Western University
Scholarship@Western

Digitized Theses | Digitized Special Collections

1995

Dynamics And Thermodynamics Of The Quasi-two Dimensional Magnetic Systems

Igor V. Rojdestvenski

Follow this and additional works at: https://ir.lib.uwo.ca/digitizedtheses

Recommended Citation
Rojdestvenski, Igor V., "Dynamics And Thermodynamics Of The Quasi-two Dimensional Magnetic Systems" (1995). *Digitized Theses*. 2574.
https://ir.lib.uwo.ca/digitizedtheses/2574

This Dissertation is brought to you for free and open access by the Digitized Special Collections at Scholarship@Western. It has been accepted for inclusion in Digitized Theses by an authorized administrator of Scholarship@Western. For more information, please contact tadam@uwo.ca, wlswadmin@uwo.ca.

National Library
of Canada

Acquisitions and
Bibliographic Services Branch

395 Wellington Street
Ottawa, Ontario
K1A 0N4

Bibliothèque nationale
du Canada

Direction des acquisitions et
des services bibliographiques

395, rue Wellington
Ottawa (Ontario)
K1A 0N4

Your file Votre référence

Our file Notre référence

NOTICE

The quality of this microform is heavily dependent upon the quality of the original thesis submitted for microfilming. Every effort has been made to ensure the highest quality of reproduction possible.

If pages are missing, contact the university which granted the degree.

Some pages may have indistinct print especially if the original pages were typed with a poor typewriter ribbon or if the university sent us an inferior photocopy.

Reproduction in full or in part of this microform is governed by the Canadian Copyright Act, R.S.C. 1970, c. C-30, and subsequent amendments.

AVIS

La qualité de cette microforme dépend grandement de la qualité de la thèse soumise au microfilmage. Nous avons tout fait pour assurer une qualité supérieure de reproduction.

S'il manque des pages, veuillez communiquer avec l'université qui a conféré le grade.

La qualité d'impression de certaines pages peut laisser à désirer, surtout si les pages originales ont été dactylographiées à l'aide d'un ruban usé ou si l'université nous a fait parvenir une photocopie de qualité inférieure.

La reproduction, même partielle, de cette microforme est soumise à la Loi canadienne sur le droit d'auteur, SRC 1970, c. C-30, et ses amendements subséquents.

Canada

DYNAMICS AND THERMODYNAMICS OF THE QUASI-TWO-DIMENSIONAL MAGNETIC SYSTEMS

by

Igor V. Rojdestvenski

Department of Physics

Submitted in partial fulfilment

of the requirements for the degree of

Doctor of Philosophy

Faculty of Graduate Studies

The University of Western Ontario

London, Ontario

March 1995

© Igor V. Rojdestvenski 1995

National Library
of Canada

Acquisitions and
Bibliographic Services Branch

395 Wellington Street
Ottawa, Ontario
K1A 0N4

Bibliothèque nationale
du Canada

Direction des acquisitions et
des services bibliographiques

395, rue Wellington
Ottawa (Ontario)
K1A 0N4

Your file Votre référence

Our file Notre référence

THE AUTHOR HAS GRANTED AN IRREVOCABLE NON-EXCLUSIVE LICENCE ALLOWING THE NATIONAL LIBRARY OF CANADA TO REPRODUCE, LOAN, DISTRIBUTE OR SELL COPIES OF HIS/HER THESIS BY ANY MEANS AND IN ANY FORM OR FORMAT, MAKING THIS THESIS AVAILABLE TO INTERESTED PERSONS.

L'AUTEUR A ACCORDE UNE LICENCE IRREVOCABLE ET NON EXCLUSIVE PERMETTANT A LA BIBLIOTHEQUE NATIONALE DU CANADA DE REPRODUIRE, PRETER, DISTRIBUER OU VENDRE DES COPIES DE SA THESE DE QUELQUE MANIERE ET SOUS QUELQUE FORME QUE CE SOIT POUR METTRE DES EXEMPLAIRES DE CETTE THESE A LA DISPOSITION DES PERSONNE INTERESSEES.

THE AUTHOR RETAINS OWNERSHIP OF THE COPYRIGHT IN HIS/HER THESIS. NEITHER THE THESIS NOR SUBSTANTIAL EXTRACTS FROM IT MAY BE PRINTED OR OTHERWISE REPRODUCED WITHOUT HIS/HER PERMISSION.

L'AUTEUR CONSERVE LA PROPRIETE DU DROIT D'AUTEUR QUI PROTEGE SA THESE. NI LA THESE NI DES EXTRAITS SUBSTANTIELS DE CELLE-CI NE DOIVENT ETRE IMPRIMES OU AUTREMENT REPRODUITS SANS SON AUTORISATION.

ISBN 0-612-03485-2

Canada

Name Igor Rogdestvenski

Dissertation Abstracts International is arranged by broad, general subject categories. Please select the one subject which most nearly describes the content of your dissertation. Enter the corresponding four-digit code in the spaces provided.

Physics / Solid State

SUBJECT TERM

0	6	1	1

SUBJECT CODE

U·M·I

Subject Categories

THE HUMANITIES AND SOCIAL SCIENCES

COMMUNICATIONS AND THE ARTS

Architecture	0729
Art History	0377
Cinema	0900
Dance	0378
Fine Arts	0357
Information Science	0723
Journalism	0391
Library Science	0399
Mass Communications	0708
Music	0413
Speech Communication	0459
Theater	0465

EDUCATION

General	0515
Administration	0514
Adult and Continuing	0516
Agricultural	0517
Art	0273
Bilingual and Multicultural	0282
Business	0688
Community College	0275
Curriculum and Instruction	0727
Early Childhood	0518
Elementary	0524
Finance	0277
Guidance and Counseling	0519
Health	0680
Higher	0745
History of	0520
Home Economics	0278
Industrial	0521
Language and Literature	0279
Mathematics	0280
Music	0522
Philosophy of	0998
Physical	0523
Psychology	0525
Reading	0535
Religious	0527
Sciences	0714
Secondary	0533
Social Sciences	0534
Sociology of	0340
Special	0529
Teacher Training	0530
Technology	0710
Tests and Measurements	0288
Vocational	0747

LANGUAGE, LITERATURE AND LINGUISTICS

Language	
General	0679
Ancient	0289
Linguistics	0290
Modern	0291
Literature	
General	0401
Classical	0294
Comparative	0295
Medieval	0297
Modern	0298
African	0316
American	0591
Asian	0305
Canadian (English)	0352
Canadian (French)	0355
English	0593
Germanic	0311
Latin American	0312
Middle Eastern	0315
Romance	0313
Slavic and East European	0314

PHILOSOPHY, RELIGION AND THEOLOGY

Philosophy	0422
Religion	
General	0318
Biblical Studies	0321
Clergy	0319
History of	0320
Philosophy of	0322
Theology	0469

SOCIAL SCIENCES

American Studies	0323
Anthropology	
Archaeology	0324
Cultural	0326
Physical	0327
Business Administration	
General	0310
Accounting	0272
Banking	0770
Management	0454
Marketing	0338
Canadian Studies	0385
Economics	
General	0501
Agricultural	0503
Commerce Business	0505
Finance	0508
History	0509
Labor	0510
Theory	0511
Folklore	0358
Geography	0366
Gerontology	0351
History	
General	0578
Ancient	0579
Medieval	0581
Modern	0582
Black	0328
African	0331
Asia, Australia and Oceania	0332
Canadian	0334
European	0335
Latin American	0336
Middle Eastern	0333
United States	0337
History of Science	0585
Law	0398
Political Science	
General	0615
International Law and Relations	0616
Public Administration	0617
Recreation	0814
Social Work	0452
Sociology	
General	0626
Criminology and Penology	0627
Demography	0938
Ethnic and Racial Studies	0631
Individual and Family Studies	0628
Industrial and Labor Relations	0629
Public and Social Welfare	0630
Social Structure and Development	0700
Theory and Methods	0344
Transportation	0709
Urban and Regional Planning	0999
Women's Studies	0453

THE SCIENCES AND ENGINEERING

BIOLOGICAL SCIENCES

Agriculture	
General	0473
Agronomy	0285
Animal Culture and Nutrition	0475
Animal Pathology	0476
Food Science and Technology	0359
Forestry and Wildlife	0478
Plant Culture	0479
Plant Pathology	0480
Plant Physiology	0817
Range Management	0777
Wood Technology	0746
Biology	
General	0306
Anatomy	0287
Biostatistics	0308
Botany	0309
Cell	0379
Ecology	0329
Entomology	0353
Genetics	0369
Limnology	0793
Microbiology	0410
Molecular	0307
Neuroscience	0317
Oceanography	0416
Physiology	0433
Radiation	0821
Veterinary Science	0778
Zoology	0472
Biophysics	
General	0786
Medical	0760

EARTH SCIENCES

Biogeochemistry	0425
Geochemistry	0996
Geodesy	0370
Geology	0372
Geophysics	0373
Hydrology	0388
Mineralogy	0411
Paleobotany	0345
Paleoecology	0426
Paleontology	0418
Paleozoology	0985
Palynology	0427
Physical Geography	0368
Physical Oceanography	0415

HEALTH AND ENVIRONMENTAL SCIENCES

Environmental Sciences	0768
Health Sciences	
General	0566
Audiology	0300
Chemotherapy	0992
Dentistry	0567
Education	0350
Hospital Management	0769
Human Development	0758
Immunology	0982
Medicine and Surgery	0564
Mental Health	0347
Nursing	0569
Nutrition	0570
Obstetrics and Gynecology	0380
Occupational Health and Therapy	0354
Ophthalmology	0381
Pathology	0571
Pharmacology	0419
Pharmacy	0572
Physical Therapy	0382
Public Health	0573
Radiology	0574
Recreation	0575
Speech Pathology	0460
Toxicology	0383
Home Economics	0386

PHYSICAL SCIENCES

Pure Sciences

Chemistry	
General	0485
Agricultural	0749
Analytical	0486
Biochemistry	0487
Inorganic	0488
Nuclear	0738
Organic	0490
Pharmaceutical	0491
Physical	0494
Polymer	0495
Radiation	0754
Mathematics	0405
Physics	
General	0605
Acoustics	0986
Astronomy and Astrophysics	0606
Atmospheric Science	0608
Atomic	0748
Electronics and Electricity	0607
Elementary Particles and High Energy	0798
Fluid and Plasma	0759
Molecular	0609
Nuclear	0610
Optics	0752
Radiation	0756
Solid State	0611
Statistics	0463

Applied Sciences

Applied Mechanics	0346
Computer Science	0984
Engineering	
General	0537
Aerospace	0538
Agricultural	0539
Automotive	0540
Biomedical	0541
Chemical	0542
Civil	0543
Electronics and Electrical	0544
Heat and Thermodynamics	0348
Hydraulic	0545
Industrial	0546
Marine	0547
Materials Science	0794
Mechanical	0548
Metallurgy	0743
Mining	0551
Nuclear	0552
Packaging	0549
Petroleum	0765
Sanitary and Municipal	0554
System Science	0790
Geotechnology	0428
Operations Research	0796
Plastics Technology	0795
Textile Technology	0994

PSYCHOLOGY

General	0621
Behavioral	0384
Clinical	0622
Developmental	0620
Experimental	0623
Industrial	0624
Personality	0625
Physiological	0989
Psychobiology	0349
Psychometrics	0632
Social	0451

ABSTRACT

In recent years a considerable research effort has been put into the understanding of the physical properties of quasi-two-dimensional magnetic systems. Theoretical investigations help to explain many current experimental results. The aim of this thesis is to study dynamic and critical properties of certain quasi-two-dimensional magnetic systems.

In the first part of the thesis (Chapters 2 and 3) the Handscomb Monte-Carlo method is applied to investigate the critical behavior of the $S=\frac{1}{2}$ Heisenberg ferromagnetic film with the number of monolayers $L\leq 3$. We confirm the renormalization group results for the two-dimensional model for a wide range of temperatures and report the effectively two-dimensional type of critical behavior for the films with L=2 and L=3.

The second part of the thesis (Chapters 4 and 5) is devoted to the development of an analytic theory of the dipole-exchange spin waves and their Brillouin light-scattering spectra in perpendicularly-magnetized magnetic films and multilayers. The time-dependent Green function technique is applied. The influence of the pinning parameter value on the magnon dipole-exchange spectrum of a single film in the case of near degeneracy of the surface mode and the nearest bulk mode is discussed. The dependences of the integrated light scattering intensities on the pinning parameter are calculated.

The degeneracy is shown to have a strong influence on the dispersion relationships for EuO films, having less importance in the case of iron films.

Next the theory is extended to the case of an exchange coupled magnetic double layer (two magnetic films separated by a non-magnetic spacer). The interlayer exchange coupling is shown to renormalize the pinning parameter at the interface between the magnetic film and the spacer for the antisymmetric SW modes.

Then we treat the case of a multilayer, consisting of a number of similar ferromagnetic layers separated by nonmagnetic spacers. The dipole-dipole and exchange coupling are included within the magnetic layers and between them. We present a semi-empirical theory for the spin wave spectra in the multilayer structures and discuss the Brillouin light scattering from spin waves in such structures.

ACKNOWLEDGEMENTS

I would like to express my most sincere acknowledgements to my supervisor, Professor M. G. Cottam whose attention and experience, accompanied by the most friendly attitude, constituted an invaluable asset of my work.

I extend my greatest gratitude to the Faculty, staff and the students of the Department of Physics and the entire University of Western Ontario, my family, friends and the whole country of Canada for making these three years of my life as pleasant and productive as they were.

Igor Rojdestvenski

TABLE OF CONTENTS Page

CERTIFICATE OF EXAMINATION ii

ABSTRACT..... iii

ACKNOWLEDGEMENTS..... v

TABLE OF CONTENTS..... vi

LIST OF FIGURES..... x

CHAPTER 1. - QUASI-TWO-DIMENSIONAL MAGNETIC SYSTEMS: MODELS AND METHODS..... 1

1.1. Introduction..... 1

1.2. Models of Magnetism..... 3

1.3. The Monte-Carlo Method in Statistical Physics.... 10

1.4. Spin Waves and Their Study by Light Scattering... 15

1.5. The Scope of the thesis..... 18

CHAPTER 2. - HANDSCOMB MONTE-CARLO METHOD FOR THE QUANTUM SPIN MODELS..... 20

2.1. Introduction..... 20

2.2. Handscomb Monte-Carlo Method. The General Formulation and Application to S=1/2 Isotropic Heisenberg Ferromagnet..... 23

2.3. A Review of Some results Obtained by Means of MCH..... 31

2.3.1. One-Dimensional Model..... 31

2.3.2. A Three-Dimensional Heisenberg Model with Defects. The Percolation Threshold..... 32

2.3.3. The Heisenberg Model with Next-Nearest-Neighbour Interactions on a Simple Cubic Lattice..... 33

2.3.4. Conclusions..... 34

2.4. The Generalization of the Handscomb Procedure.... 35

2.5. Applications of the Handscomb Method to Some Other Models..... 42

2.5.1. Heisenberg Model with four-Spin Interactions. 42

2.5.2. Modelling of a Heisenberg Antiferromagnet and XY model..... 43

2.5.3. MCH Method for S=1/2 Ising Model in Transverse Field..... 46

2.5.4. Some Recent Modifications of the Handscomb Method..... 47

CHAPTER 3. - MONTE-CARLO SIMULATION OF THE CRITICAL PROPERTIES OF QUASI-TWO-DIMENSIONAL HEISENBERG SYSTEMS..... 50

3.1. Introduction..... 50

3.2. Critical Properties of Quantum 2D Ferromagnets... 53

3.3. Thin Heisenberg Films with Number of Monolayers M<4..... 63

3.4. Two-Monolayer Film with a Diluted Upper Layer.... 72

3.5. Influence of Interlayer Exchange on the Critical

Properties of a Two-Layer Film..... 83

3.6. Conclusions..... 87

CHAPTER 4. - BRILLOUIN LIGHT SCATTERING FROM DIPOLE-EXCHANGE MICROWAVE SPIN WAVES IN MAGNETIC FILMS..... 88

4.1. Introduction..... 88

4.2. Fundamentals of Light Scattering from Spin Waves..... 91

4.2.1. The Differential Cross Section for BLS..... 91

4.2.2. 180^0 Backscattering from a Perpendicularly Magnetized Film..... 98

4.3. Non-Hybridized Spin Waves and Green Functions.... 99

4.4. Brillouin Light Scattering from Non-Hybridized Spin Waves..... 102

4.5. Hybridized Spin Waves and Green Functions..... 109

4.6. Brillouin Light Scattering from Hybridized Spin Waves..... 116

4.7. Modifications of Pinning Conditions..... 124

4.8. Conclusions..... 125

CHAPTER 5. - SPIN WAVE SPECTRA IN THE MAGNETIC MULTILAYER STRUCTURES..... 128

5.1. Introduction..... 128

5.2. Spin Wave Spectrum for the Exchange-Coupled

Double Layer Spectrum..... 133

5.3. Numerical Results and Applications for Surface Waves..... 139

5.4. Spin Wave Spectrum in Multilayers with Interlayer Exchange and Dipole Coupling. A Semi-Empirical Approach..... 145

5.4.1. The Hamiltonian and the Spin Wave Representation..... 145

5.4.2. Multilayer Energy Density in the CSWM Approximation..... 149

5.4.3. Calculation of the Matrix Elements..... 152

5.4.4. Analysis of the Obtained Expressions..... 158

5.4.5. Numerical results..... 163

5.5. Conclusions..... 167

CHAPTER 5. - CONCLUSIONS..... 168

REFERENCES..... 171

VITA..... 181

LIST OF FIGURES

Figure — Page

1. The finite scaling analysis of the susceptibility for a one-layer film. 58

2. The temperature dependence of the longitudinal susceptibility for a one-layer film. 59

3. The finite scaling analysis of the correlation range for a one-layer film. 61

4. The temperature dependence of the correlation range for a one-layer film. 62

5. The finite scaling analysis of the susceptibility for a two-layer film. 65

6. The temperature dependence of the susceptibility for a two-layer film with $J^T = J^B$. 66

7. The temperature dependence of the correlation range for a two-layer film. 67

8. The temperature dependence of the surface-surface correlator for a two-layer film. 68

9. The temperature dependence of the susceptibility for a three-layer film. 70

10. The susceptibility data for a two-layer field with diluted upper layer. 76

11. Exchange renormalization versus occupancy concentration for a film with a diluted upper layer. 77

12. Exchange parameter as a function of the film density..... 82

13. The temperature dependence of the susceptibility for a two-layer film with $J^T=0.1J^B$ and $J^T=0.3J^B$. 85

14. The temperature dependence of the susceptibility for a two-layer film with $J^T=0.02J^B$ and $J^T=0.04J^B$. 86

15. The ferromagnetic film of thickness , showing the coordinate axes and the directions of the incident (I) and scattered (S) light beams for a general BLS backscattering geometry. 92

16. The SW frequencies plotted against the in-plane wave vector q for a Fe film in the nondegenerate case. 106

17. The SW dispersion relations for a Fe film. 118

18. The SW eigenfrequencies versus pinning d for a Fe film. .. 119

19. The SW dispersion relations for a EuO film for two different values of the pinning parameter. 120

20. The integrated intensities of the BLS for a Fe film with

backscattering angle equal to 45° versus pinning parameter d. 122

21. The integrated BLS intensities and SW frequencies (see inset) for a EuO film as functions of film thickness L. 123

22. The shift in the perpendicular SW wave vector as a function of d. 126

23. The geometry of a typical multilayer structure. 129

24. The dependences of the imaginary perpendicular SW wavenumbers on the interlayer exchange coefficient. 141

25. The dependences of the surface SW frequencies on the interlayer exchange coefficient. 143

26 The dependences of the integrated intensities of Brillouin light scattering from the surface SW on the interlayer exchange coefficient. 144

27. The boundaries of the bulk bands for multilayers with different numbers of layers. 164

28. Dispersion branches for multilayers with different values of the interlayer exchange. 165

The author of this thesis has granted The University of Western Ontario a non-exclusive license to reproduce and distribute copies of this thesis to users of Western Libraries. Copyright remains with the author.

Electronic theses and dissertations available in The University of Western Ontario's institutional repository (Scholarship@Western) are solely for the purpose of private study and research. They may not be copied or reproduced, except as permitted by copyright laws, without written authority of the copyright owner. Any commercial use or publication is strictly prohibited.

The original copyright license attesting to these terms and signed by the author of this thesis may be found in the original print version of the thesis, held by Western Libraries.

The thesis approval page signed by the examining committee may also be found in the original print version of the thesis held in Western Libraries.

Please contact Western Libraries for further information:
E-mail: libadmin@uwo.ca
Telephone: (519) 661-2111 Ext. 84796
Web site: http://www.lib.uwo.ca/

CHAPTER 1.

QUASI-TWO-DIMENSIONAL MAGNETIC SYSTEMS: MODELS AND METHODS

1.1. INTRODUCTION

In recent years a considerable research effort has been put into the understanding of the physical properties of quasi-two-dimensional magnetic systems. Here we classify such systems as crystals having translational invariance in two out of three spatial dimensions, i.e. thin films, slabs, semi-infinite and finite thickness multilayers with alternating magnetic/nonmagnetic layers.

The main goals of the current research in this field are as follows. First, a number of physical phenomena occurring due to the effectively reduced dimensionality are of interest for numerous industrial applications such as microwave devices and magnetic recording heads. The phenomenon of giant magnetoresistance in magnetic multilayers, which is currently believed to exist due to the exchange interaction between the magnetic layers via a nonmagnetic spacer, might serve as an example. Another example is soliton propagation in magnetic films.

Second, the industrial need for the production of magnetic thin films and multilayers with given physical properties, such as surface and bulk interaction parameters, gives rise to a technology of non-destructive testing of these materials. Hence, it is necessary to

to develop experimental techniques for the sake of such testing together with theoretical investigations to interpret the experimental results and to determine the required parameters. An example might be the technique of Brillouin light scattering from the spin waves (SW) in magnetic films and slabs that enables an investigator to obtain the spectra of SW excitations. These spectra can serve as a source of information about the parameters of the system and the quality of its production.

Third, many physical phenomena in the systems in question are interesting from the point of view of fundamental science, such as thermodynamics and critical properties of ultrathin ferromagnetic films. Theoretical investigations in this area help to explain many current experimental results, such as the critical properties of thin ^{3}He films on a graphite substrate. Moreover, extensive use of different techniques and their combinations in research of such physically rich objects as quasi-two-dimensional magnetic systems provides for further development of the methods themselves. Useful analogies, pointed out as the research progresses, might then be extensively used far away from the traditional realm of theoretical physics, such as the utilization of the Monte-Carlo method in the transport and neural network analysis.

The aim of the present thesis is to study dynamic, thermodynamic

and critical properties of certain quasi-two-dimensional systems. The structure of this introductory chapter is as follows. In Section 2 we discuss some different models of magnetism, which are relevant to the thesis. In Section 3 we discuss the foundations of the classic Monte-Carlo method as applied to the problems of statistical physics. Section 4 deals with a general survey of the basic theory of spin waves in magnetic thin films and multilayers and the Brillouin light scattering from these spin waves. Section 5 concludes this introductory Chapter, explaining the contents of the subsequent thesis chapters.

1.2. MODELS OF MAGNETISM

The nature of the interaction that produces ordering in magnetic crystals has been described by Heisenberg (Ref. 1) in 1928. He showed that this interaction is electrostatic and originates in the quantum-mechanical exchange interaction. In simple terms, the Fermi-Dirac statistics of the electrons provides for the Pauli principle to be in effect, which principle states that there cannot be more than one electron in one quantum state. This means, in turn, that the spin parts of the electron wave functions can only have the symmetry properties such that then total two-electron wave function

be antisymmetric. The operator of the total Coulomb interaction energy of a pair of neighbouring one-electron ions, 1 and 2, calculated within the framework of the first order perturbation theory and accounting for the symmetry of the wave functions, has then the following form:

$$H = -2J\,\mathbf{S}_1\cdot\mathbf{S}_2 + \text{const.} \qquad (1)$$

In Eq. (1) $\mathbf{S}_1$ and $\mathbf{S}_2$ are the spin-1/2 operators of the two electrons, J is called the "exchange parameter" and can be calculated in terms of the overlap integral of the electronic wave functions. For a crystal containing many such ions, since the Coulomb interaction is a pair interaction, the total exchange energy is represented as a sum of the pair terms of all the interacting ions. Adding then the Zeeman energy term due to the interaction with the external magnetic field H (in the z direction), we obtain then what is called the isotropic $S=\frac{1}{2}$ Heisenberg quantum Hamiltonian:

$$H = -g\mu_B H \sum_t S_t^z - 2\sum_{t>t'} J_{tt'}\,\mathbf{S}_t\cdot\mathbf{S}_{t'} \qquad (2)$$

where μ_B is the Bohr magneton and g is the Lande factor. The summation in the second sum, in principle, has to be accomplished over all the pairs of spins in the lattice. However, $J_{tt'}$, as being defined via the overlap integrals, decreases abruptly as a function of the distance between the sites t and t'. That is why a commonly

used approximation is a so-called nearest neighbour interaction, in which $J_{tt'}$ is assumed to be nonzero only for the pairs of spins which are adjacent on the lattice. The expression (2) can be generalized to many electron ions, and in this case the general spin S operators are being used (see, e.g. Ref. 2).

The signs and the values of the exchange parameter depend on the lattice structure and dimensionality. A negative exchange parameter in Eq. (2) corresponds to the case of an antiferromagnet or a ferrimagnet, while for a ferromagnet this sign is positive.

The Hamiltonian (2) corresponds to the simplest case of an isotropic magnetic material with only exchange interaction in effect. The crystallographic anisotropy may result in an anisotropy in the exchange interaction itself, changing the exchange energy term in (2) as follows (see, e.g. Ref. 2):

$$-\sum_{t>t'} J_{tt'}(S_t^x S_{t'}^x + S_t^y S_{t'}^y + \Delta S_t^z S_{t'}^z), \qquad (3)$$

with Δ being the anisotropy parameter. Equation (2) corresponds to the case of $\Delta=1$. In the extreme case of a very strong anisotropy, $\Delta>>1$, the above model becomes the Ising model, while the case of $\Delta=0$ corresponds to the so-called XY model. In this thesis, however, when discussing the statistical, thermodynamic and critical properties of the Heisenberg model, we will assume it to be in the form (2).

Along with the exchange, much weaker relativistic spin-spin and spin-orbital interactions might come into effect. These interactions result, in particular, in the single-ion anisotropy, which in a non-cubic crystal might be described by adding to (2) a term of the form (see, e.g. Ref. 3, 4):

$$-K\sum_{t}(S_t^z)^2 - F\sum_{t}[(S_t^x)^2 - (S_t^y)^2]. \qquad (4)$$

It is important sometimes as well to account for the dipolar interactions of the spins. The corresponding energy for two spins situated at lattice sites i and j, can be written microscopically in the form (see, e.g. Ref. 4):

$$g^2\mu_B^2\left[\frac{\mu_o}{4\pi}\right]\left[\frac{\mathbf{S}_i\cdot\mathbf{S}_j}{|\mathbf{r}_{ij}|^3} - \frac{3(\mathbf{S}_i\cdot\mathbf{r}_{ij})(\mathbf{S}_j\cdot\mathbf{r}_{ij})}{|\mathbf{r}_{ij}|^5}\right] \qquad (5)$$

Here we use the standard notations of μ_o being the magnetic permeability of the free space.

Very often the total magnetic Hamiltonian is rewritten in the so-called "continuous medium approximation". That is, if we assume the size of the system to be much greater than the size of an elementary lattice cell, we can introduce a position dependent macroscopic local magnetization vector, $\mathbf{M}(\mathbf{r})$, which is a thermal average of the sum of the spin operators in a macroscopically small vicinity of the position $\mathbf{r}$, which vicinity is, nevertheless, assumed

to be effectively infinite on the microscopic scale (see, e.g. 3, 5, 6). In this approximation the Heisenberg isotropic exchange interaction energy density term may be rewritten in the form:

$$- 2\pi\alpha\int dr\left(\nabla \mathbf{M}(r)\right)^2 \qquad (6)$$

where the renormalized exchange parameter α can be expressed in terms of the microscopic exchange parameter, the lattice constant a, and the equilibrium static magnetization M_o of the sample. For example, for a simple cubic lattice with the nearest-neighbour exchange interaction J we have:

$$\alpha \cong \frac{SJa^2}{2g\mu_B M_o}, \qquad (7)$$

We should note here that in the discussed approximation the kinetic stages of the evolution of the system have been accounted for in the process of averaging $\mathbf{M}(r)$ (Ref. 5). Hence, this description is valid only for a long wave, hydrodynamic stage of the evolution of the system.

As well as for the microscopic model (2), it is possible in the continuous medium approximation to account for different kinds of anisotropies in a way that is analogous to (6) (see, e.g. 3, 4). In particular, this can be done for the dipolar interaction energy, which is conveniently obtained in the continuous medium approximation from the solution of the Maxwell's equations (usually in the

magnetostatic limit) with the boundary conditions corresponding to the shape of the sample (See Ref. 7). We will leave further discussions of different contributions to the total energy density of a ferromagnetic thin film until Chapter 4.

The characteristic features of the dynamic and thermodynamic properties of finite-size macroscopic crystals are largely dependent on the shape and dimensionality. When studying the critical phenomena, the dimensionality determines the type of the phase transition and the values of the critical temperature and the critical exponents. A traditional example might be the $S=\frac{1}{2}$ Ising model on a simple cubic lattice, which has been solved exactly in one and two dimensions and vastly investigated by means of different numerical and analytical methods in three and more dimensions (see, e.g. Ref. 8). This model displays no phase transition in one dimension, a second order transition in two and three dimensions, and becomes exactly solvable by the mean field approximation in four or more dimensions. Another example, the isotropic Heisenberg model in two dimensions, is discussed in Chapter 3 together with the description of the critical behaviour of the quasi-two dimensional models (i.e., thin ferromagnetic Heisenberg films), which are finite in one dimension and infinite in the two others.

For the dynamic phenomena the reduction of the dimensionality of

the system is accompanied by a reduction of its translational invariance. This results in the occurence of additional types of excitations, such as surface and interface excitations. These excitations are characterized by having their amplitude localized in the vicinity of a surface (interface) of a crystal and decaying, typically exponentially, with the distance away from it (see Ref. 9 for a review). As well, the arrangement of the atoms at the surfaces and interfaces might differ from that in the bulk. This means that the parameters of the surface exchange and effective anisotropies may be different from the corresponding bulk values, which affects the spectra of the excitations of the system.

Normally the surface and interface parameters participate in the boundary condition equations for the variable part of magnetization. The procedure of deriving these boundary conditions in the continuous medium approximation is described in Ref. 10 in terms of the variational principle for the effective field. As an example, we can quote the case of the Hamiltonian of a thin ferromagnetic film sample with a single-ion anisotropy and magnetized perpendicularly to the film surface. The boundary condition has the simple form

$$\frac{\partial \mathbf{m}}{\partial z} + d_1 \mathbf{m}\Big|_{z=0} = 0 , \qquad \frac{\partial \mathbf{m}}{\partial z} + d_2 \mathbf{m}\Big|_{z=-L} = 0 \tag{8}$$

where $\mathbf{m}$ is the varying (or fluctuating) part of the total

magnetization, z is a coordinate in the direction perpendicular to the film surface, d_1 and d_2 are the pinning parameters (related to the surface anisotropy constant, as explained in Chapter 4) at the top (z=0) and the bottom (z=-L) surfaces of the film. The limiting cases of $d_{1,2}=0$ and $d_{1,2}=\infty$ correspond to totally "free" and totally "pinned" surface spins, respectively.

1.3. THE MONTE-CARLO METHOD IN STATISTICAL PHYSICS

Since its invention in 1953 (Ref. 11) the Monte-Carlo (MC) method has proved itself to be a powerful tool for the investigation of statistical, thermodynamic and critical properties of a multitude of physical systems (see, e.g. Ref. 12 and references therein). It happened to fill the gap between the theoretical approaches to the mentioned phenomena and an experimental study of them. Rapid growth of computer technologies encouraged the wider utilization of the MC technique, its applications now being spread over the entire domain of statistical physics and related disciplines.

The simplified general scheme of the MC technique can be formulated as follows. Let us have a canonic ensemble with the Hamiltonian $\mathcal{H}$. For the partition function Z and the canonic average value of any physical variable operator A, denoted here as $\langle A \rangle_c$, we may write:

$$Z = \mathrm{Tr}\left[\exp\{-\beta H\}\right], \qquad \langle A\rangle_c = \frac{1}{Z}\,\mathrm{Tr}\left[A\exp\{-\beta H\}\right] \tag{9}$$

where $\beta=1/(k_B T)$, T denotes temperature (in K) and k_B is Boltzmann's constant. Let $\{|\Phi_i\rangle\}$ be a complete orthonormal basis in the space of the wave functions for this system. Then, by definition of a trace operation we have:

$$\langle A\rangle_c = \frac{\sum_i \langle\Phi_i|\left(A\exp\{-\beta H\}\right)|\Phi_i\rangle}{\sum_i \langle\Phi_i|\left(\exp\{-\beta H\}\right)|\Phi_i\rangle} \tag{10}$$

Now let us assume that our set $\{|\Phi_i\rangle\}$ diagonalizes the operators H and A simultaneously,

$$H|\Phi_i\rangle = E_i|\Phi_i\rangle,\ A|\Phi_i\rangle = A_i|\Phi_i\rangle, \tag{11}$$

which implies

$$[A,H] \equiv AH - HA = 0. \tag{12}$$

Then we rewrite (10) as follows:

$$\langle A\rangle_c = \frac{\sum_i A_i \exp\{-\beta E_i\}}{\sum_i \exp\{-\beta E_i\}} = \sum_i A_i\, p_i,$$

$$p_i = \frac{\exp\{-\beta E_i\}}{\sum_j \exp\{-\beta E_j\}} \qquad (13)$$

If $p_i \geq 0$ for all i, then we can treat $\{p_i\}$ as a *probability distribution*, having

$$\langle A \rangle_c = \langle A_i \rangle_p \qquad (14)$$

In Eq. (14) we denote the average with the probability distribution $\{p_i\}$ as $\langle\ \rangle_p$.

The basic idea of the MC method is to simulate the random sampling of the functions $|\Phi_i\rangle$ from the set $\{|\Phi_i\rangle\}$, which is then called the *sample space*, with the probability distribution $\{p_i\}$. Once the procedure for such a sampling is achieved, the thermal averages $\langle A \rangle_c$ are calculated as the arithmetic averages of the values of A_i corresponding to the $|\Phi_i\rangle$ which occur in the process of sampling.

The way the random sampling is usually realised is in applying the concept of a *Markovian process*, or *Markov chain* (see, e.g. Ref. 12). Within the framework of this approach the sampling is accomplished as a sequence of transitions between two configurations - initial, $|\Phi_i\rangle$ and final, $|\Phi_j\rangle$, the probabilities of these transitions depending only on the canonic weights, $\exp\{-\beta E_i\}$ and $\exp\{-\beta E_j\}$ of the two configurations involved and not depending on the previous transitions. These *transition probabilities*, $\Pr(\Phi_i \rightarrow \Phi_j)$, may be proved to provide finally for the *limit distribution* p_i, as

the number of the transitions, or *steps*, in the sequence goes to infinity, on the condition that they obey the *detailed balance equation*:

$$Pr(\Phi_j \rightarrow \Phi_i)\, p_j = Pr(\Phi_i \rightarrow \Phi_j)\, p_i \qquad (15)$$

We should note here that the transition probabilities $Pr(\Phi_i \rightarrow \Phi_j)$ are not uniquely defined by (15). Different systems of transition probabilities provide for different *numerical dynamics*, the choice of the dynamics affecting only the convergence rate and the uncertainties. The most often used dynamics is the *Metropolis dynamics*, where

$$Pr(\Phi_i \rightarrow \Phi_j) = \min\,(1,\ \exp\{-\beta(E_j - E_i)\}) \qquad (16)$$

The generalized scheme of the MC method then looks as follows:

1. Set the system of transition probabilities $Pr(\Phi_i \rightarrow \Phi_j)$ according to a chosen dynamics;

2. Start from a certain initial state, $|\Phi_K\rangle$ chosen from a sample space, $\{|\Phi_i\rangle\}_{i=1}^{M}$;

3. Jump from state $|\Phi_K\rangle$ to state $|\Phi_L\rangle$ with the probability $Pr(\Phi_K \rightarrow \Phi_L)$, otherwise remain in $|\Phi_K\rangle$ with the probability $\left(1-Pr(\Phi_K \rightarrow \Phi_L)\right)$;

4. Wait for the reaching of equilibrium, when it may be considered that the frequencies of occurrence of the states $|\Phi_K\rangle$

with any κ are close enough to the probabilities p_κ, and start averaging.

For a very thorough discussion of the properties of the MC method we refer the reader to the Ref. 12. Among the advantages of the MC method one can mention the following:

1) The method in principle is *exact* in the mathematical sense, i.e. its realizations, albeit with some exclusions, do not contain any approximations other than the ones implied by the theoretical model used. The results obtained are accurate apart from the statistical errors which in principle can be made as small as desired if the time of calculation is long enough.

2) The MC technique very often appears to be the only one suitable for studying the properties of systems with complex interactions, deviating from the nearest neighbour interactions.

3) Though the traditional MC method does not provide accurate information on the dynamic properties of a system under consideration, it yields knowledge of the equilibrium configurations.

A classic example of utilization of the MC method is the spin S Ising model with the Hamiltonian having the form:

$$H = -g\mu_B H \sum_t S_t^z - 2\sum_{t>t'} J_{tt'} S_t^z S_{t'}^z, \qquad (17)$$

with S_t^z being the z-component of the operator of spin located at the

site t. For this model the functions $|\Phi_K\rangle$ are the well known *spin configurations:*

$$|\Phi_K\rangle = |\sigma_1,\sigma_2,\sigma_3, \ldots . ,\sigma_{N-1},\sigma_N\rangle \qquad (18)$$

where σ_1 = -S, S+1,...., S-1, are z-projections of the spin-S operators. It is interesting to note that the model (17) does not have any intrinsic dynamics in the sense of the Hamiltonian equations of motion. Thus there is no ab initio preference for the choice of the MC dynamics.

1.4. SPIN WAVES AND THEIR STUDY BY LIGHT SCATTERING

The concept of magnetic spin waves, or magnons, was introduced by Bloch in 1930 (Ref. 13). Empirically one can describe the magnons as small deviations from the spin ground state of the lattice, which propagate in a wave-like manner. For the magnons to be well defined, the magnetic thermodynamic state has to have a well defined order parameter. Hence, the magnetic crystal has to be either at low (compared to T_c) temperatures or magnetized to saturation by an external magnetic field. The concept of magnons was at first applied to describe the deviations of the temperature dependence of the magnetization of a ferromagnet at low temperature from the prediction of the mean-field theory (Ref. 13).

A mathematical introduction of the magnon formalism can be based on the bosonisation of the spin Hamiltonian by means of one of the well-known transformations, such as the Holstein-Primakoff transformation (see, e.g. Ref. 14). The Hamiltonian equations of motion for the magnons are usually linearized within the approximation of the number of magnons at the same lattice site (or with the same wave vector) being small compared to the 2S value. After that these equations are Fourier transformed in the spatial and in the time dimensions. The result is the dependence $\omega(\mathbf{q})$ of the frequencies of the magnons on the spatial wave vector $\mathbf{q}$. These frequences describe completely the system of non-interacting magnons which by their definition are quantized and obey the Bose-Einstein statistics. The analogous procedure in the continuous medium approximation is based on the linearization of the Hamiltonian equations of motion with respect to the small parameter which is the deviation of the local variable magnetization $\mathbf{M}(r)$ from the static magnetization $\mathbf{M}_o$ of the sample (see, e.g. Ref. 10). However, in the continuous medium approximation, the magnetic excitations are no longer quantized, as the Hamiltonian becomes a classical one.

The mechanism of light scattering from the spin waves was described first by Elliott and Loudon (Ref. 15). Namely, the light is scattered by the magnetic permeability fluctuations which occur due

to the existence of magnons. The first observation of spin waves by light scattering was made in 1966, when Fleury et al (Ref. 16) used the Raman scattering technique to study the excitation of spin waves and spin-wave pairs in the antiferromagnet FeF_2. Extensive studies of Raman light scattering in many other antiferromagnets followed shortly afterwards. However, it was several years later before the innovation of a multipass Fabry-Perot spectrometer made possible the observation of ferromagnetic and ferrimagnetic spin waves by the technique of Brillouin light scattering (BLS). The first BLS measurements of spin waves (Refs. 17, 18) were reported in 1973 for the ferrimagnet yttrium iron garnet (YIG) and in 1974 for the ferromagnet $CrBr_3$.

More recently there have been BLS studies of spin waves in opaque ferromagnets, and on thin films and multilayers, with a view to studying spin waves at surfaces. The first experiments (Refs. 19, 20) were performed for EuO and for Fe and Ni, using BLS at a single surface of a thick sample. They showed scattering from localized surface spin waves, as well as a modification of the bulk spin-wave properties. Subsequent BLS studies were reported for ferromagnetic thin films (Ref. 21), double-layer systems (Ref. 22), and superlattices (Ref. 23). In general, BLS spectroscopy has now developed into a convenient and sensitive technique for studying the

spin-wave spectra and the magneto-optical properties of films and multilayers.

1.5. THE SCOPE OF THE THESIS

The present thesis is devoted to the investigation of the dynamic, thermodynamic and critical propertes of magnetic thin films and multilayers by means of different numerical and analytical methods. The outline of the thesis is as follows.

The next two chapters deal with the MC methods as applied to quantum spin systems. In Chapter 2 we formulate in detail the Handscomb MC technique applied to various quantum spin models. We illustrate our discussion with a review of the results for the thermodynamic and critical properties of these models obtained by the Handscomb method.

In Chapter 3 we investigate the thermodynamic properties of very thin (i.e., having several monoatomic layers) S=1/2 simple cubic Heisenberg isotropic ferromagnetic films. We discuss the application of various methods to the two-dimensional Heisenberg model. We then present the results of our numerical simulation, by means of the Handscomb method, of the above films with different values of the parameters.

In Chapters 4 and 5 we investigate the spin wave spectra and their study by Brillouin light scattering (BLS) from magnetic thin

films and multilayers. We assume the continuous medium approximation to be in effect. In Chapter 4 we develop the formalism of light scattering from the spin waves in thin films within the framework of the Green function theory. We study the dependences of the SW spectrum and the BLS integrated intensities on the wave vector and surface parameters in the cases of optically transparent and opaque thin films.

Chapter 5 is devoted to the investigation of the SW spectra and the BLS phenomena from magnetic multilayers with the interlayer dipole and exchange interactions. We study the cases of a symmetric bilayer with the layers coupled via Hoffmann boundary conditions, and a general case of a multilayer. Numerical results are presented for some spectra of the surface excitations and the BLS integrated intensities.

In the concluding Chapter 6 we underline the basic results of this research and discuss some further possible developments in related areas.

CHAPTER 2.

HANSCOMB MONTE CARLO METHOD FOR THE QUANTUM SPIN MODELS

2.1 INTRODUCTION

In this chapter we shall concentrate on discussing some details of the application of MC technique to quantum systems. The straightforward application of the Metropolis scheme does not work in the case of quantum systems, as explained below. We apply here the term "quantum" to specify the systems with the Hamiltonian operator being a sum of non-commutative terms. In this sense the well known Ising model becomes "classical" though its Hamiltonian is an operator expressed in terms of spin operators for each lattice site.

The main feature of the quantum (in the above sense) models is that it is very often impossible to achieve a complete basis for random sampling within the framework of the MC method, meeting the requirement of Eq. (11). Indeed, for the case of the "classical" Ising model, one readily knows that the appropriate set is the complete set of eigenfunctions of z-projection of the total spin operator. If, however, we modify the Ising model, e.g., to obtain the so-called Ising model in a transverse (or x-directed) field (IMTF), then to calculate the needed set of eigenfunctions alone one would need to solve a system of $2^N \times 2^N$ equations, N being the total number of sites in the lattice. It is easy to figure out that for N being of the order of 1000, the total calculation time even on the most

up-to-date computer would be comparable with the lifetime of the Universe.

To overcome the above mentioned difficulty the following approaches are used:

1. Trotter-Suzuki approach. In this approach the limit Trotter formula is utilized:

$$\exp(\hat{A}+\hat{B})=\lim_{m\to\infty}\left[\exp(\hat{A}/m)\,\exp(\hat{B}/m)\right]^m \qquad (19)$$

with A and B being the non-commuting parts of the Hamiltonian. This method reduces the D-dimensional quantum system with nearest-neighbour interactions to the (D+1)-dimensional classic Ising model with more complicated and, generally, temperature-dependent interactions. The derivations are analogous to those used in the path-integral technique for the quantum field theory. Once the transformation to a classical model is accomplished, one can apply the classical Metropolis technique (Ref. 11) to it. A detailed review of the advantages and applications of this method is given in Ref. 24.

However, we lose one of the advantages of the MC method, namely, the procedure requires additional approximations to be made. Indeed, in not being able to take the limit of $m\to\infty$ *exactly*, one has to limit oneself to large but finite values of m, the system size in the additional, (d+1)-th dimension, then extrapolating the results to $m\to\infty$. This means that even for a finite size system the results

obtained by the described technique are *approximate in principle* even for an infinite time of calculations, whilst a standard MC process gives exact results where applicable. Moreover, serious problems are reported (Ref. 25) to have occurred with the convergence of the extrapolation involved.

2. Handscomb approach. Here the operator exponent is expanded into the operator series

$$\exp(\hat{A}) = \sum_{r=1}^{\infty} \frac{(\hat{A})^r}{r!} . \qquad (20)$$

If $\hat{A}$ consists of a sum of non-commuting operators then the r-th power of $\hat{A}$ will be represented as a sum of all possible combinations of these operators to the different powers, the sum of all the powers being equal to r. Handscomb in Refs. 26, 27, making use of this expansion, suggested a method of MC simulation of thermodynamic and critical properties of S=1/2 quantum Heisenberg ferromagnet. This approach was then developed by Lyklema in Refs. 28, 29.

The purpose of this Chapter is to give a detailed account of the MC method by Handscomb (MCH) in application to the quantum spin lattice systems. In Section 2 we give an outline of the MCH method in its original formulation and discuss its application to a $S=\frac{1}{2}$ isotropic Heisenberg ferromagnet. Section 3 is devoted to a brief review of the numerical results obtained by means of the MCH technique for the quoted model. In Section 4 a generalization of the

method is suggested, and in Section 5 we discuss the modifications of the original technique to the $S=\frac{1}{2}$ isotropic Heisenberg ferromagnet with multispin interactions, Heisenberg antiferromagnets and Ising model in a transverse field.

2.2 HANDSCOMB MONTE-CARLO METHOD. THE GENERAL FORMULATION AND APPLICATION TO S=1/2 ISOTROPIC HEISENBERG FERROMAGNET.

In this section we discuss the MCH method in its original formulation. Let us start with the quantum system with the Hamiltonian:

$$H = H_0 + \sum_{i=1}^{N} H_i, \quad [H_0, H_i] = 0, \ \forall\, i \tag{21}$$

The canonic average $\langle \hat{A} \rangle_c$ of any physical variable operator $\hat{A}$ can be written for this case as follows:

$$\langle \hat{A} \rangle_c = \frac{\mathrm{Tr}\left[A e^{-\beta H} \right]}{\mathrm{Tr}\left[e^{-\beta H} \right]} = \frac{\sum_{r=0}^{\infty} \frac{(-\beta)^r}{r!} \sum_{C_r} \mathrm{Tr}\left\{ \hat{A} H_{i_1} \ldots H_{i_r} e^{-\beta H_0} \right\}}{\sum_{r=0}^{\infty} \frac{(-\beta)^r}{r!} \sum_{C_r} \mathrm{Tr}\left\{ H_{i_1} \ldots H_{i_r} e^{-\beta H_0} \right\}}, \tag{22}$$

where $\sum_{C_r}$ denotes the summation over all the ordered r-element sets of indices $C_r \equiv \{i_1, \ldots, i_r\}$, $1 \le i_k \le N_0$. Before proceeding further we should note the following two points. First, in (22) the

transposition of the infinite summation and the trace operation is undertaken. This transposition is possible without testing for uniform convergence because we work with finite size systems only. For such systems the operator H has finite dimension and, hence, the trace operation is equivalent to a finite summation. Second, the request for C_r to be ordered is a consequence of the fact that, in general,

$$\left[H_{i_1}, H_{i_k}\right] \neq 0, \quad i \neq k. \tag{23}$$

The sets C_r, introduced at this stage can be treated as the ordered Mayer diagrams, following Ref. 30, with their elements corresponding to different H_i terms in the Hamiltonian.

Having then defined the quantities

$$\pi(C_r) = \frac{(-\beta)^r}{r!} \mathrm{Tr}\left\{H_{i_1} \ldots H_{i_r} e^{-\beta H_0}\right\}, \tag{24}$$

$$Q_A(C_r) = \frac{1}{\pi(C_r)} \frac{(-\beta)^r}{r!} \mathrm{Tr}\left\{A\, H_{i_1} \ldots H_{i_r} e^{-\beta H_0}\right\}, \tag{25}$$

$$\chi_\pi(C_r) = \mathrm{sign}\, \pi(C_r), \tag{26}$$

$$P(C_r) = \frac{|\pi(C_r)|}{\sum_{r, C_r} |\pi(C_r)|}, \tag{27}$$

under the condition that

$$\forall\, C_r,\ \pi(C_r)\neq 0,\ \sum_{r,C_r} |\pi(C_r)| < +\infty, \tag{28}$$

we can rewrite (22) in the form:

$$\langle \hat{A} \rangle_c = \frac{\sum_{r,C_r} \Omega_A(C_r)\chi_\pi(C_r)P(C_r)}{\sum_{r,C_r} \chi_\pi(C_r)P(C_r)}\ ,\ \forall C_r,\ P(C_r)>0,\ \sum_{r,C_r} P(C_r) = 1. \tag{29}$$

Now the set of all C_r, $0 \le r \le +\infty$, may be treated as a discrete space with the probability distribution $P(C_r)$. Within this assumption expression (29) takes the form of a ratio of the mathematical expectations of two random variables:

$$\langle A \rangle_c = \frac{\langle\, \Omega_A(C_r)\chi_\pi(C_r)\,\rangle_P}{\langle\, \chi_\pi(C_r)\,\rangle_P}\ , \tag{30}$$

where $\langle\ \rangle_P$ means averaging with the distribution $P(C_r)$ and the sets C_r represent the random events.

Let us design the Markovian *stochastic procedure* (SP) of the random walk in the space of the C_r sets. This SP should generate by iterations the ergodic Markov chain with the required limit distribution (27) starting from an arbitrary initial state. Let us introduce two types of steps of SP:

1. Step "forward" with the increase of the C_r length, r:

$$C_r \longrightarrow C_r i = C_{r+1};$$

2. Step "backwards" with the decrease of the C_r length, r:

$$C_r = iC_{r-1} \longrightarrow C_{r-1}. \qquad (31)$$

As well, let us introduce the probability of choice of "forward" (Step 1) direction, f_r:

$$0 < f_r \leq 1, \qquad (32)$$

and the probability p(i) of a particular realization of a step "forward", i.e. of picking up a certain term, H_i, to include it into a C_r set,

$$p(i)>0,\ 1 \leq i \leq N_0\ ,\ \sum_{i=1}^{N_0} p(i) = 1\ . \qquad (33)$$

The stochastic procedure suggested by Handscomb is as follows:

1. We choose step "*forward*" with the probability f_r (step "*backwards*" is chosen, respectively, with the probability $(1-f_r)$, then **GO TO 2.**

2. **IF** the step "*forward*" is chosen, **THEN** we choose the index i added to C_r with the probability p(i) and with the probability $T^*(C_r, C_r i)$ we go to the **NEW** state $C_r i$, **OTHERWISE** (with the probability $(1-T^*(C_r, C_r i))$ the state does not change. **GO TO 3.**

ELSE we perform the transition $C_r \equiv iC_{r-1} \longrightarrow C_{r-1}$ with the probability $T^-(iC_{r-1}, C_{r-1})$ **OTHERWISE** (with the probability $(1-T^+(C_r, C_r i))$ we accomplish the cyclic transposition:

$$C_r \equiv iC_{r-1} \longrightarrow C_{r-1} i \equiv C'_r \tag{34}$$

3. After accomplishing the step we modify the estimators and the summators and **GO TO 1**.

The proof that this system of the transition probabilities generates the required limit distribution $P(C_r)$ can be found in Ref. 26. The functions T^+ and T^- are described by the following relationships:

$$T^+(C_r, C_r i) = \min\left[1, \frac{(1 - f_r)\,\pi(C_r i)}{f_r\, p(i)\, \pi(C_r)}\right],$$

$$T^-(iC_{r-1}, C_{r-1}) = \min\left[1, \frac{f_{r-1}\, p(i)\pi(C_{r-1})}{(1 - f_r)\pi(iC_{r-1})}\right], \tag{35}$$

and, in practice (Refs. 28, 29, 31, 32), it is enough to choose f_r and $p(i)$ as follows:

$$p(i) = 1/N_o, \ \forall i, \ f_r = (1 + \delta_{r0})/2 \ . \tag{36}$$

The application of the above technique to the S=1/2 isotropic Heisenberg model is based on the transformation of the Hamiltonian (Eq. (2)) to the form (21), where

$$H_0 = - g\mu_B H \sum_t S_z^t + N_0 J(0)/2, \qquad J(0) = \frac{1}{2} \sum_{t,\, t \neq t'} J_{tt'},$$

$$H_1 = - J_{tt'} E(t,t'), \tag{37}$$

and

$$E(t,t') = \frac{1}{2} \left\{ 1 + 4(S_t \cdot S_t) \right\} . \tag{38}$$

The operator $E(t,t')$ interchanges the spin variables in the lattice sites t and t'. The operator chains $H_{i_1} \ldots . H_{i_r}$ in this representation appear to be the permutation operators of the form:

$$P(C_r) = \prod_{j=1}^{r} E(t,t') \tag{39}$$

It also can be shown (Ref. 27) that for the discussed model,

$$\pi(C_r) = \frac{\beta^r}{r!} \left[\prod_{j=1}^{r} J_{t_j t'_j} \right] \left[\prod_{j=1}^{k(C_r)} 2\cosh(a_j \beta\mu H) \right], \tag{40}$$

where a_j is the length of the j-th cycle, $\{a_j\}$, of the permutation $P(C_r)$, and $k(C_r)$ is the total number of the cycles of $P(C_r)$. The expressions for the estimators of different thermodynamic values are:

1. Magnetization (Ref. 27)

$$M_z = \left\langle (2\mu/N) \sum_t S_z^t \right\rangle_k = \frac{\mu}{N} \left\langle \sum_{j=1}^{k(C_r)} a_j \tanh (a_j \beta\mu H) \right\rangle_P; \tag{41}$$

We note here that the magnetization in this approach identically vanishes with zero applied magnetic field. This is due to the fact

that the symmetry of the system with respect to a reversal of the applied field is taken into account at the stage of calculating the trace of the individual diagrams. This provides for the inability to identify within this approach the spontaneous breaking of symmetry that is producing non-zero magnetization.

2. Internal energy (Ref. 27)

$$E = \langle H \rangle_k = -NHM_z - \frac{\langle r \rangle_P}{\beta} + \frac{N_0 J(0)}{2}; \qquad (42)$$

3. Uniform longitudinal susceptibility in the zero field (Ref. 27):

$$\frac{k_B T \chi_0}{\mu^2} = \frac{1}{N} \left\langle \sum_{j=1}^{k(C_r)} a_j^2 \right\rangle_P ; \qquad (43)$$

4. Static spin-spin correlator

$$\langle S_i^z S_j^z \rangle_k = \frac{1}{4} \langle G_{ij} \rangle_P, \text{ where}$$

$$G_{ij} = \begin{cases} 1, \text{if the both spins belong to the same cycle, } \{a_1\} \\ 0, \text{if the both spins belong to different cycles.} \end{cases} \qquad (44)$$

The major problem in applying this relatively simple scheme to real systems is the problem of signs. Equation (29) is a ratio of two infinite sums and is well defined if all the terms in the denominator have the same sign. Otherwise, if attempting to do a MC summation of a series with an approximately equal number of negative

and positive terms, one ends up with a considerable uncertainty, that increases dramatically if the series in question is in the denominator. In practice (Refs. 28, 29) the Handscomb method appears to be applicable only to the systems for which the overwhelming majority of the quantities χ_{α} have the same sign. Going then to Eq. (40) we may conclude that this implies that all the elements $J_{t_j t'_j}$ of the exchange interaction matrix should be positive. This restricts the applicability of the method in its original form to ferromagnetic systems (see as well Section 2.5).

Another difficulty in using this method straightforwardly for systems different from the isotropic $S=\frac{1}{2}$ is that, in general, the majority of the terms in (22) for any arbitrary model will be equal to zero, thus leaving us with a very unrepresentative system of probabilities. In this case, most of the computer time would be spent on accounting for the configurations that contribute to the averages with zero weight.

The mentioned problems are commonplace in theoretical and computer particle physics, when one deals with any kind of diagrammatic or path integral technique in application to fermionic systems. The way to deal with both above shortcomings is to seek an appropriate representation of the Hamiltonian. Indeed, one always has the liberty to add an arbitrary constant to the Hamiltonian. By doing so, sometimes it becomes possible to reformulate an original

Hamiltonian in such a way that the problem of signs is eliminated. As well, modifying the Markov chain rules and the transition probabilities, one can achieve a procedure of random walk only over the subspace of the states with nonzero weights. However, there is no way to sketch any kind of universal scheme for this for an arbitrary Hamiltonian. We shall postpone the discussion of these situations until Section 2.5.

2.3 A REVIEW OF SOME RESULTS OBTAINED BY MEANS OF MCH

In this section we review some of the results obtained by the MCH method for different kinds of $S=\frac{1}{2}$ isotropic Heisenberg ferromagnets in comparison with some other analytical and numerical approaches. We discuss the results for the one-dimensional Heisenberg chain, a three-dimensional nearest neighbour simple cubic lattice system with defects, and the three-dimensional model with next-nearest-neighbour interaction. Though there are various results for the two-dimensional Heisenberg ferromagnet, we shall postpone the discussion of them until Chapter 3.

2.3.1. One-dimensional model

The thermodynamic properties of the one-dimensional quantum Heisenberg ferromagnet were investigated by the technique in question in Refs 28, 29, 33 and 34. The application of the quantum MC methods led to conflicting results for the critical index γ for a

susceptibility: γ=1.32 - the Trotter-Suzuki approach (Ref. 25); γ=1.75 - MCH (Ref. 29); γ=2 - MCH (Ref. 34). These differences are likely to have been caused by insufficient system size, N≤200, and insufficiently low temperatures in most calculations.

2.3.2 A three-dimensional Heisenberg model with defects. The percolation threshold.

A problem of a regular ferromagnetic structure with vacancy-type defects attracted attention because of the dependence of the critical properties on the concentration of the defects, as well as the geometry and dimensionality of the model. The problem of the phase transitions in this model is closely connected to another problem of statistical physics, namely, the percolation problem. If the concentration of the defects is sufficiently high, the spins, connected by a ferromagnetic interaction, are able to form only finite-size clusters. Hence, it is impossible for a system to form a magnetically ordered state. A minimal concentration of the magnetic sites, at which the formation of an infinite cluster becomes possible, is called the percolation threshold, p_c. A detailed insight into the percolation problem in connection with the MC methods can be found in Chapter 8 of Ref. 12. Some recent results are reported in Refs. 35 - 36.

In Ref. 37 a three-dimensional Heisenberg model on a simple cubic lattice with vacancy-type defects has been studied by means

of the MCH method. The Hamiltonian of the model reads:

$$H = -2\sum_{i,j} J\xi_i\xi_j \, \mathbf{S}_i \cdot \mathbf{S}_j \,, \qquad (45)$$

where $\xi_i=1$, if the site i is occupied by a magnetic ion and $\xi_i=0$ otherwise. The size of the systems under investigation was 8×8×8 with the periodic boundary conditions applied. It was found that, with the increase of the concentration of the defects, the phase transition temperature T_c^* shifted towards lower temperatures, and the maximum value of the specific heat (as a function of temperature) decreased. As well, a linear extrapolation to the value $T_c^*=0$ gives the percolation threshold as 30%, which coincides very well with the estimates of the percolation threshold for a simple cubic lattice obtained by other methods.

2.3.3. The Heisenberg model with next-nearest-neighbour interactions on a simple cubic lattice.

As a generalization of the Handscomb method for the Heisenberg system with first and second neighbour exchange interactions, a modelling of the three-dimensional ferromagnet with the Hamiltonian:

$$H = -2J_1 \sum_{nn} \mathbf{S}_i \cdot \mathbf{S}_j - 2J_2 \sum_{nnn} \mathbf{S}_i \cdot \mathbf{S}_j \qquad (46)$$

has been accomplished in Ref. 37. The first sum in (46) is over the nearest neighbours, whilst the second is over the next-nearest neighbours. The values of the interaction constants were taken as

J_1/k_B=0.28 K and J_2/k_B=0.056 K, respectively, corresponding to the material $CuK_2Cl_4 \cdot 2H_2O$. In this case the utilization of the MCH method gave the authors an opportunity to move further into the fluctuation region than any analytical approach would allow and to determine some critical characteristics of the phase transition.

2.3.4. Conclusions

The presented examples of the utilization of the MCH procedure clearly show that the method is capable of producing new insights into the critical phenomena for the quantum Heisenberg model. Its convergence rate, though usually less than of the analogous standard MC scheme, appeared to be sufficient for most of the applications. Among other advantages of the MCH procedure it is worth mentioning that the utilized representation of the partition function itself provides for additional information about the magnetic ordering in the system. For example, the cycles of the permutations occurring in (22) - (25) are likely to be associated with the clusters, as the trace of a $P(C_r)$ operator is contributed to only by the spin configurations having all the spins in them aligned in the same direction. As well, because the formation of the equilibrium permutations in the MC process is ruled by the structure of the interactions in the system, the cycles tend to form connected areas of the lattice, similar to the true magnetic domains.

2.4 THE GENERALIZATION OF THE HANDSCOMB PROCEDURE

It has been already mentioned in Section 2.2 that due to the sign problem and the null weight problem one cannot apply straightforwardly the Handscomb method to systems different from the isotropic Heisenberg model, for which it was originally devised.

The original MCH does not account for the situations when the Hamiltonian contains interaction terms of different origin. For example, if we treat the Heisenberg model with additional four-spin interactions, some of the terms H_i in the Hamiltonian (21) would be the usual Heisenberg terms while others would correspond to the four-spin interactions. Hence, an appropriate procedure of the Handscomb type would incorporate two different types, or "channels", of step "forward". In turn, the definition of the C_r sets has to be appropriately modified, as now we have two sets of indices forming it, i.e. the bi-index from the Heisenberg part and the quarto-index from the four-spin interaction part. In general, one has to construct a sort of multichannel procedure to account for different types of interaction. Moreover, this multichannel procedure might happen to be more effective even in the case of a relatively simple Hamiltonian. For example, the insertion into C_r, when stepping forward, of not a single index but an appropriate combination of them, e.g. a four-spin or a two-spin loop, may lead to a better convergence of the process if the channels incorporate well the intrinsic geometry and

dimensionality of the interaction in the system.

In this section we propose a general scheme for a modified multichannel stochastic procedure of the MCH, that can help one to obtain the transition probabilities once the Hamiltonian is appropriately rewritten and the procedure is sketched. It can be shown that most of the existing modifications of MCH are particular cases of the presented formalism.

Suppose we have a series of the form:

$$\sum_G \pi(G)A(G) = \left\{ \sum_G \pi(G) \right\} \left\{ \sum_G A(G) \frac{\pi(G)}{\sum_G \pi(G)} \right\}, \tag{47}$$

$$\pi(G)>0 \ (a), \qquad \sum_G \pi(G)<+\infty \ (b), \tag{48}$$

where G is the summation variable of any origin, e.g. number, vector, operator, multi index, etc., $G \in \mathbf{G}$. To construct a Markov chain with the limit distribution

$$P(G) = \frac{\pi(G)}{\sum_G \pi(G)}, \qquad \sum_G P(G) = 1, \tag{49}$$

it is necessary to derive the equations for the set of one step transformations together with the transition probabilities, leading to the given limit distribution. If (48) is satisfied, then, according to the results of Ref. 38, for the desired transition probabilities it is enough to satisfy the following relation:

$$\sum_{G' \in G^1(G)} \pi(G')pr(G' \longrightarrow G) = \pi(G), \qquad (50)$$

where $pr(G' \longrightarrow G)$ is the probability of a transitio.. from the state G' to the state G, and $G^1(G)$ is the set of values of parameter G' from which it is possible to reach G by one step of the Markovian process. Here we call $G^1(G)$ the *one-step vicinity of G*. If the Markov chain is reversible, that means

$$\forall\, G' \in G^1(G) \Rightarrow G \in G^1(G'),$$

then, together with (50) the condition of the detailed balance is fulfilled:

$$\pi(G')pr(G' \longrightarrow G) = \pi(G)pr(G' \longrightarrow G). \qquad (51)$$

Let us introduce the set Γ^1 of transformations over G that transform G' into G by one step of the stochastic procedure:

$$\Gamma^1 \ni \Gamma_x : G' \longrightarrow G,\ G' \in G^1(G), \qquad (52)$$

where index x numerates the transformations in Γ^1. In simple terms, Eq. (52) states that we denote the operators of the transitions $G' \longrightarrow G$ by Γ_x. Later we construct the Markovian process as a sequence of transformations Γ_x.

The structure of the Markovian process has to provide for the completeness of the coverage of the sample space. This means that the set of one-step transformations has to be designed in such a way that it is possible to reach any state, G'', from any state, G', by a

finite number of steps. A rigorous algebraic definition will then read:

$$\forall G,\ G'' \in G, \exists\ \ \Gamma(G',G'')=\prod_{i=1}^{m}\Gamma_{x_i},\ \Gamma_{x_i}\in\Gamma^1, \forall i,\ \ G''=\Gamma(G',G'')\cdot G'',\ m<+\infty \tag{53}$$

Let us define as well the set of Γ^{π} transformations that conserve $\pi(G)$, i.e. transform the state G into some G' with the same weight $\pi(G)$:

$$\Gamma^{\pi} \ni \Gamma^{\pi}_{Y} \ :\ \ G\longrightarrow G,\quad \pi(G)=\pi(\Gamma^{\pi}_{Y}\cdot G')=\pi\left[(\Gamma^{\pi}_{Y})^{-1}\right]\cdot G'), \tag{54}$$

where Y numerates the set Γ^{π}.

Having made the basic definitions, we now can start designing the necessary structure of the Markovian process. Let the set Γ^1 be organized as follows:

$$\Gamma^1=\Gamma^1_F\cup\Gamma^1_R\ ;\ \forall\Gamma_x\in\Gamma^1_F\ \exists!\Gamma'_x\in\Gamma^1_R,\ \exists!\Gamma^{\pi}_x\in\Gamma^{\pi},\ \Gamma'_x=(\Gamma_x)^{-1}\cdot\Gamma^{\pi}_x \tag{55}$$

Namely, we assume that our transformation set Γ^1 consists of two subsets, Γ^1_F and Γ^1_R, of the transformations, such that a subsequent application of a transformation from Γ^1_F and a corresponding transformation from Γ^1_R to G produces the state G" with the same weight as G. The meaning of the introduced structure of $\Gamma^1(G)$ may be clarified as follows. Suppose the set Γ^{π} contains only a unit element, i.e. the transformation G ——>G. Then, for each

transformation Γ from Γ_F^1, Γ_R^1 contains Γ^{-1} .and vice versa. It means in turn that our Markovian process consists of reversible steps, and the detailed balance equation (51) holds. This is characteristic for most of the classical MC procedures, where in principle one can come back to the initial state by just two subsequent steps, direct and inverse. For example, for a Metropolis procedure for the Ising model the set of transformations contains the flips of the individual spins, which are self-inverse.

We are interested, however, in a more general type of irreversible procedure, when one cannot generally reach the initial state by just two subsequent steps. Thus we only require by (55) that we should be able to reach in two steps, direct and "pseudoinverse", a state which has the same weight as the initial.

Let us introduce the function $q(G,\Gamma)$:

$$q(G,\Gamma): G\times\Gamma^1 \longrightarrow [0,1], \quad \sum_{\Gamma_x\in\Gamma^1} q(G,\Gamma) = 1, \quad \forall G \in G \qquad (56)$$

which we later use as a probability distribution of the realizations of certain steps in the Markovian process.

Having established the structure of the set of necessary transformations, let us now use the following procedure for the construction of Markov chain:

1. With the probability $q(G,\Gamma_x)$ we choose the transformation

$\Gamma_x \in \Gamma^1$ of the initial state G as a step of Markov chain.

2. Then we construct the function $T(G,\Gamma_x)$.

3. We perform the transformation $G \longrightarrow \Gamma_x \cdot G$ with the probability $T(G,\Gamma_x)$ and go to the next step (item 1).

4. Else (i.e. with the probability $(1-T(G,\Gamma_x))$):

a) If $\Gamma_x \in \Gamma^1_F$ then we conserve the initial state and go to item 1.

b) If $\Gamma_x \in \Gamma^1_R$ then we assume the new state as $G'=\Gamma^{\pi}_x G$, Γ^{π}_x being defined by (56) and go to item 1.

We should note here that the completeness (53) of the set Γ^1 provides for the ergodicity of the so constructed Markov chain. It can be shown (Ref. 34) that the given stochastic procedure has the limit distribution (49) provided we assume:

$$B(G,\Gamma_x) = \frac{q\left([(\Gamma^{\pi}_x)^{-1}\Gamma_x]\cdot G,\ \Gamma_x^{-1}\Gamma^{\pi}_x\right)\pi(\Gamma_x \cdot G)}{q(G,\Gamma_x)\ \pi(G)},\quad \text{if } \Gamma_x \in \Gamma^1_F\ ;$$

$$B(G,\Gamma_x) = \frac{q\left(\Gamma_x \cdot G,\ \Gamma^{\pi}_x\Gamma_x^{-1}\right)\pi(\Gamma_x \cdot G)}{q(G,\Gamma_x)\ \pi(G)},\quad \text{if } \Gamma_x \in \Gamma^1_R;$$

$$T(G,\Gamma) = \min(1,\ B(G,\Gamma)). \qquad (57)$$

The proof that (57) provides for the correct limit distribution is somewhat analogous to the one suggested in Ref. 25 for a particular set of the transition probabilities used by Handscomb and is not presented here.

The irreversible procedures with non-trivial Γ^{π} appear to be very useful in situations where the sample space elements are chain-like and at each step we introduce changes in the edges of the chain. If no special measures are accomplished, it takes a long time for the inner parts of the chain to be transformed within the MC process.

The perfect example of the above is the original Handscomb procedure, for which we can identify G objects as C_r index sets, Γ^{π}_F and Γ^{π}_R as, respectively, operations of addition of an index to the right edge of C_r and elimination of an index at the left edge. The set Γ^{π} is represented by a cyclic transposition. Then the probability set $q(G, \Gamma^{\pi}_F)$ corresponds to the Handscomb probability of drawing out an index for inclusion after the right edge of C_r, multiplied by the probability of the choice of the step forward, f_r. $q(G,\Gamma^{\pi}_R)$ is just the probability of step backwards, $(1-f_r)$. With this correspondence it is easy to show that the probability normalization condition (56) holds because of (33) and the Eqs. (57) become equivalent to (35).

Using the approach developed here we are able to set up a Handscomb-like procedure for an arbitrary model. As soon as the set of necessary transformations is established in the form (55), the procedure takes the form quoted above with the choice factors calculated by means of Eq. (57).

2.5 APPLICATIONS OF THE HANDSCOMB METHOD TO SOME OTHER MODELS

In this section we will discuss how to modify the original Handscomb method for different spin Hamiltonians in view of the results of the previous section.

2.5.1 Heisenberg model with four-spin interactions

A generalization of the MCH technique to the $S=\frac{1}{2}$ Heisenberg ferromagnet with multispin exchange on a simple cubic lattice has been accomplished in Ref. 32. The Hamiltonian of the system under consideration was taken as follows:

$$H = -2J \sum_{ij} \mathbf{S}_i \cdot \mathbf{S}_j - 2 \sum_{klmn}' K_{klmn} (\mathbf{S}_k \cdot \mathbf{S}_l)(\mathbf{S}_m \cdot \mathbf{S}_n), \qquad (58)$$

where $K_{klmn} \equiv K > 0$ in the case when the nearest neighbours (kl) and (mn) belong to an elementary plaquette on the lattice; each plaquette is considered twice in the summation. Having used the operator identity (38), the Hamiltonian (58) can be transformed to:

$$H = -(J-K) \sum_{i=1}^{N_b} E(t_i, t_i') - \frac{K}{2} \sum_{i=N_b+1}^{2N_b} E(t_i, t_i') E(t_i'', t_i'''), \qquad (59)$$

where $N_0 = 2N_b$ and t_i, t_i', t_i'', t_i''' with $N_b + 1 \leq i \leq 2N_b$ belong to the vertices of an elementary plaquette.

The way to generalize MCH for the described system is analogous to that decribed in Section 2.4. In the MC procedure we introduce additional steps of a new type - simultaneous addition to or elimination from C_r of a tethrade, i.e. pair of transposition

operators, corresponding to the four-spin interaction. Utilizing the above multichannel MC scheme (see Section 2.4) one can write the expressions for the transition probabilities. The results of the investigation of the critical properties of the three-dimensional quantum ferromagnet with the Hamiltonian (58), modelled by means of modified MCH, are presented in Ref. 32. The calculations made it possible to draw a phase diagram of the model. The comparison of the MCH results and the results of other approaches shows that the latter may lead to significant errors in critical temperature estimation.

2.5.2. Modelling of a Heisenberg antiferromagnet and XY model.

As shown earlier (see Section 2.2), the applicability of MCH to the quantum system depends on the possibility of defining a system of weights for the elements of the sample space, $P(C_r)$. The weights have to meet the conditions of normalization and non-negativity. In the case of a ferromagnet (Refs. 27, 28) the partition function Z of the system and the thermal averages of the physical variables $\hat{A}$ may be easily defined via the MC average of non-negative estimators, Ω_A, all the factors $\chi_\pi(C_r)$ in (26), (29, (30) being equal to +1.

In the case of an antiferromagnet, however, $\chi_\pi(C_r)=1$ for the C_r with even r and $\chi_\pi(C_r)=-1$ for the odd r. This leads not only to a significant change in the estimator for any physical variable, which has now alternating signs, but as well the average is defined as a ratio of two sign-alternating series (30).

In Refs. 28, 29 an attempt has been made to utilize this idea for the case of one-dimensional quantum $S=\frac{1}{2}$ antiferromagnet. It was found that the practical applicability of the quoted approach was limited to sufficiently high temperatures.

As discussed in Ref. 39, given the partition function representation in the form (see (29)):

$$Z = \sum_{r,C_r} \chi_{\pi}(C_r)P(C_r) \qquad (60)$$

one can easily see how the sign problem actually occurs. In the process of a random walk along the sample space of C_r, every next MC step changes, as a rule, the length of C_r by 1, and hence the positively defined value Z is represented as a small difference of large quantities, each of which grows significantly as the temperature is lowered. In these circumstances the statistical errors, inherent in MC methods, do not allow one to achieve a reasonable uncertainty. The situation gets worse when the values of partition function (60) are substituted into the denominator of (30) for the canonic averages.

In Ref. 33 there was reported an interesting application of MCH to the case of a one-dimensional quantum XY model (that is, a model, described by Eq. (3) with $\Delta=0$). The Hamiltonian was rewritten in the form:

$$H = -J \sum_{k=1}^{2N_b} h_k, \qquad h_k = S^{+}_{t_k} S^{-}_{t'_k} \qquad (61)$$

The bond from site t_k to site t'_k in this case has a direction ("past" to "future", as in the path integral technique) and the C_r set corresponds to an ordered *directed* diagram (Ref. 30). To organize a random walk only within the subspace of C_r with nonzero weight one has to devise a stochastic procedure as an insertion (extraction) of an even number of operators h_k.

In Refs. 39, 41, 42 a modification of MCH applicable to the Heisenberg antiferromagnet has been developed. The Hamiltonian is represented as follows:

$$-\beta H = \frac{\beta J}{2} \sum_{ij} (h_{ij}^2 - h_{ij}) + \text{const}, \qquad (62)$$

The expansion of the exponentials in (22) is accomplished in the same fashion as before and the states C_r with the nonzero weights have the subscripts of the h_{ij} operators forming the closed loops on the lattice. For a square lattice, for example, it becomes the requirement of an even number of the h_{ij} operators in C_r. This automatically eliminates the sign alternation problem in the partition function and thermal averages (see Eq. (29)). However, a new set of difficulties occurs in how to form these closed loops from the restrictions on the possible orientations of the spins within one loop, similar to those occurring in the cycles of permutation $P(C_r)$ (see Section 2.2). In Refs. 41, 42, the thermal dependences of the critical properties of the planar Heisenberg ferromagnet were

investigated by means of MCH.

2.5.3. MCH method for S=1/2 Ising model in transverse field

The transverse Ising model (IMTF) is described by the following Hamiltonian:

$$H = H_{IS} + H_{\omega} + H_{\Omega} + \text{const}; \quad H_{\Omega} = -\Omega \sum_{i=1}^{N} S_i^x ;$$

$$H_{IS} = -(1/2) \sum_{(i,j)}^{N} J_{ij} S_i^z S_j^z ; \qquad H_{\omega} = -\omega \sum_{i=1}^{N} S_i^z ; \qquad (63)$$

where N is the total number of spins in the lattice, ω and Ω are the reduced longitudinal and transverse magnetic fields, respectively and J_{ij} is the exchange parameter. The model is applicable to certain physical phenomena, such as phase transitions in KDP-type ferroelectrics and rare-earth magnets (Refs. 43, 44) and is of theoretical interest itself, because it is one of the simplest quantum spin lattice models.

One of the possibilities to extend the MCH procedure to the case of the IMTF is to use the following representation of the Hamiltonian (63):

$$H_{\omega} = -\omega \sum_{i=1}^{N} \left[2A_i^-(\alpha) + A_i^+(\alpha) \right] ; \qquad H_{\Omega} = -\Omega \sum_{i=1}^{N} \left[S_i^+ + S_i^- \right] ;$$

$$H_{IS} = -(1/4) \sum_{\substack{i \neq j, \\ J_{ij} > 0}}^{N} J_{ij} \left[A_i(\alpha)\, A_j(\alpha) + A_i(\alpha)\, A_j(\alpha) \right] -$$

$$(1/4)\sum_{\substack{i\neq j,\\ J_{ij}<0}}^{N}|J_{ij}|\left[A_i(\alpha)\,A_j(\alpha)+A_i(\alpha)\,A_j(\alpha)\right]\Big\}\ ;$$

$$A_i^{\pm}(\alpha)=(1\pm\alpha)S_i^+S_i^- + (1\mp\alpha)S_i^-S_i^+\ ; \qquad (64)$$

Now the C_r sets consist of the elements of the following types:

$$A_i^-(\alpha),\ A_i^+(\alpha),\ A_i^+(\alpha)A_j^-(\alpha),\ A_i^+(\alpha)A_j^+(\alpha),\ A_i^-(\alpha)A_j^-(\alpha),$$

$$A_i^-(\alpha)A_j^+(\alpha),\ S_i^+ \text{ and } S_i^-\ . \qquad (65)$$

The algorithm for random sampling of the operator sets consisting of the elements (65) is presented in Ref. 45. The results show a very good correspondence with the known analytical and numerical results for different types of the exchange interaction.

The above methods appeared to be practical for one-dimensional systems. We must note, however, that all the procedures are universally appropriate for any dimensionality and any kind of interaction. However, this must be carefully tested in each case, because theoretical applicability gives no warranty of a good convergence in the numerical experiment.

2.5.4. Some recent modifications of the Handscomb method

Here we shall discuss two recent modifications to the original Handscomb procedure. As these modifications allow one to extract additional information using basically the same scheme, our

discussion will be much less detailed than in the previous sections.

First, the Handscomb expansions (22) and the procedure of a random walk itself allows one to obtain information about the high temperature expansion coefficients of the investigated model. In Ref. 46 the authors suggested an approach, in which they at first, using expressions of the type of (40), devise a MC scheme to calculate several coefficients of the high temperature expansion. Utilizing the fact that the dependence of the coefficients in their representation is monotonic with respect to the power of the inverse temperature, the authors of Ref. 46 apply an interpolation procedure. Their results show that the method is capable of calculating up to the order of 100,000 coefficients for the specific heat, entropy, internal energy and the magnetic susceptibility. The comparison of their data with the results of the exact high temperature expansions and other analytical approaches confirms the suitability of their method.

A generalization of the Handscomb method for the general spin-S Heisenberg model has been achieved in Ref. 47. The main idea is as follows. As it is often difficult to evaluate directly the traces of the operator chains appearing in the expansion (22), one may expand traces as the sums over all the sets of configurations of the corresponding diagonal matrix elements. These matrix elements are usually much more simple to evaluate. Then, if one treats as an

element of the configuration space a direct product of the space of the spin configurations and the space of C_r sets, then the weights of the elements of the configuration space are the diagonal elements corresponding to certain C_r sets. Using a representation of a C_r set similar to the path integral trajectory, the author achieves something close to the Trotter-Suzuki method (see Section 2.1) and MCH. The actual simulations have been done for S=1 and $S=\frac{3}{2}$ and the values of the critical exponent γ are presented.

Finally, the authors of Ref. 48 devised a method of evaluating the free energy of a Heisenberg ferromagnet using the MCH method. The problem of the estimation of the free energy lies in the fact that the statistical weights are normalized by the partition function itself. That is why the partition function, and hence the free energy as its logarithm, is hard to calculate within the framework of the MC method at one temperature. The general idea suggested in Ref. 48 is to include sweeping over a range of temperatures into the Handscomb procedure and thus calculate the free energy, using some artificial set of probabilities to accomplish the jumps from one temperature to another. The results presented in Ref. 48 include the free energy for the 2D Heisenberg ferromagnet in comparison with the results of the spin-wave approach by Takahashi (Ref. 49).

CHAPTER 3.

MONTE-CARLO SIMULATION OF THE CRITICAL PROPERTIES OF QUASI-TWO-DIMENSIONAL QUANTUM HEISENBERG SYSTEMS

3.1. INTRODUCTION

Recently there has been experimental work (e.g., see Refs. 50, 51, 52, 53, 54, 55) to investigate the magnetic properties of quasi-two-dimensional (quasi-2D) ferromagnetic systems. For example, $[C_6H_5(CH_2)_nNH_3]_2CuBr_4$ has been interpreted as a quasi-2D Heisenberg nearly-isotropic ferromagnet (Ref. 55) with the ratio of the intralayer exchange to the interlayer interaction parameter being as low as 0.04. The temperature of the second-order phase transition was found from the susceptibility data to be around 10 K in this material, depending on the structural index n. Also the magnetization and longitudinal susceptibility of 2.5 monoatomic layers of ^3He adsorbed on graphite are reported to be well described by high-temperature expansions and other theories for 2D Heisenberg ferromagnets (Refs. 50, 51, 52, 53, 54).

There are several papers where different analytical and numerical methods are applied to study the 2D Heisenberg model with spin $S = \frac{1}{2}$. We shall discuss these methods in detail later in this chapter. At this stage we shall sketch the main problems arising

when one attempts to deal with such systems. First, according to the Mermin-Wagner theorem (Ref. 56), there is no phase transition at finite temperatures in 2D. This fact complicates greatly the analytical approaches based on Green-function techniques. Indeed, in most Green-function formulations, one introduces a certain decoupling scheme (or other approximation), and that means usually some nonzero order parameter being involved. This becomes too rough an approximation in 2D, where the dynamics of ferromagnetic ordering are far from being understood. Some interesting results have been obtained (see Refs. 49, 57) by using the condition of zero magnetization at T = 0 as a constraint for the variational entropy principle for the 2D model in a boson representation. However, the expressions were found to need corrections from second-order perturbation theory. When the critical temperature is equal to zero, the MC results become very sensitive to finite-size effects, and this becomes increasingly significant as the temperature is reduced. Thus, when attempting to do a MC calculation, one has to accomplish a finite-scaling analysis and to determine for what range of temperatures the results are valid.

The situation becomes even more involved if we try to investigate quasi-2D systems, for example, thin films consisting of 2 and 3 monolayers. For such systems the Mermin-Wagner theorem is no longer applicable and the main question is whether the critical

temperature is zero, as in the purely 2D case, or not. Obviously, any kind of the mean-field theory or random-phase approximation are unreliable and likely to produce a spurious phase transition at $T \neq 0$. Also these thin films should be good models for the experiments (Ref. 50), and so it is interesting to obtain their properties by an independent numerical or analytic approach.

We should note here as well that the use of quantum statistics is required, especially in the case of $S = \frac{1}{2}$. This can be understood from the fact that the classical limit of the Heisenberg ferromagnet, the Ising ferromagnet, has a well-defined phase transition in 2D.

In this chapter we investigate the critical properties of ultrathin monocrystalline thin films described by the $S = \frac{1}{2}$ isotropic Heisenberg ferromagnetic Hamiltonian on a simple cubic lattice and with the number of monolayers $L \leq 3$ by means of the MCH technique described in Chapter 2. The outline of this Chapter is as follows. In Sec. 3.2 we review the existing results for 2D Heisenberg ferromagnets and present our calculations of the critical behavior of the longitudinal susceptibility and the correlation range. Section 3.3 is devoted to the critical behavior of thin Heisenberg films with two and three layers. We present the results of our MC calculations together with a simple theoretical interpretation of their meaning. In Sec. 3.4 we discuss the critical behavior of a film consisting of two monoatomic layers, one of which is diluted, that has some

correspondence to the experiment of Ref. 50. In Sec. 3.5 we study the influence of varying the interlayer interaction on the longitudinal susceptibility of a two-layer film. In the concluding Section 3.6 we summarize the obtained results.

3.2. CRITICAL PROPERTIES OF QUANTUM 2D FERROMAGNETS

The critical properties of quasi-2D spin systems have recently been studied by a number of analytical and numerical methods. Under discussion were the type of the phase transition, as well as the critical behavior of the uniform longitudinal susceptibility and the correlation range in 2D. Now it is considered as established that the $S = \frac{1}{2}$ Heisenberg ferromagnet with nearest-neighbor interaction displays no phase transition in 2D at finite temperatures, in accordance with the Mermin-Wagner theorem (Ref. 56). However, some high-temperature expansion results admit the possibility of a Kosterlits-Thouless-type phase transition (Ref. 58, 59).

In Ref. 33 susceptibility data for the 2D quantum Heisenberg model were reported for system sizes $N = L^2$, with L = 8, 16, and 24, in the temperature interval $0.4 \leq T/J \leq 1.3$. Here J is the nearest-neighbor exchange and we use units such that $k_B = 1$ and the Bohr magneton $\mu_B = 1$. Although an extrapolation to infinite size was not done for $T/J < 1.0$, where the results display a size-dependence, the authors concluded that the L-dependence of χT is similar to that

for the 1D system and is drastically different from the 3D model.

In Ref. 41 the authors made a detailed investigation of the temperature dependences of the correlation function and correlation range within the temperature interval $0.4 \leq T/J \leq 10$. We note that their Hamiltonian differs from the one used here and in Refs. 28, 29, and 33 by a factor of two. Hence the quoted temperature interval corresponds to $0.8 \leq T/J \leq 20$ in our notation. Under consideration were the systems with the linear sizes L = 10, 20, and 30 with free as well as periodic boundary conditions. The temperature behavior of the correlation range ξ was compared to the results of the high-temperature expansions (Ref. 61) and low-temperature spin-wave theories (Ref 49, 57).

The low-temperature behavior of correlation range and the susceptibility was studied in Ref. 62 both by the MCH method and the momentum shell renormalization group approach. A good coincidence of the results of MC simulation and the low-temperature approximation for the longitudinal susceptibility χT and the correlation range ξ in the form

$$\chi T = C_{\chi} \left[\frac{C_{\xi}}{2\pi} \right]^2 2^7 \left[\frac{T}{2J} \right]^3 \exp\left\{ \frac{2\eta_{\chi}\pi J}{T} \right\} , \tag{66}$$

$$\xi \sim (T/J)^{1/2} \exp\left\{ \frac{\eta_{\chi}\pi J}{T} \right\} , \tag{67}$$

with $\eta_{\chi} = 1$ for $S = \frac{1}{2}$, was reported. It is worth mentioning, however, that the lowest temperature for which this coincidence has

been checked is $T/J = 0.77$.

In Ref. 63 the MCH method was applied to obtain the temperature dependences of the internal energy E/NJ, susceptibility χT, and static correlation functions $\langle S_i S_j \rangle$ of the 2D Heisenberg ferromagnet in the temperature interval $0.3 \leq T/J \leq 20$, with the system size L varying from 16 to 80. Periodic boundary conditions were assumed. It was found that the energy, unlike the susceptibility, did not show a monotonic dependence on the system size and was described adequately by the low-temperature expansion within the temperature range $T/J \leq 0.9$. For $T/J > 0.8$ a good correspondence of the calculated susceptibility values with the quantum high-temperature expansion results occurred. For $T/J \leq 0.7$ the size dependence started to be significant.

Within the temperature interval $0.8 \leq T/J \leq 3.2$ the susceptibility temperature dependence was found to be well described by the low-temperature limit of a modified spin-wave theory by Takahashi (Refs. 49, 57):

$$\chi T = aT \exp\{2\pi bJ/T\}, \qquad (68)$$

with $a = 0.211$ and $b = 0.615$. However, starting from the temperature $T/J = 0.7$, deviations were reported to occur and when $0.3 \leq T/J \leq 0.5$ the susceptibility χT was described as a linear function of the inverse temperature:

$$\chi T = -C + bJ/T \qquad (69)$$

This dependence was treated as an evidence that the critical index of the susceptibility is 2 for the 2D system.

In summary, there are many inconsistencies in the results by different authors about the type of the zero-temperature phase transition as well as the critical indices themselves. To clarify the situation we make further calculations (see also Refs. 64, 65) of the critical behavior of the 2D S = $\frac{1}{2}$ isotropic Heisenberg ferromagnet.

To find the correlation range ξ we first calculate the static correlation function, Eq. (64). In doing this, we take into account only the pairs of spins that belong to the same monolayer and the radius vector r_{ij}, ($r_{ij} = |r_i - r_j|$), being parallel to one of the boundaries of the plane. Within this assumption the spins are separated by a distance equal to an integer multiple of the lattice constant. Our procedure to evaluate G_{ij} is as follows:

1. At each step of the Markov chain we make a random choice of the lattice site i;

2. We choose randomly the distance r_{ij} so that it does not exceed L/2;

3. We define the second lattice site j as having one of the two in-plane coordinates equal to that of i and the second in-plane coordinate shifted by r_{ij}, taking account of in-plane periodic

boundary conditions;

4. We use Eq. (44) for G_{ij}, and we calculate its average $\langle G_{ij} \rangle$ along the Markov chain. Finally, we calculate the correlation range as:

$$\xi = \left[\left(\sum_i r_{ij}^2 \langle G_{ij} \rangle \right) / \left(\sum_i \langle G_{ij} \rangle \right) \right]^{1/2} . \qquad (70)$$

We note here that the above expression for ξ is approximate and differs from that applied in Ref. 62, and that is why our correlation range results slightly differ from theirs. However, our procedure provides for good convergence of the results due to the good convergence of the correlation functions.

We calculate the susceptibility and correlation range for systems with the number of sites $N = L^2$, where L = 10, 15, 20, 30, 40, 60, 80, and 120 within the temperature interval $0.4 \leq T/J \leq 1.3$. The Markov chains are as long as 200 MCsteps/spin for $T/J \geq 1$ to 500 MCsteps/spin for $0.4 \leq T/J \leq 1$. The averaging is made over the second half of the Markov chain, the first half being left for the relaxation. For the purpose of extrapolation of our susceptibility results to the infinite lattice we plot $\ln(\chi T/J)$ versus ln(L) (Fig. 1). Using this plot we can make a reliable extrapolation to the infinite lattice for the temperatures down as low as $T/J \approx 0.5$, corresponding to $T/J = 0.25$ with the hamiltonian taken as in Ref. 62.

To check the validity of the expression (66) we plot $\ln(\chi T/T^3)$ *vs.* inverse temperature J/T in Fig. 2. It can be seen that the data

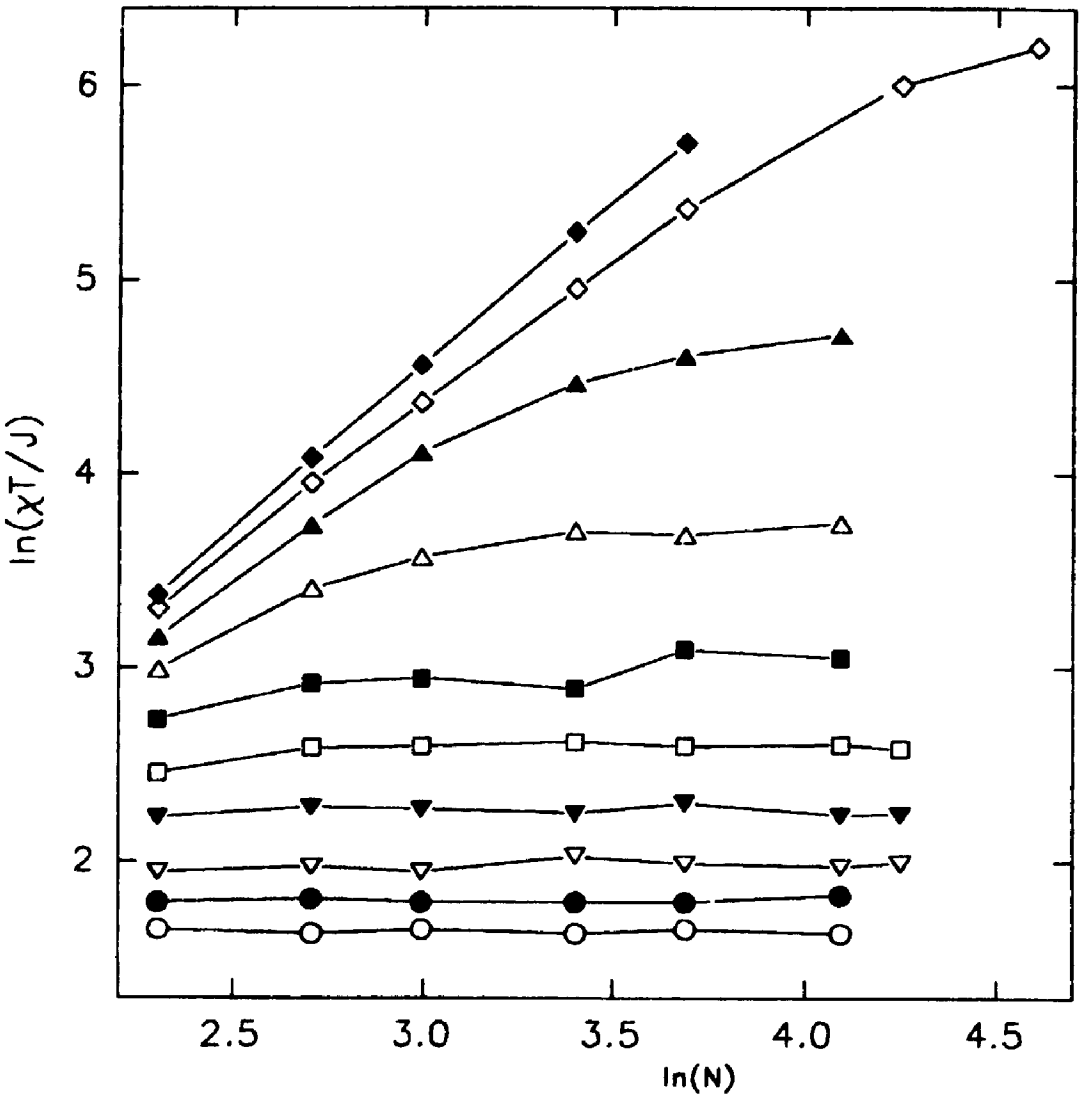

Fig.1. The finite scaling analysis of the susceptibility for a one-layer film. Legend: ○ T/J=1.3; ● T/J=1.2; ▽ T/J=1.1; ▼ T/J=1.0; □ T/J=0.9; ■ T/J=0.8; △ T/J=0.7; ▲ T/J=0.6; ◇ T/J=0.5; ◆ T/J=0.4

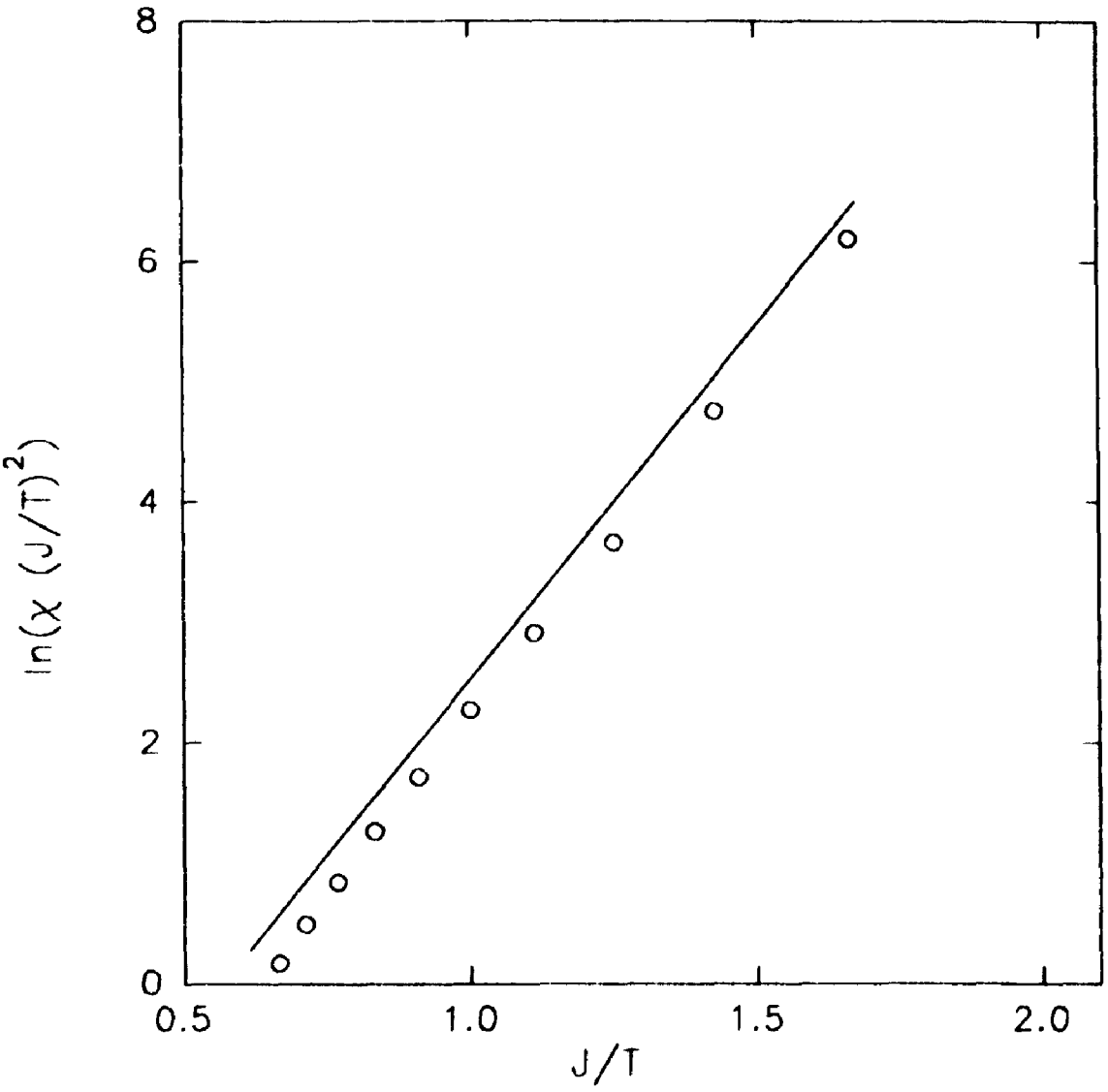

Fig. 2. The temperature dependence of the longitudinal susceptibility for a one-layer film. The MCH data (circles) give a fit close to $5.99J/T - 3.77$, and the solid line is $5.92J/T - 3.51$, as from Ref. 19.

fit the straight line with the slope equal to 5.99 within the entire investigated temperature interval, the theoretical slope being equal to 2π for $S^2 = 1/4$. We note that our fit is better than the value of 5.92 obtained in Ref. 62. The insignificant difference in the vertical intercept is due to a different normalization of the susceptibility. We conclude that our results confirm the validity of the expression (66) for a wider range of temperatures than before. The difference between our conclusions and those of Refs. 63 and 66 is probably due to the fact that finite size effects may mask the difference between the expressions (66) and (68). This is supported by the fact that, at low temperatures $T/J \leq 0.5$, a linear size of 80 spins is not enough to approximate the infinite system. We can use either Eq. (66) or Eq. (68) for ξ to deduce the linear size appropriate to lower temperatures where $L/2 \gg \xi$. Our results should be more reliable because larger systems are investigated.

In Fig. 3 we plot our results for the in-plane correlation range ξ for different linear sizes of the film L. The presented dependence of ξ on L gives an opportunity to make the extrapolation to the infinite-size lattice for the temperatures $T/J \geq 0.6$.

The comparison between our results and the expression (67) for ξ are shown in Fig. 4. The slope of the straight line approximating the obtained dependence of $\ln\left(\xi(J/T)^{1/2}\right)$ *vs.* J/T is 2.8, which is close to the theoretical value of π for $S = 1/2$.

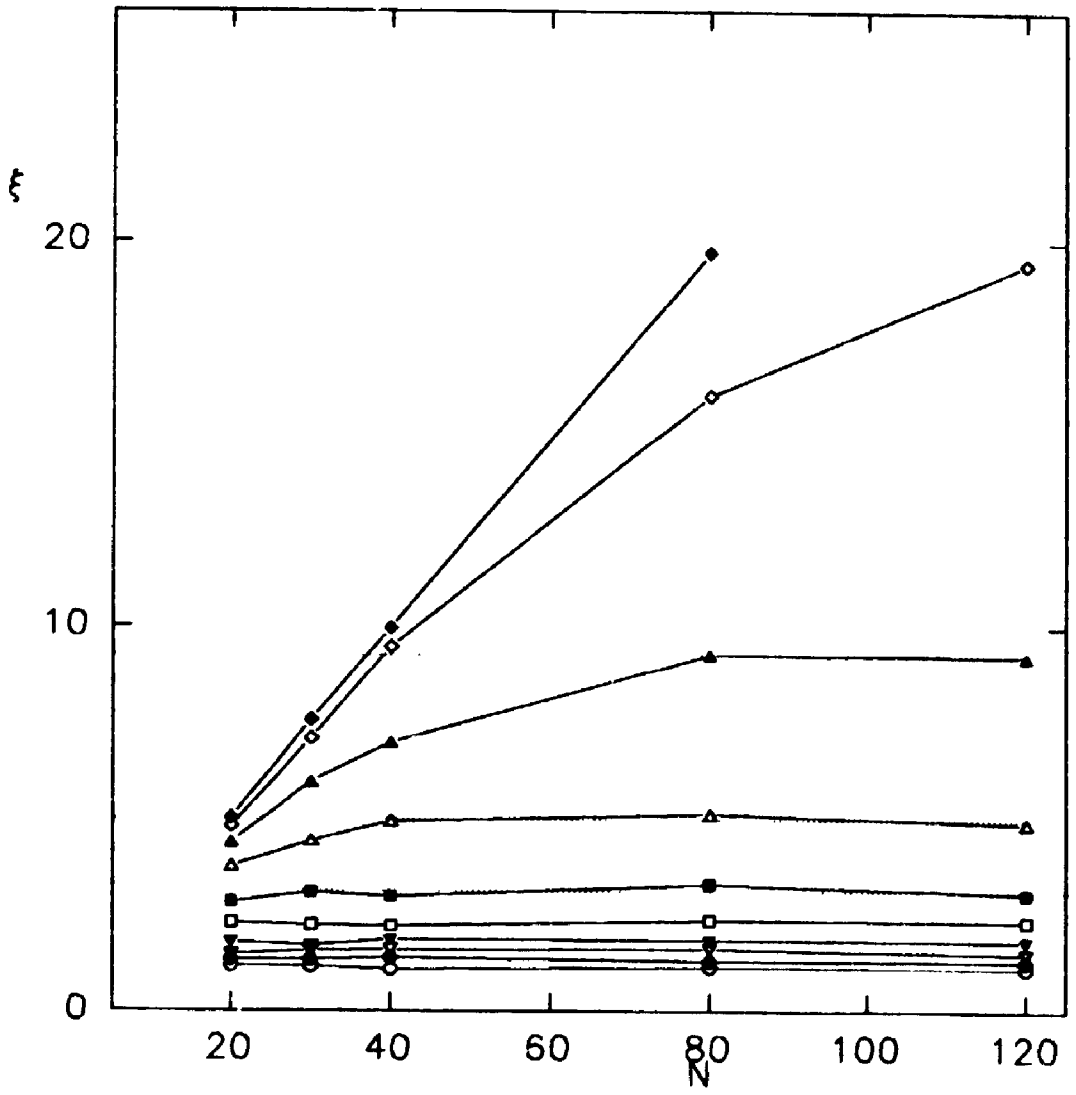

Fig.3. The finite scaling analysis of the correlation range ξ for a one layer film. Legend : ○ T/J=1.3; ● T/J=1.2; ▽ T/J=1.1; ▼ T/J=1.0; □ T/J=0.9 ■ T/J=0.8; △ T/J=0.7; ▲ T/J=0.6; ◇ T/J=0.5; ○ T/J=0.4.

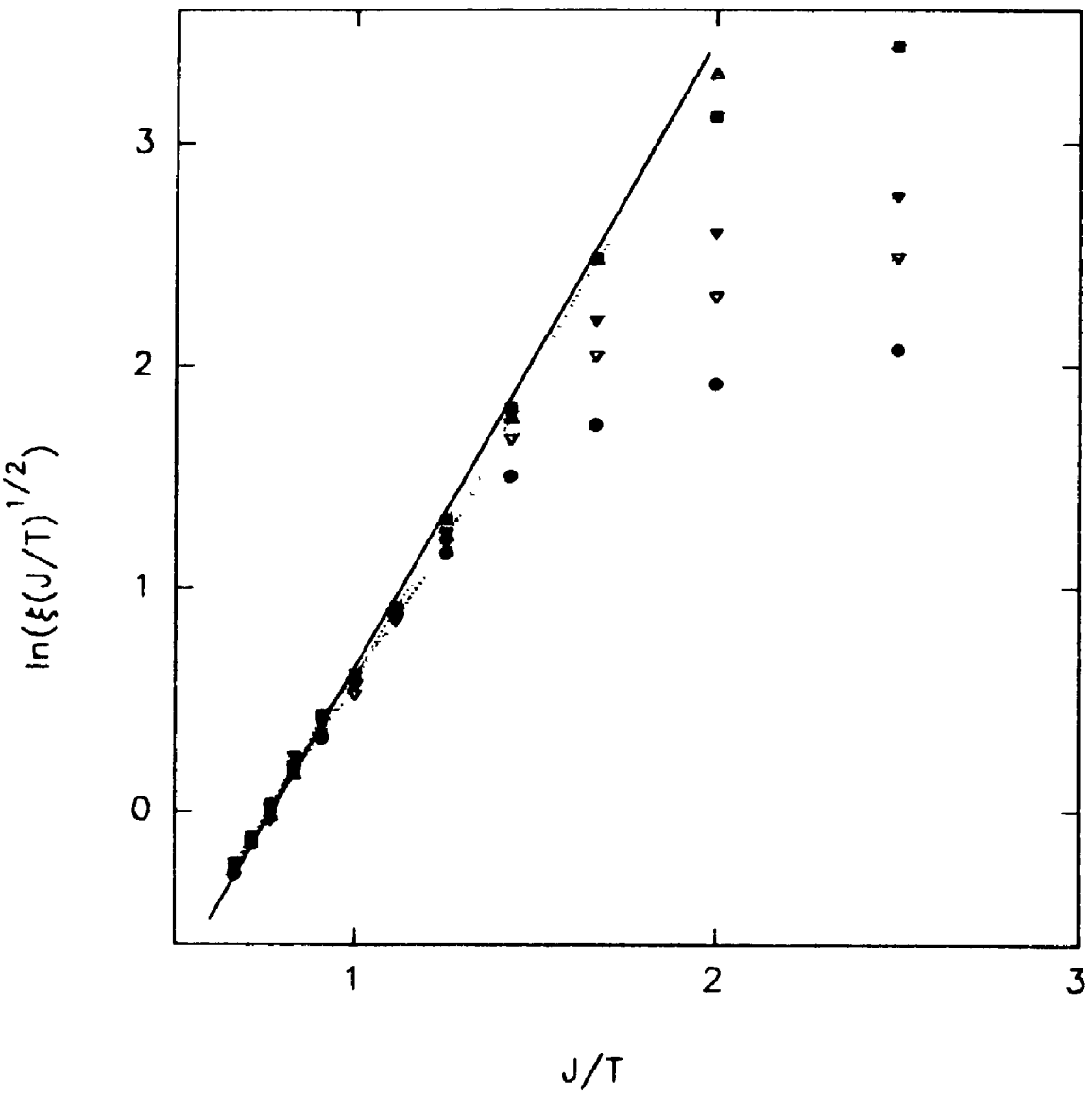

Fig.4. The temperature dependence of the correlation range ξ for a one-layer film. Linear size: • 20; ▿ 30; ▾ 40; ▪ 80; ▵ 120. The solid line represents a fit to the function $2.8J/T - 2.1$.

3.3. THIN HEISENBERG FILMS WITH NUMBER OF MONOLAYERS M ≤ 4

The objective in this thin-film study is to examine the type of critical behavior and to look for possible 2D-3D crossovers. Let us consider the thin film as a crystal having two equal surfaces in one direction and to be infinite in the others. The Hamiltonian of a S = $\frac{1}{2}$ Heisenberg ferromagnet with nearest-neighbor interactions and the above geometry can be written in the following general form:

$$H = -2\sum_{p=1}^{M}\sum_{(i\,j)} J^{B}\mathbf{S}_i^p\cdot\mathbf{S}_j^p - 2\sum_{q=1}^{M-1}\sum_{i} J^{T}\mathbf{S}_i^q\cdot\mathbf{S}_i^{q+1}, \qquad (71)$$

where the first sum is responsible for the interaction of the spins within layer p, and the second term is the contribution of the interlayer interaction. The sums are taken over pairs of nearest neighbors in both cases. This model has been used in the numerical calculations of the longitudinal susceptibility in zero field as well as the in-plane correlation range.

As the MC method permits one to work only with finite crystals, we quote the procedure to approximate the infinite crystal by the finite system. The usual way to do this for bulk systems is to introduce periodic boundary conditions. In order to simulate a thin film we can use periodic boundary conditions for those directions in which the crystal is infinite, keeping free boundary conditions for the surfaces of the film.

First we examine the case of a *two-monolayer* film. Under

consideration are systems with the in-plane linear size L = 10, 20, 30, 40, 60, and 80 spins. In Fig. 5 we show our finite scaling analysis, making the conclusion about the possibility to extrapolate our data to the infinite-lattice case for temperatures $T/J^B \geq 0.9$.

The results of investigating the temperature dependence of the susceptibility when $J^T = J^B$ are presented in Fig. 6. This provides evidence that the susceptibility displays a 2D behavior of the same type as in Eq. (66) but with the power in the exponential equal to 12.1, which is close to 4π. As well, our results for ξ (see Fig. 7, (a)) satisfy the expression (67) with the exponential power equal to 5.8, which is approximately twice our value 2.8 for the 2D system.

We calculate the surface-surface correlation function $\langle G_{ij} \rangle$, taking i and j to belong to the opposite surfaces of the film, and its temperature dependence is presented in Fig. 8. We note that, within the investigated temperature interval, this correlation function is rather close to the saturation value 0.25, implying that the surface spins are well correlated.

Similar conclusions are found for the case of $J^T = 2J^B$ (see Fig. 7, (b)). For the exponential power in Eq. (67) we get the value 5.9 and the surface-surface correlations for this case are stronger than previously.

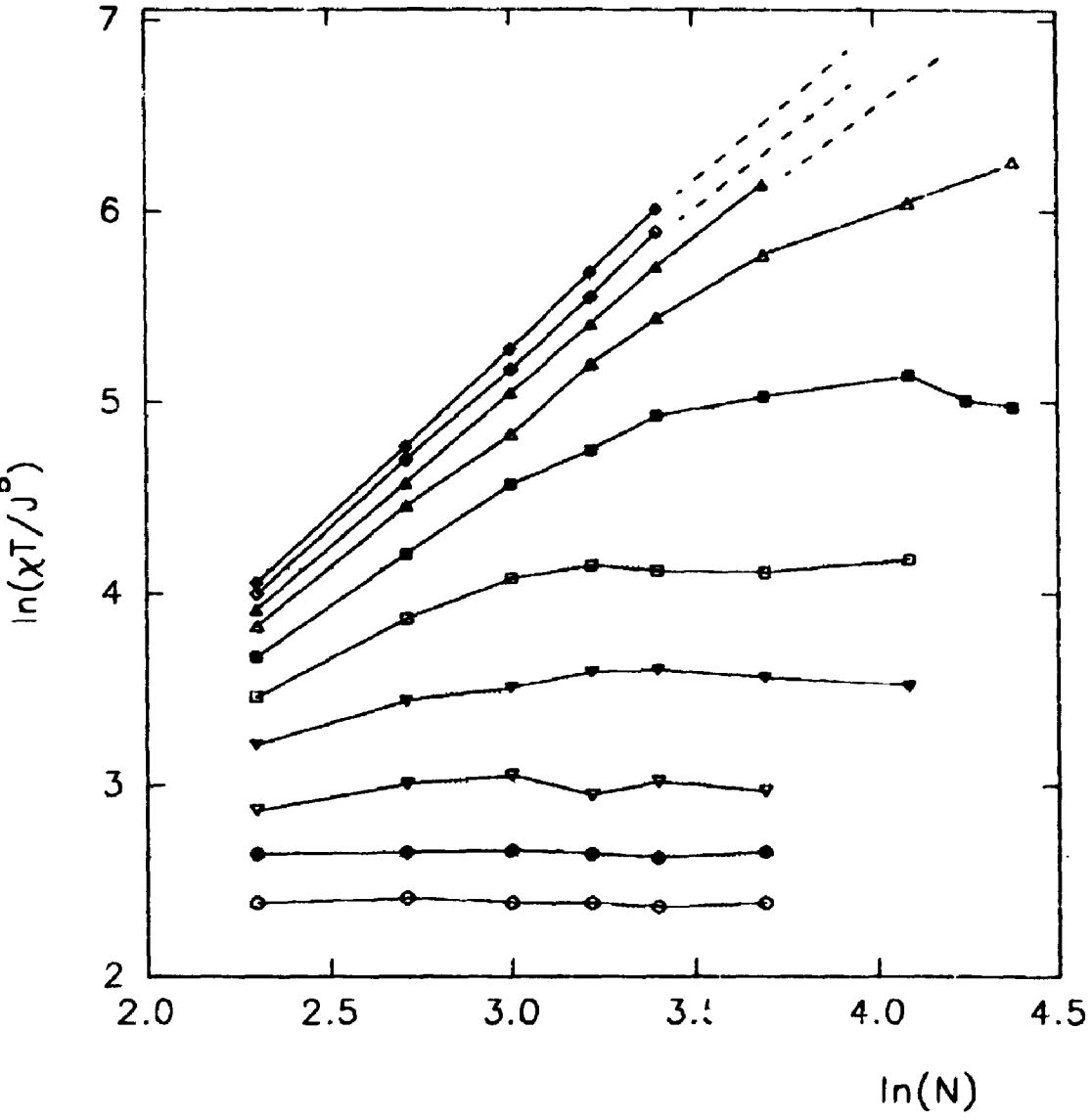

Fig.5. The finite scaling analysis of the susceptibility for a two-layer film with $J^T=J^B$. T/J^B=: ○ 1.5; ● 1.4: ▽ 1.3; ▼ 1.2; □ 1.1; ■ 1.0; △ 0.9; ▲ 0.8; ◇ 0.7: ◆ 0.6

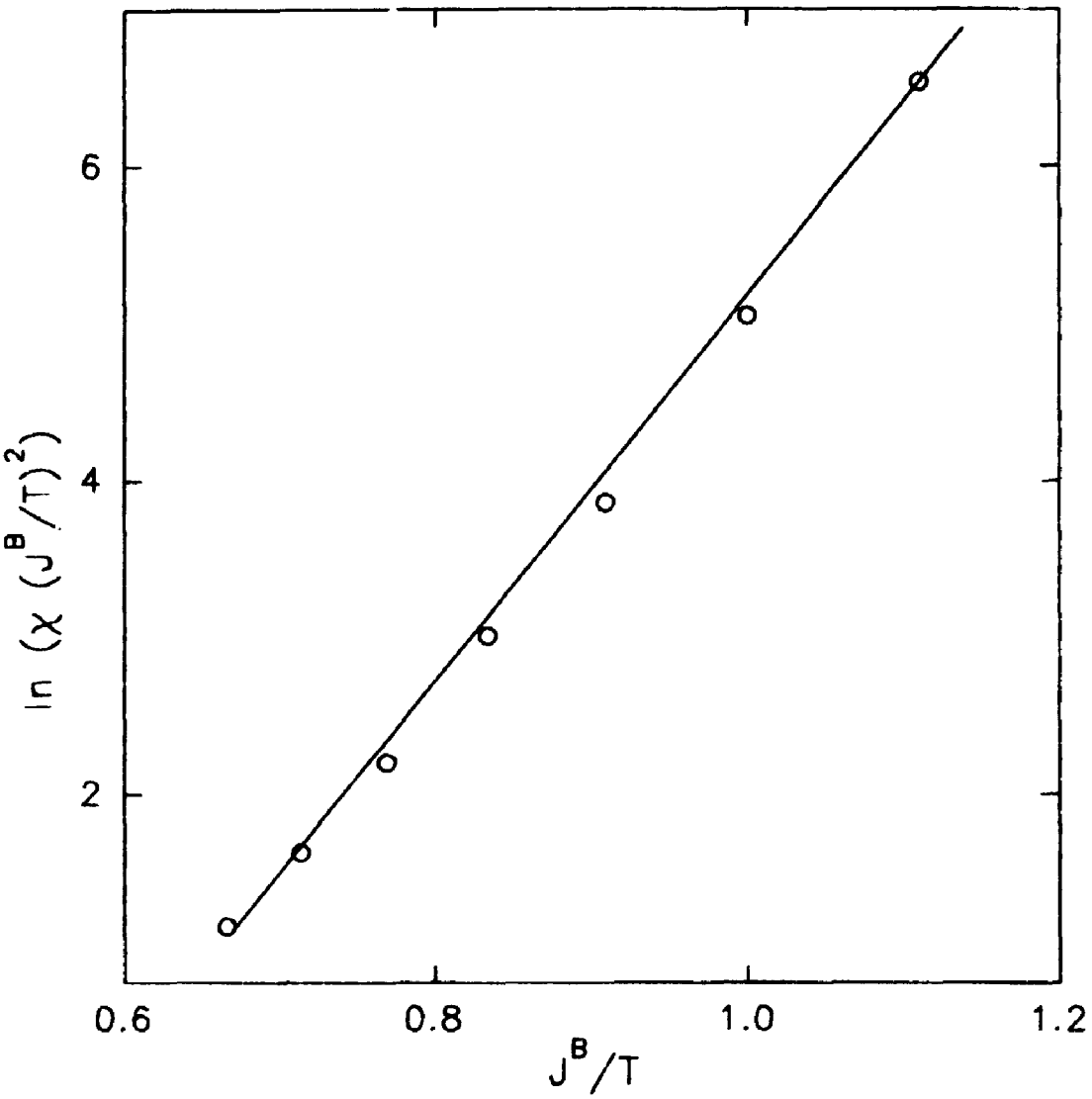

Fig.6. The temperature behavior of the susceptibility for a two-layer film with $J^T=J^B$. The MCH points are extrapolated to the infinite lattice. The solid line represents function 12.1J/T − 7.0

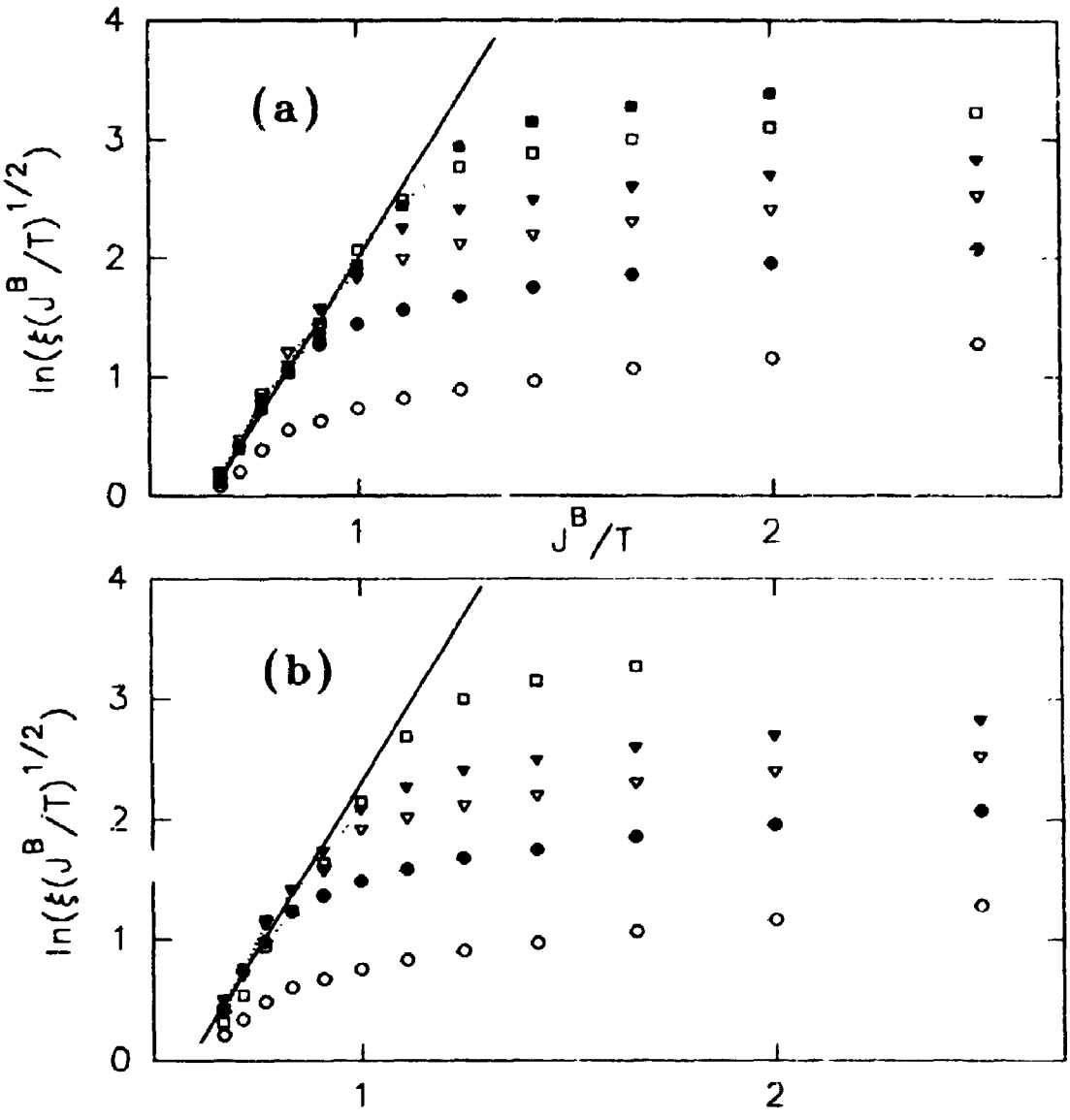

Fig 7. The temperature dependence of the correlation range for the two-layer film with (a) $J^T=J^B$; (b) $J^T=2J^B$. N=: ○ 10; ● 20; ▽ 30; ▼ 40; □ 60; ■ 80. Solid line is a fit to the function $5.8J^B/T - 3.8$ (a) and $5.9J^B/T - 3.6$ (b).

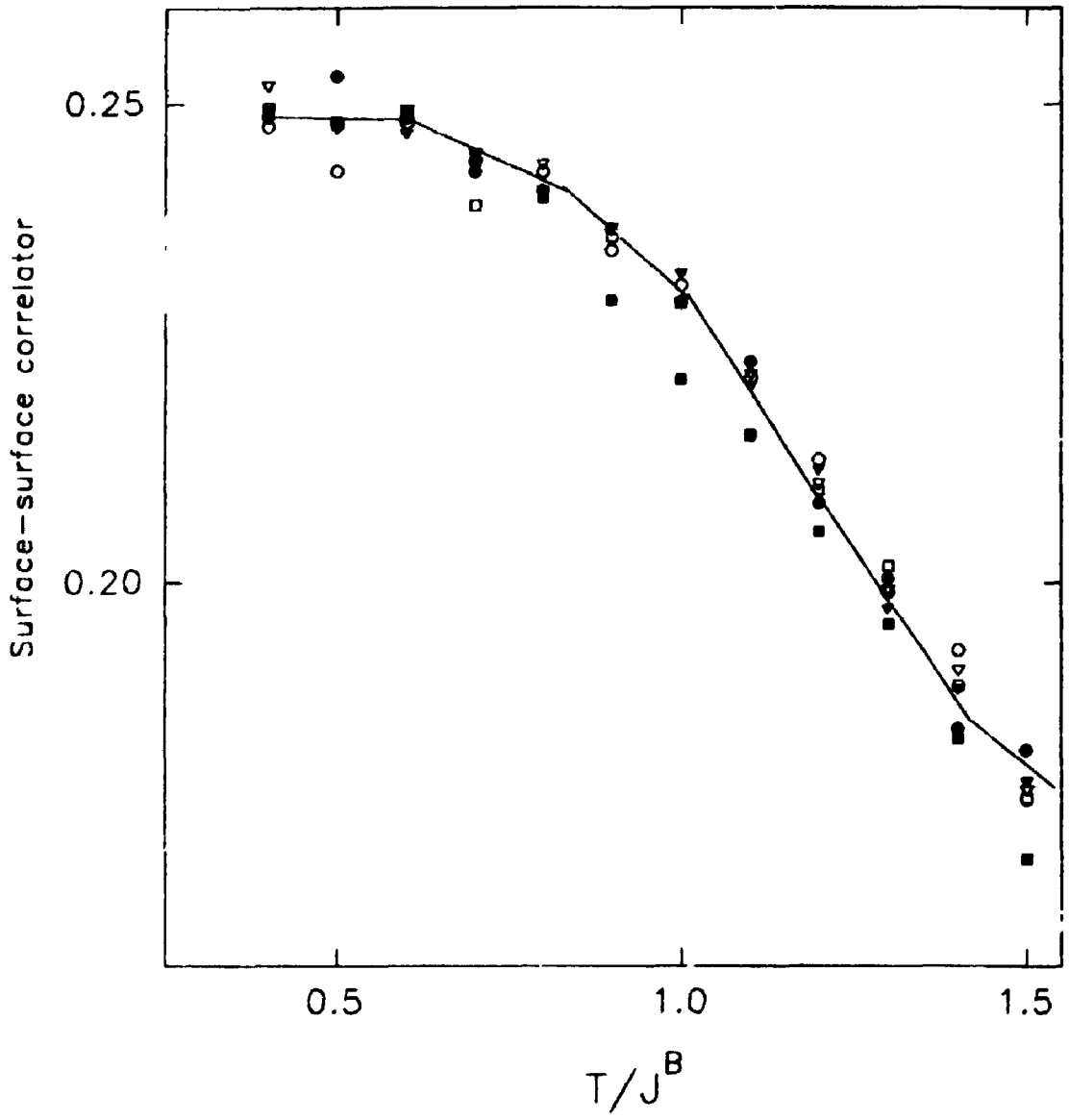

Fig.8. The temperature dependence of the surface-surface correlator for a two-layer film with $J^B=J^T$. The notations are similar to those in Fig.7. The solid line is a guide to eye.

Next we discuss *three-monolayer films.* We have accomplished simulations for the films with the linear sizes L = 10, 20, 30, 40, and 60 spins and $J^T = J^B$. The susceptibility results are presented in Fig. 9. In this case, when trying to fit our results to the 2D dependence (66), we get the exponential power equal to 18 which is close to 6π.

We treat our results as evidence that, in certain temperature intervals and for $J^T \gtrsim J^B$, the temperature dependences of the susceptibility and the correlation range obey the 2D results of Eqs. (66) and (67) with J replaced by MJ, M being the number of the monolayers in the film. We present here a simple arguments to support this conclusion for the two-layer film. Having used a well-known transformation from spin operators to transposition operators for the $S = \frac{1}{2}$ case (e.g., see Eq. 38), we can rewrite the Hamiltonian as

$$H = -\sum_{p=1}^{2} \sum_{(i\,j)} J^B E^p_{ij} - 2 \sum_{l} J^T E^{12}_l + \text{const} , \qquad (72)$$

where E^p_{ij} and E^{12}_l are, respectively, the transposition operators for the sites i and j within the pth layer and between the sites l in layers 1 and 2. The first term represents the energy of the exchange interactior within the layers and the second sum is the exchange interaction energy between the layers. When the surface-surface correlations are strong, the most significant contribution to the

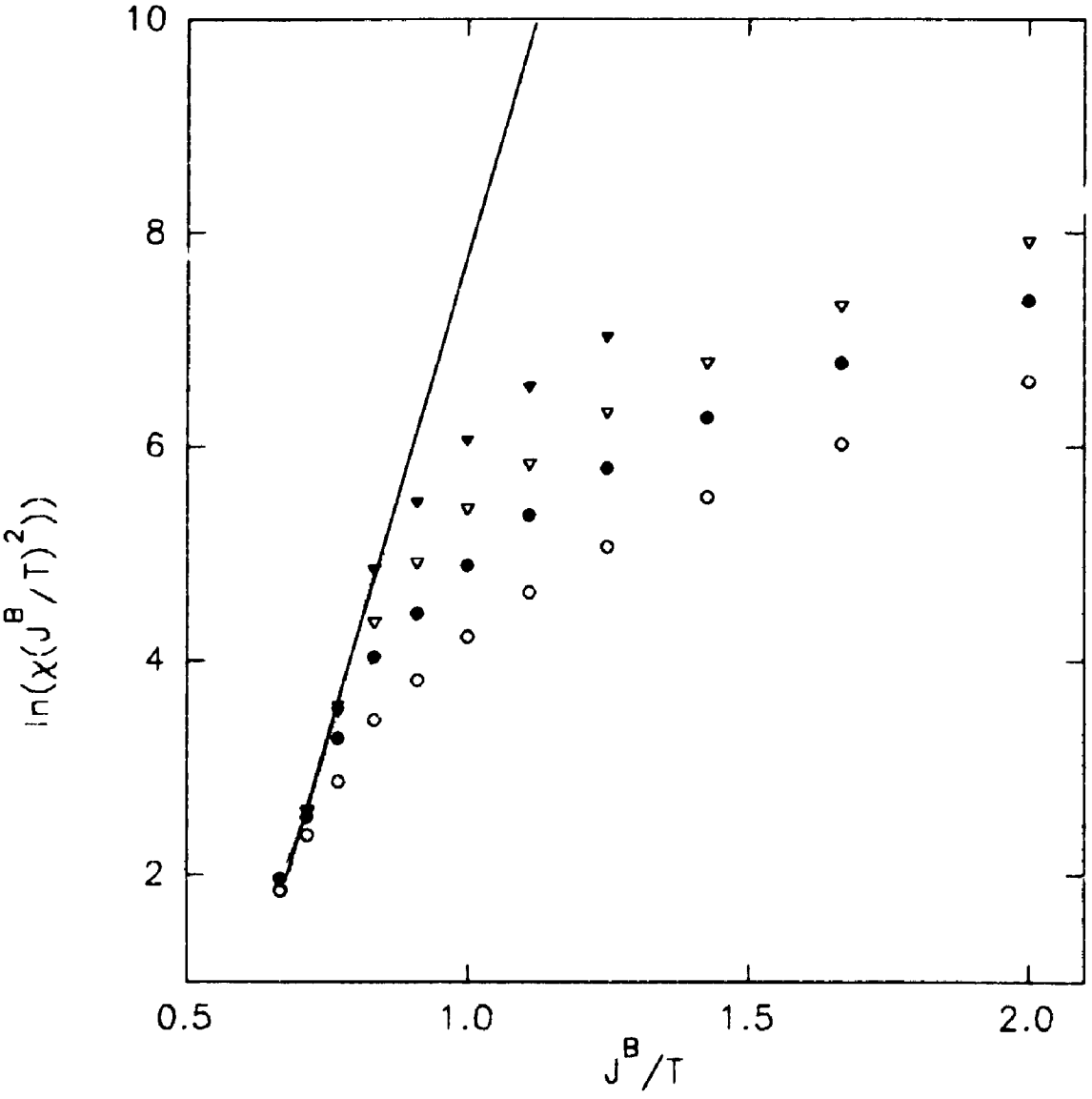

Fig.9. The temperature behavior of the susceptibility for a three-layer film with $J^T=J^B$. N=: ○ 10; ● 20; ▽ 30: ▼ 40; □ 60. Solid line is fit to the function $18J^B/T-10$.

thermodynamic properties is given by the spin configurations in which the z-projection values of the spin operators (along the direction perpendicular to the film surface) are the same throughout the film thickness. For these configurations the transposition operators in the second term are equal to the identity operator, giving a term that is effectively constant. For the same configuration the first term can be written effectively as

$$\sum_{(ij)} 2J^{B}E_{ij} \quad . \tag{73}$$

This corresponds to the Hamiltonian of the 2D model with the exchange renormalized to the value $2J^{B}$. Of course, this simple explanation lacks rigor but it makes the conclusion from our numerical results plausible.

Our results may provide an explanation of the fact that the direct nuclear exchange parameter $J = 2.1$ mK for ^{3}He, quoted in Ref. 50 as a result of fitting to the 2D analytical expressions, is higher than might be expected. In the discussion of the experimental results, the authors of Ref. 50 assumed that only one of two completed monolayers of ^{3}He was magnetized, thus forming a 2D Heisenberg system. However, if we assume both monolayers to be magnetized, we fit the same 2D temperature dependences of the susceptibility and the correlation range, but now the fitting exchange parameter corresponds to 2J. In this case J would be half

the value quoted in Ref. 50.

We emphasize that the analysis of our results cannot give us a conclusive proof that the behavior of the system remains 2D to T = 0. This is because in our MC calculations we use large but finite lattices and long but finite Markov chains. However, for the investigated temperature interval, the transverse (or interlayer) correlations were shown to be close to saturation and so did not give rise so far to any kind of finite-temperature phase transition. This is consistent with the 2- and 3-monolayer films being effectively 2D down to at least close to T = 0.

3.4. TWO-MONOLAYER FILM WITH A DILUTED UPPER LAYER

Heisenberg ferromagnets with dilution have been recently studied by experimental (Refs. 67, 68, 69, 53), theoretical (Refs. 70, 71), and numerical (Refs. 35, 36, 37, 72) methods. Our aim here is to obtain the dependences of the critical behavior on the concentration of either spins or bonds present in the system. The usual way to do this is to study how T_c depends on the concentration. In the 2D Heisenberg model, however, as the critical temperature is zero even for the non-diluted case, we may try to interpret the results for the diluted system by examining the parameters of the 2D behavior, as given by Eqs. (66) and (67), to deduce their dependence on the occupancy concentration.

A simple theory for the diluted 2D model is presented in Ref. 70, based on a modified spin-wave theory (Refs. 49, 57). The main result suggested in this paper is that the behavior of the diluted system remains 2D down to a percolation-limit concentration (i.e., 0.5 for the bond percolation or 0.69 for the site percolation), the exchange being renormalized by a factor of (2m-1) where m is the bond-occupancy concentration. The comparison of this theory with the MC calculations (Ref. 72) displays some discrepancy. A possible origin of this discrepancy may be that instead of Eq. (67) they used an expression analogous to Eq. (68) for the correlation range. Our numerical calculations, as mentioned above, provide for the use of Eqs. (66) and (67) rather than (68).

Here, following Refs. 65 and 73, we study the effects of an incomplete layer for the two-layer film. For simplicity, we consider a Heisenberg film consisting of two monoatomic layers, of which one is complete, i.e., all the sites are occupied by spins, and the second is diluted or incomplete, having a random distribution of vacant sites with a given concentration. For this purpose, we rewrite the Hamiltonian as follows:

$$H = -2 \sum_{(ij)} J^1_{ij} \mathbf{S}^1_i \cdot \mathbf{S}^1_j - 2 \sum_{(pq)} J^2_{pq} \mathbf{S}^2_p \cdot \mathbf{S}^2_q - 2 \sum_{l} J^T_l \mathbf{S}^1_l \cdot \mathbf{S}^2_l \,, \qquad (74)$$

where the superscripts 1 and 2 refer to the layer number while the subscripts label the positions of the sites in the film plane. As in

Sec. 3.3 we assume in-plane periodic boundary conditions.

To introduce incompleteness into the second layer, we make the following assumptions for the exchange interactions:

(i) $J^1_{ij} \equiv J$ for all the pairs of nearest neighbors, i and j;

(ii) To construct J^2_{pq} and J^T_l we first introduce the fractional concentration x of the occupied sites, where $0 < x \leq 1$ and $x = 1$ stands for the complete second layer. Then, using this concentration as the probability for the single site to be occupied, we construct the vacancy distribution within the second layer. After that, we put $J^2_{pq} = 0$ if either of the sites p and q is vacant, otherwise we put $J^2_{pq} = J$ if both are occupied. Similarly, we put $J^T_l = 0$ if in the second layer the site l is vacant, otherwise $J^T_l = J$. We note that in our simple model we do not account for the possibility of the interlayer exchange being different from the in-plane exchange.

For our calculations we choose the same temperature interval as before, i.e., $0.7 < T/J < 1.3$. Based on our previous simple finite-scaling analysis for this interval for the one- and two-monolayer films (see Sections. 3.2 and 3.3), we assume that a square with the linear size equal to 70 sites represents the infinite system fairly well. We remark that the finite-size effects were reported to be more important for diluted systems than for systems without structural disorder (Ref. 12). However, in our case, having made several test calculations, we did not observe these effects to

be significant in the chosen temperature interval. All the other details of the computer simulation, including the lengths of the MC runs, are similar to Secs. 3.2 and 3.3.

The analysis of the numerical results for the temperature dependences of the longitudinal susceptibility includes making fits to an expression of the form (66) and defining the exchange renormalization index η_χ. We note that the exponential power in Eq. (66) is $2\pi\eta_\chi J/T$ ($\cong 6.28\eta_\chi J/T$). However, we in this work and others (Ref. 62) obtained this power for the one-monolayer system as $\sim 6\eta_\chi J/T$. The difference might be due either to systematic numerical error or to an inaccuracy in the derivation of Eq. (66). For the calculation of η_χ, we use our value 6 instead of 6.28 from Eq. (66).

In Fig. 10 we present the results of this fitting procedure for several values of the concentration x. We conclude that the investigated system displays effectively 2D behavior with the values of η_χ lying between those for two-monolayer and one-monolayer systems. When x is small, η_χ appears to be close to 1 and only weakly dependent on x. For larger x values, η_χ appears to depend strongly on x, dropping rapidly from $\eta_\chi \cong 1.5$ for $x = 0.8$ to $\eta_\chi \cong 1.2$ for $x = 0.6$.

We also plot η_χ versus concentration x in Fig. 11. This shows that, for $x > 0.7$, η_χ decreases with decreasing x in such a way that the tangent line to this dependence is pointing to the limit of

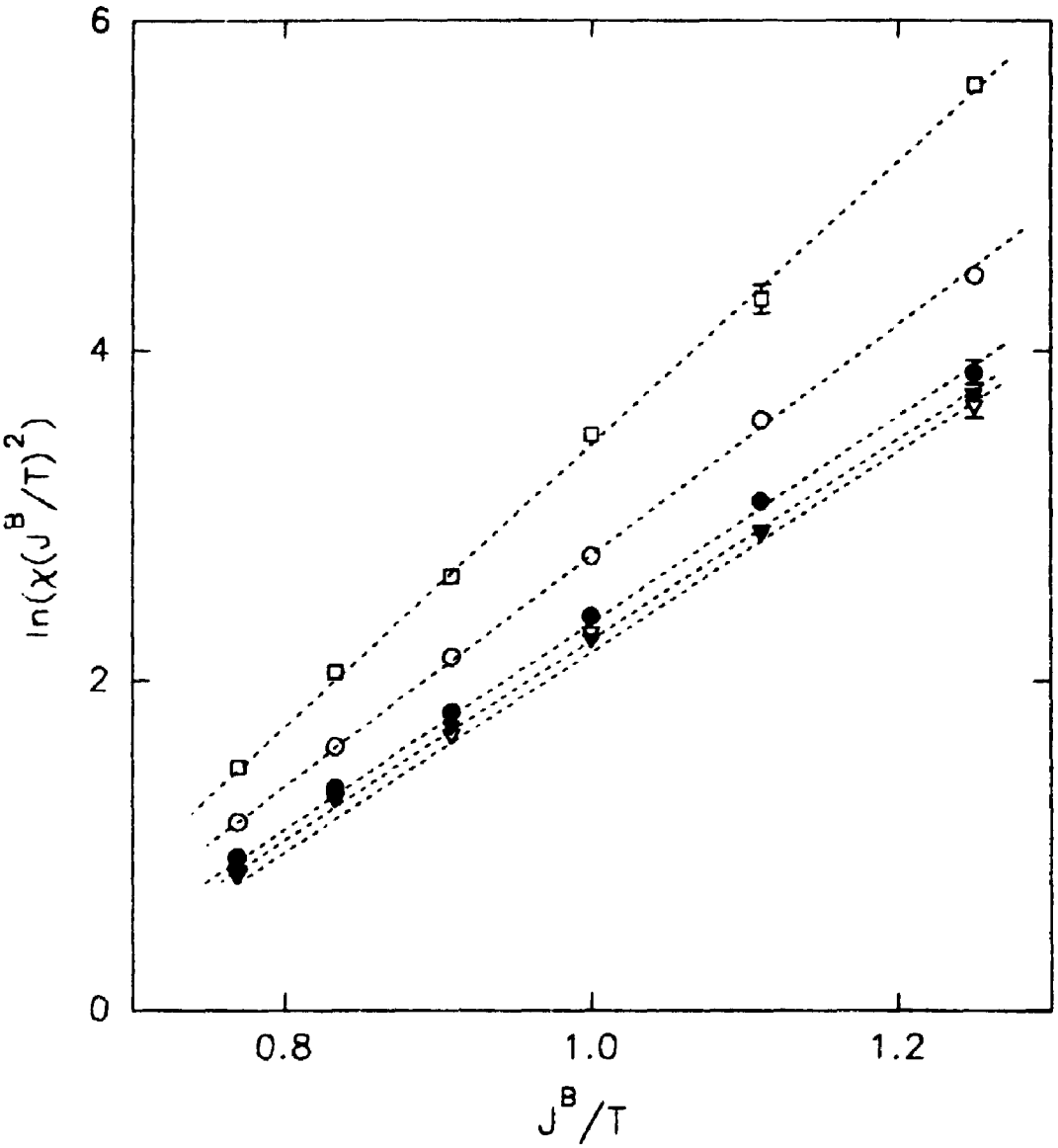

Fig.10. The susceptibility data for a two-layer film with diluted upper layer. Legend: □ x=0.8; ○ x=0.6; ● x=0.4; ▽ x=0.2; ▼ x=0.1

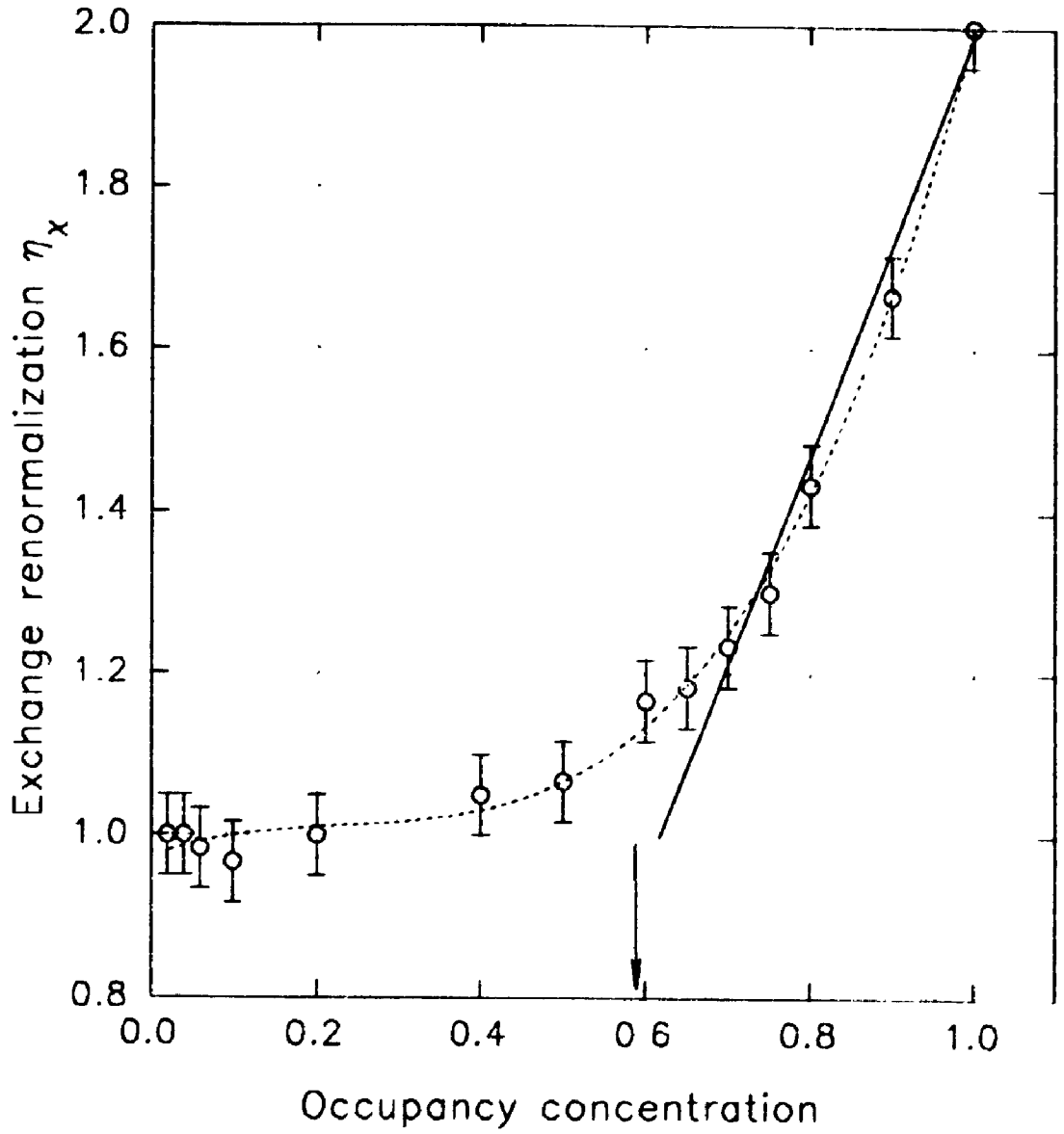

Fig.11. Exchange renormalization vs occupancy concentration for a film with diluted upper layer. The arrow points at the percolation limit for a s.c. lattice.

purely 2D behavior ($\eta_\chi = 1$) approximately at the 2D percolation limit $x \cong 0.6$ (see, e.g., Ref. 12). We note here that the this tangent line corresponds well to the theory of Ref. 70, reformulated in terms of site percolation. However, when x becomes less than 0.7, substantial deviations from this tangent line occur, making the crossover interval from two-layer to one-layer behavior as wide as $0.3 < x < 0.7$. Finally, for $x < 0.3$ the curve flattens to almost a horizontal line.

A simple qualitative interpretation of these results can be provided by the percolation theory. The magnetic long-range order in the incomplete layer, being taken separately, depends on the existence of exchange paths connecting the spins in the plane. If the number of the bonds is insufficient to form the mentioned paths, then the long-range order vanishes. However, in the presence of the second (complete) layer, the spins in the upper layer can be connected by paths that avoid the broken bonds in the upper layer and partially go through the lower layer. When the occupancy concentration x is sufficiently high, the main ordering in the upper layer occurs due to the paths lying within this layer. This situation can be adequately described by the 2D percolation theory, with the result that the tangent line points straight to the percolation limit. However, in the vicinity of the percolation threshold, the paths involving both of the layers play a significant

role, thus flattening the curve in the range of intermediate values of x. Finally, for small values of x, the total number of spins in the upper layer becomes so small that they do not contribute significantly to the susceptibility of the whole system. Moreover, the paths connecting the remaining spins in the upper layer then lie mostly in the lower layer, contributing to the lower layer susceptibility.

The results depicted in Fig. 11 might be useful in the context of a rough interpretation of the data from Refs. 52 and 53, where the dependence of the magnetization on the coverage by a second monoatomic layer was studied. The system was assumed (Refs. 52, 53) to be a Heisenberg magnet on a triangular lattice, with the first layer completed with the density ~0.114 atoms/$Å^2$. It is very difficult to design an adequate model for the above described system, as with the change of the total film density different processes occur, such as solidification of the second layer, changes of the structure of the higher layers, incommensurate structures in different layers, etc. In Refs. 52 and 53 the authors assumed the first layer to be effectively paramagnetic with the exchange constant being lower than 50μK, whereas in the second layer, when it is complete, the exchange is quoted as being about 2.1 mK. As well, the authors of Refs. 52 and 53 discount the possibility of exchange interaction between the first and second layers, admitting the

possibility of an interlayer exchange between the second and higher layers.

We wish to point out that our MC simulations (Refs. 65, 73) provide for an alternative explanation (compared with that in Refs 52 and 53) of the coverage dependence of the effective exchange energy (see, e.g. Ref. 52, Fig.3a) and the coverage dependence of the magnetization (Ref. 54, Fig.4). First, the low-temperature second-layer magnetization, presented in Ref. 54 (Fig.4) displays a typically percolative dependence on the coverage, analogous to that of the calculated magnetic susceptibility in Ref. 65 (see Fig.2), obtained within the assumption of a strong intralayer coupling in the first layer and a strong interlayer coupling. The percolation limit can be roughly estimated as ~65% coverage by the second layer. This value is closer to the percolation limit of a square lattice (59%), than a triangular lattice (50%). However, this minor inconsistency might be attributable to a complicated structure of an interlayer interaction. Moreover, due to the interlayer interactions, the effective percolation limit of the two-layer system, defined as an intercept of the tangent line to the curve for high coverages with the line of exchange renormalization equal to unity, increases up to 62% for the square lattice case. The above correspondence between the results for the two systems in question seems to be consistent with a strong interlayer exchange coupling in the ^{3}He films.

The above arguments also hold when analyzing the effective exchange energy dependence on the total film density. Assuming the first layer density to be constant and equal to ~0.114 atoms/Å^2 (the value quoted in Ref. 54) we see that the maximum effective exchange parameter J corresponds to the second layer coverage being ~100% of the first layer coverage, the total density therefore being about 0.228 atoms/Å^2 (Fig.3a of Ref. 52 and Fig.9 of Ref. 54). This largest value of J is approximately twice the smallest value. This behaviour also supports the model of strong exchange coupling in the first layer and strong interlayer coupling. We should mention here that in our MC calculations of the exchange renormalization we use the same theory of the two-dimensional Heisenberg magnet (Ref. 62), as do the authors of Ref. 52, 53 and 54. The only difference is that we use for our fits the expressions for the susceptibility, while they are using the saturation magnetization equation.

We also made an attempt to compare our exchange renormalization data for a two-layer film, taken from Ref. 73, with the results of Ref. 52 (Fig.3a). For densities less than 0.228 atoms/Å^2 we assumed the second layer to be incomplete. For the part of the data corresponding to the total densities greater than 0.228 atoms/Å^2 we made a very crude assumption that the system restructures itself in such a way that a first layer can be considered incomplete. Also, as a rough approximation, we used our previous data (Ref. 65) for the

PM-1 3½"x4" PHOTOGRAPHIC MICROCOPY TARGET
NBS 1010a ANSI/ISO #2 EQUIVALENT

1.0
1.1
1.25
1.4
1.6
2.8
3.2
3.6
4.0
2.5
2.2
2.0
1.8

PRECISION[SM] RESOLUTION TARGETS

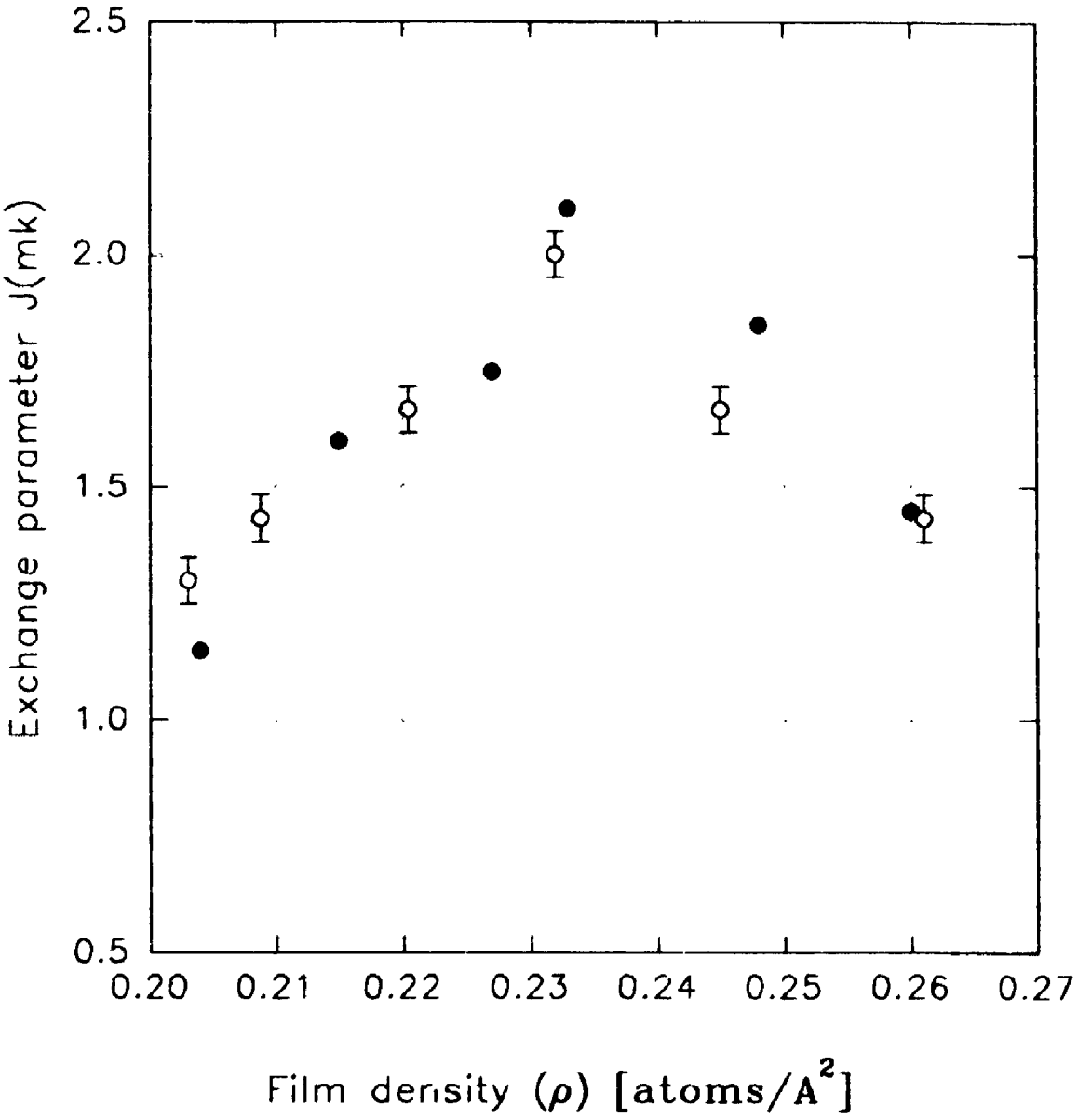

Fig.12. Exchange parameter as function of the film density. The first layer density is assumed to be 0.116 atoms/A^3. Intralayer exchange approx 1 mk, interlayer exchange >1mk. Solid circles – experiment (Ref. 53); open circles – MCH.

square lattice. The results of the comparison show a remarkable correspondence for such a crude model, as can be seen from Fig. 12. We do not have to account for any systematic uncertainties occurring because of the fitting procedure which is the same for both sets of data. In general, the correspondence in Fig. 12 is very good for densities less than 0.23 atoms/$Å^2$ (incomplete second layer). The deviation in the second part of the curve (first layer "incomplete") are larger, probably due to the crudeness of our approximation for this region.

In conclusion, we would suggest further experimental investigation of the system in question, attempting to evaluate the possible effect of the interlayer exchange and the influence of the second and higher layers on the intralayer exchange in the first layer.

3.5. INFLUENCE OF INTERLAYER EXCHANGE ON THE CRITICAL PROPERTIES OF A TWO-LAYER FILM

In Sec. 3.2 we discussed the effectively 2D behavior of the two-layer Heisenberg film with $J^T > J^B$ in the Hamiltonian (71). For other values of J^T, however, one might expect deviations of the critical properties of the susceptibility from the general form of Eq. (66). Indeed, in the limit case of $J^T = 0$ the two layers become independent 2D systems without any renormalization of exchange. In

principle, the change in the behavior as J^T increases from zero might occur either continuously, producing a smooth dependence of the η_χ parameter on the J^T value, or in the form of a crossover. Here we discuss our results for the critical behavior of the longitudinal susceptibility of the two-layer film within a range of values of J^T.

The linear size of the investigated system is L = 70 spins. All the details of the MC calculations are the same as in the previous sections, together with the conclusions about the temperature interval of their applicability. The interpretation of the numerical results is again based, where appropriate, on Eq. (66).

In Fig. 13 (a,b) we display the susceptibility dependences on the inverse temperature for the values J^T/J^B = 0.1 and 0.3. We can distinctly see a crossover between two effectively 2D regimes, as exhibited by the pronounced change in the slope of the straight line on the plots. The crossover region shifts to higher temperatures with increasing J^T. This behavior confirms our statement about the importance of the saturation of the transverse correlations on the magnetic ordering in the system. When the temperature is lower than the crossover temperature, the slope of the line is approximately the same for all the values of J^T (corresponding to $\eta_\chi \cong 1.8$) and is close to our value for the case of $J^T = J^B$ ($\eta_\chi \cong 2.0$). Above the crossover, the parameter η_χ displays a dependence on the value of J^T (see Fig. 13, (a)).

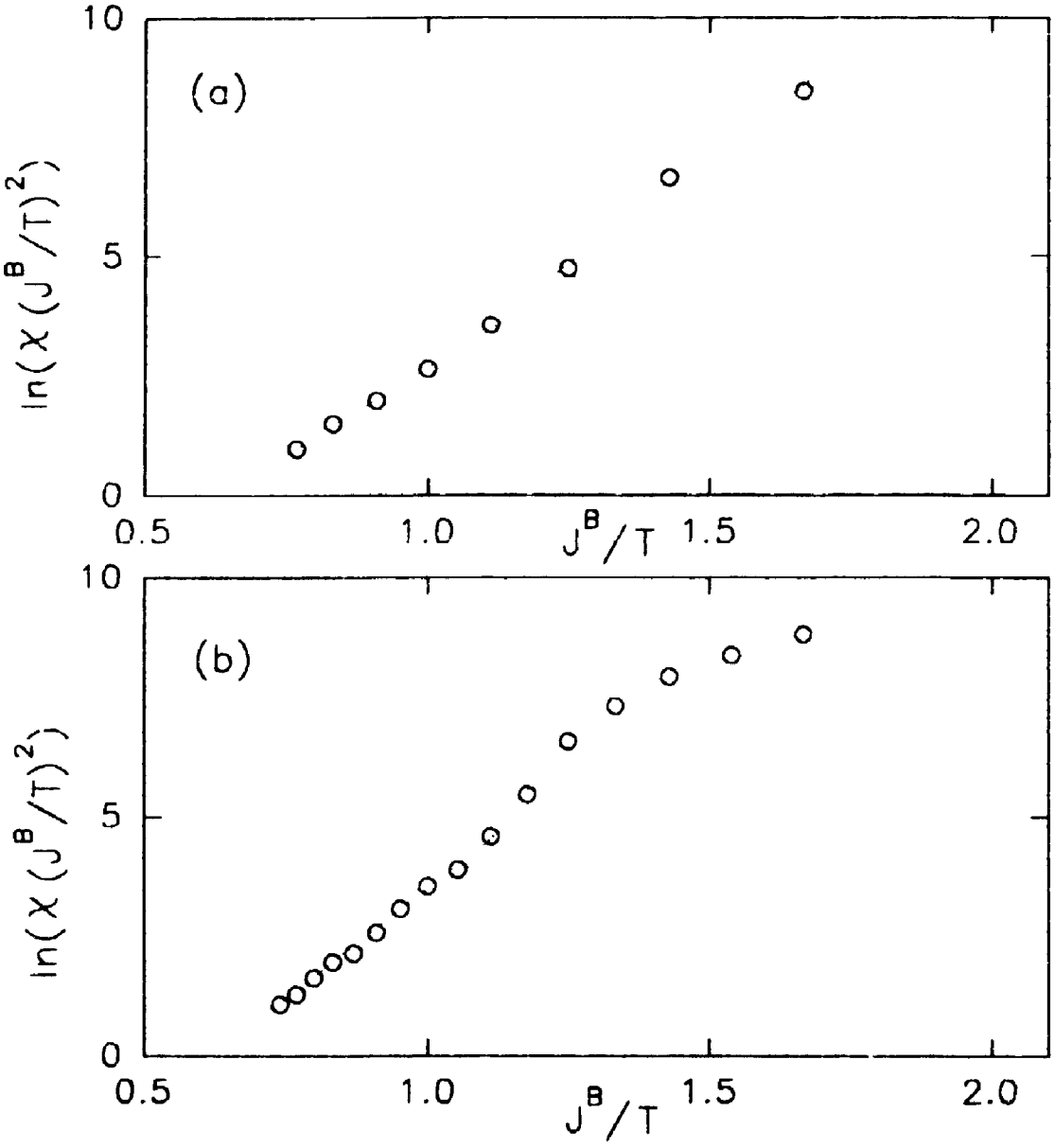

Fig. 13. Temperature behaviour of a two-layer film with (a) $J^T=0.1J^B$ and (b) $J^T=0.3J^B$. The lines are guides to the eye.

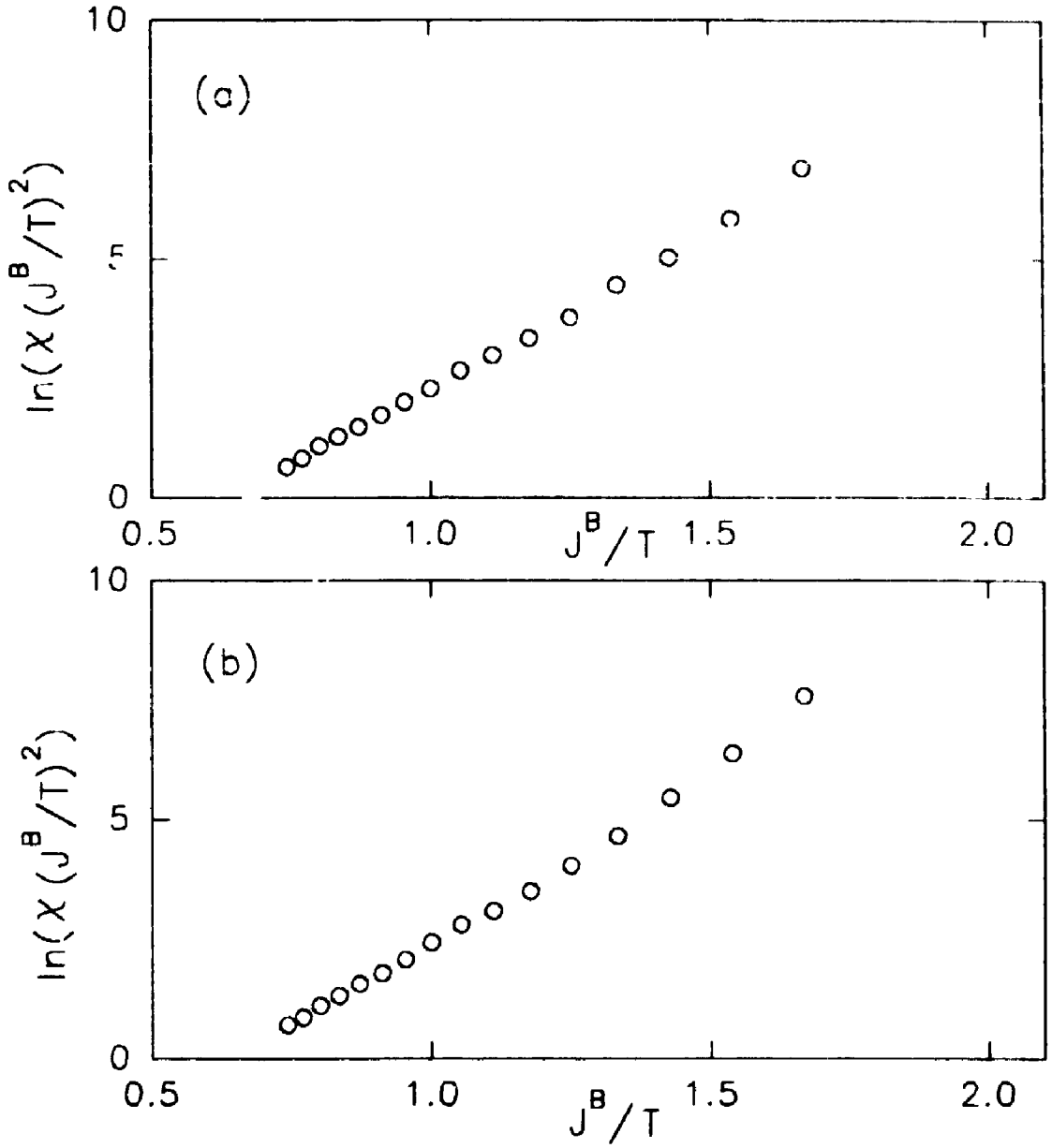

Fig. 14. Temperature behaviour of a two-layer film with (a) $J^T=0.02J^B$ and (b) $J^T=0.04J^B$. The lines are guides to the eye.

We also investigated the case of a very weak interlayer interaction, taking $J^T/J^B = 0.02$ and 0.04 (see Figs. 14 (a,b)). We conclude that even a weak interlayer interaction provides for changes in the critical behavior of the two-layer film, as within the chosen range of J^T the exchange renormalization η_λ appears to be different from the purely 2D value of 1 for $J^T = 0$.

3.6 CONCLUSIONS

The presented results of the numerical simulation of the critical properties of $S = \frac{1}{2}$ Heisenberg thin films provide for three main conclusions:

1. The thin film displays the effective 2D behavior with the in-plane exchange parameter being renormalized;

2. The renormalization of the exchange depends on the number of monolayers in the film, the site dilution, and the value of the interlayer interaction.

3. The mechanism providing for the crossover to the 2D behaviour is the saturation of the surface-surface correlations in the film.

The obtained results illustrate new types of behavior and also they should be helpful in the attempt to develop an analytic theory for such films. Our investigations of the Heisenberg ferromagnetic thin films have resulted in several publications (see Refs. 64, 65, 73).

CHAPTER 4.

BRILLOUIN LIGHT SCATTERING FROM DIPOLE-EXCHANGE MICROWAVE SPIN WAVES IN MAGNETIC FILMS

4.1. INTRODUCTION

A brief introduction to spin waves (SW) and their study by Raman and Brillouin light scattering was given in Section 1.4. A general description of the progress (up to about 1986) in light scattering from spin waves can be found in the book by Cottam and Lockwood (Ref. 4). Some review accounts, dealing mainly with Brillouin light scattering (BLS) measurements in magnetic films and multilayers, have been given (for example) by Grunberg (Refs. 74, 75) and Dutcher (Ref. 76).

From the kinematics of BLS it is easily deduced (Ref. 4) that the spin waves participating in the light scattering have wave vectors $\mathbf{q}$ close to the Brillouin zone center. Typically $|\mathbf{q}|$ is of order 10^6 cm^{-1}, although the value depends on the laser wavelength, the scattering geometry, and the refractive index of the magnetic medium. Usually this corresponds to the region of *dipole-exchange spin waves*, in which the long-range magnetic dipole-dipole interactions and the short-range exchange interactions both influence the spin-wave properties. Approximate descriptions of BLS in ferromagnets can be obtained in some cases by using magnetostatic

theory; for example, the early experiments (Refs. 92, 93) on BLS from EuO, Fe, and Ni showed strong scattering from a surface spin wave that approximated to the Damon-Eshbach surface magnetostatic mode (Ref. 77). However, light scattering experiments performed in different magnetic materials in thin-film and multilayer geometries have shown conclusively (Refs. 74, 75) that a full theory of BLS from magnetic excitations should take into account both the dipole-dipole and exchange interactions in the material, as well as the anisotropies at the surfaces and interfaces of the sample.

The earlier theories of BLS from dipole-exchange spin waves (SW) in ferromagnetic films (Refs. 78, 79) give, in general, a good overall picture of the process and are in fair agreement with the experimental data. These light-scattering theories use essentially the same description of the dipole-exchange SW spectrum of the film as developed originally by De Wames and Wolfram (Ref. 80, see also Refs. 81 - 83). In this approach the initial system (consisting of a linearized Landau-Lifshitz equation for the magnetization, Maxwell's equations in the magnetostatic limit, and electrodynamic and exchange boundary conditions) is reduced to a bicubic equation for the values of SW wave number. This equation can then be solved numerically to obtain the frequencies of the SW modes. Consequently the theory of BLS from dipole-exchange SW modes involves lengthy numerical calculations, whether one uses a treatment based on Green

functions (Ref. 78) or on the application of statistical mechanics to the SW normal modes of the film (Ref. 79).

In this Chapter we elaborate a theory of light scattering from magnetic excitations in ferromagnetic films which takes into account the relevant interactions and, moreover, yields explicit *analytical* expressions for the light-scattering cross sections from surface and bulk SW modes (Refs. 84 - 87).

In order to achieve this we use the tensorial Green-function method introduced by Vendik and Chartorizhskii (Ref. 78) and later further developed by Kalinikos and Slavin (Refs. 89, 90, 91, 92) for the dipole-exchange SW spectrum. The advantage of this method lies in the fact that it yields a simple approximate analytical solution for the SW frequencies in films, while still giving sufficient accuracy for practical applications. The method also allows one to obtain explicit analytical expressions for the SW linear-response functions which can then be employed to obtain analytically the BLS cross section. We illustrate the advantages of our approach by examining in detail the particular case of a perpendicularly magnetized ferromagnetic film with antisymmetric exchange boundary conditions. However, we also for completeness include the generalizations to other magnetization directions and to other boundary conditions.

4.2. FUNDAMENTALS OF LIGHT SCATTERING FROM SPIN WAVES

In this section we provide an account of the kinematics of BLS from the surface of a magnetic film. In particular, we obtain an expression for the differential scattering cross section for a general geometry and for general orientation of the static magnetization in the film, and we discuss the form of the magneto-optical coupling. Then we consider in more detail the results for the case of a 180° backscattering geometry and a perpendicularly magnetized film.

4.2.1 The differential cross section for BLS

We assume a general geometry (see Fig. 15) of backscattering from the upper surface of a ferromagnetic film of thickness L deposited on a nonmagnetic substrate. The axes X, Y, and Z are related to the film surface as shown, and do not necessarily coincide with the direction of static magnetization. The incident (I) and scattered (S) light beams are at angles θ_I and θ_S, respectively, to the Z axis and are in different vertical planes if angle $\phi \neq 0$. The special cases of a 180° backscattering geometry ($\theta_I = -\theta_S$, $\phi = 0$) and a 90° scattering geometry ($\theta_I + \theta_S = 90°$, $\phi = 0$) are typical of many surface BLS experiments.

From the translational symmetry in the XY plane, it follows that the excitation wave vector q parallel to the surface has components given by

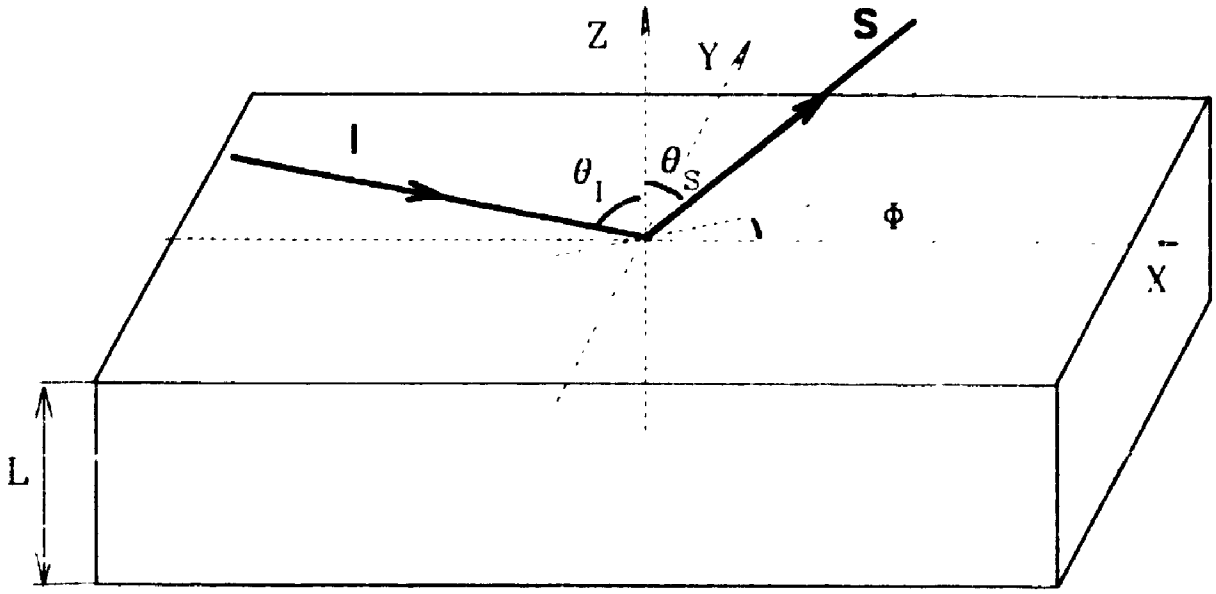

Fig. 15. The ferromagnetic film of thickness L, showing the coordinate axes and the directions of the incident (I) and scattered (S) light beams for a general BLS backscattering geometry.

$$q_X = (\omega_I/c)\sin\theta_I - (\omega_S/c)\sin\theta_S\cos\phi \ ,$$

$$q_Y = -(\omega_S/c)\sin\theta_S\sin\phi \qquad (75)$$

where ω_I and $\omega_S = (\omega_I - \omega)$ are the frequencies of the incident and scattered light, c is the velocity of light in vacuum, and the medium above the film ($Z > 0$) is assumed to have refractive index equal to 1. The cases of Stokes and anti-Stokes scattering correspond to $\omega > 0$ and $\omega < 0$ respectively. Denoting the wave vector of the light *inside* the film (with complex dielectric function ε for an optically absorptive medium) by **k**, we have

$$k_I^Z = (\omega_I/c)[\varepsilon - \sin^2\theta_I]^{1/2} \ ,$$

$$k_S^Z = (\omega_S/c)[\varepsilon - \sin^2\theta_S]^{1/2} \qquad (76)$$

as the complex components perpendicular to the surface. From the property of translational symmetry parallel to the surface, the in-plane components of the incident and scattered light wave vector inside the film are real and correspond to $k_I^X = (\omega_I/c)\sin\theta_I$, $k_I^Y = 0$, $k_S^X = (\omega_S/c)\sin\theta_S$, and $k_S^Y = (\omega_S/c)\sin\theta_S\sin\phi$.

The Green-function formalism for calculating the differential cross section for BLS in magnetic films is already well established (see, e.g., Refs. 4, 78, and 93) with most studies being for the case of tangentially-magnetized films. The scattering process may be divided into three stages:

Stage 1. The incident light with wave vector k_I and frequency ω_I is

partially transmitted from the vacuum region ($Z > 0$) to the magnetic film, where its wave vector becomes $\mathbf{k}_I$. The electric-field component μ ($\mu = X,Y,Z$) in the film is given simply by $f^\mu E_I^\mu$, where E_I^μ is the electric field in the vacuum and the the Fresnel coefficients f^μ are

$$f^X = 2k_I^Z/(k_I^Z + \epsilon k_I^Z) , \quad f^Y = 2k_I^Z/(k_I^Z + k_I^Z) ,$$

$$f_I^Z = f^X k_I^Z/k_I^Z \tag{77}$$

Stage 2. The incident light in the film interacts with a spin wave with wave vector $\mathbf{Q} = (\mathbf{q}, \kappa_n)$ and frequency ω. The components of $\mathbf{q}$ are real and given by Eq. (75), but the κ_n may be complex in general. Either κ_n is real for bulk modes, taking a series of discrete values as discussed later, or κ_n is complex (usually pure imaginary) for surface modes. The interaction produces a polarization in the film, and we denote its Fourier components by $P_{int}\exp[i(\mathbf{K}\cdot\mathbf{r}-\omega_S t)$ where $\omega_S = \omega_I - \omega$ and $\mathbf{K} = \mathbf{k}_I - \mathbf{q}$.

Stage 3. The induced polarization in the film produces a scattered beam with wave vector k_S and frequency ω_S in the vacuum region ($Z > 0$). The solution for the corresponding electric field gives

$$E_S^\mu = (\omega_S/\epsilon_o c)\exp(ik_S\cdot r)\sum_{q,\nu}\psi(B + \kappa_n)g^{\mu\nu}P_{int}^\nu \tag{78}$$

Here $B = (k_I^z + k_S^z)$ is a complex quantity depending on the optical wave vectors in the film, and we define

$$\psi(x) = [1 - \exp(ixL)]/x \tag{79}$$

The matrix $\mathbf{g}$ describes the transmission of the scattered beam through

the surface at Z = 0:

$$g = R \begin{pmatrix} \dfrac{-(c/\omega_S)k_S^Z k_S^Z}{\varepsilon k_S^Z + k_S^Z} & 0 & \dfrac{-(c/\omega_S)k_S^Z k_S^X}{\varepsilon k_S^Z + k_S^Z} \\ 0 & \dfrac{\omega_S/c}{k_S^Z + k_S^Z} & 0 \\ \dfrac{(c/\omega_S)k_S^Z k_S^X}{\varepsilon k_S^Z + k_S^Z} & 0 & \dfrac{(c/\omega_S)(k_S^Z)^2}{\varepsilon k_S^Z + k_S^Z} \end{pmatrix} R^{-1} \qquad (80)$$

where

$$R = \begin{pmatrix} \cos\phi & -\sin\phi & 0 \\ \sin\phi & \cos\phi & 0 \\ 0 & 0 & 1 \end{pmatrix} \qquad (81)$$

Using the above results for the scattered electric field, it is now straightforward to deduce the BLS cross section, which is proportional to $|E_S|^2$. The general expression for the differential cross section for scattering into an elementary solid angle $d\Omega$ with frequency between ω_S and $\omega_S + d\omega_S$ has the form (Ref. 4)

$$\frac{d^2h}{d\Omega d\omega_S} = [n(\omega) + 1]\ \mathrm{Im}\left[\sum_{n,n'} \psi(B + \kappa_n)^* \psi'(B + \kappa_{n'}) \times \sum_{\nu,\nu',\delta,\delta'} F(\nu,\delta,\nu',\delta') \ll (\chi^{\delta\nu})^* ; \chi^{\delta'\nu'} \gg \right] \qquad (82)$$

where the n and n′ refer to summations over the discrete SW modes of

the film, $n(\omega)$ is the Bose-Einstein thermal factor, and the indices ν, δ, ν', δ' refer to Cartesian components. The function F depends on the electric field polarizations, the optical transmission coefficients at the surface, and the scattering geometry. In terms of the quantities defined above, it is given by

$$F(\nu,\delta,\nu',\delta') = -\frac{\bar{A}\omega_I\omega_S^3\cos^2\theta_S}{2\pi^2c^4}\sum_{\mu,\mu'} e_S^{\mu}e_S^{\mu'}(f^{\nu})^{*}f^{\nu'}e_I^{\nu}e_I^{\nu'}(g^{\mu\delta})^{*}g^{\mu'\delta'} \tag{83}$$

where e_I is the unit polarization of the incident beam, and we assume that the polarization e_S is selected ir the scattered beam. Also $\bar{A}$ is the area of the film surface through which the scattered beam emerges. Finally the term in Eq. (82) of the form $\langle\langle\chi^{*};\chi\rangle\rangle$ is a Green function (Ref. 94), where χ is a component of the magnetization-dependent susceptibility tensor, which corresponds to the polarization P_{int}.

The susceptibility χ can be expanded (Ref. 4) in terms of components of the totai magnetization M in the film. If we suppose that the film has its static magnetization M_o along the z axis of a xyz coordinate system, the light scattering from single spin waves can occur in two ways: (i) *linear magneto-optical coupling*, involving terms in χ proportional to M^x and M^y, and (ii) *quadratic magneto-optical coupling*, involving terms $M^xM^z + M^zM^x$ and $M^yM^z + M^zM^y$. Usually the quadratic parts can be simplified by replacing

terms like $M^x M^z$ by $M^x M_o$ (ignoring quantum fluctuations in the z component), and M^x and M^y can then be replaced by the fluctuating magnetizations m^x and m^y, respectively. For a ferromagnetic material with cubic symmetry, the appropriate form of χ for substitution into Eq. (82) is

$$\chi = \begin{pmatrix} 0 & 0 & 2M_oGm^x - Km^y \\ 0 & 0 & 2M_oGm^y + Km^x \\ 2M_oGm^x + Km^y & 2M_oGm^y - Km^x & 0 \end{pmatrix} \quad (84)$$

where K and G are the coefficients of linear and quadratic magneto-optical coupling, respectively. They are proportional to the Faraday rotation and the magnetic linear birefringence, respectively, in the ferromagnet. We note from Eq. (84) that χ is antisymmetric in the case of linear magneto-optic coupling only (G = 0) and symmetric in the case of quadratic coupling only (K = 0); this property can be used in BLS experiments to distiguish between the two contributions (Ref. 4). From Eqs. (82) and (84) it follows that the light-scattering cross section is expressible in terms of the four basic Green functions $\langle\langle (m^x)^*; m^x \rangle\rangle$, $\langle\langle (m^x)^*; m^y \rangle\rangle$, $\langle\langle (m^y)^*; m^x \rangle\rangle$, and $\langle\langle (m^y)^*; m^y \rangle\rangle$. Their evaluation in terms of the dipole-exchange SW theory will be given later in this chapter.

It should be emphasized that Eq. (77)- (83) apply provided the magnetic film is sufficiently thick and/or opaque that light scattering processes involving multiple reflections at the lower film

surface (at Z = -L) can be neglected. The generalized formalism to include such effects is known (Ref. 93), and we shall later make use of this.

4.2.2. 180° Backscattering from a Perpendicularly Magnetized Film

We now consider the specific form of the expression for $d^2h/d\Omega d\omega_S$ in the case of 180° backscattering ($\theta_I = -\theta_S \equiv \theta$, $\phi = 0$) with crossed polarizations ($e_I \cdot e_S = 0$). This would be typical of many BLS experiments. Also it is assumed that the film is magnetized perpendicular to its surfaces, and so the XYZ and xyz axes coincide.

Consider first the case where the incident polarization is in the vertical plane, so that $e_I = (\cos\theta, 0, \sin\theta)$, and therefore the scattered polarization is $e_S = (0, 1, 0)$. The differential cross section is found from Eqs. (82)- (84) to be

$$\frac{d^2h}{d\Omega d\omega_S} = -\frac{\bar{A}\omega_I\omega_S^3\cos^2\theta\sin^2\theta}{2\pi^2c^4}\,[n(\omega)+1]\,|f^z g^{yy}|^2 \times$$

$$\mathrm{Im}\Big[\sum_{n,n'}\psi(B+\kappa_n)^*\psi(B+\kappa_{n'})\,\{\,|K|^2 \times$$

$$\langle (m^x)^*;\, m^x\rangle + 2M_o G^* K\,\langle (m^y)^*;\, m^x\rangle +$$

$$2M_o G\,K^*\langle (m^x)^*;\, m^y\rangle + 4M_o^2|G|^2\,\langle (m^y)^*;\, m^y\rangle\,\}\Big] \qquad (85)$$

On the other hand, if the polarizations are $e_I = (0, 1, 0)$ and $e_S = (\cos\theta, 0, \sin\theta)$, the required expression is

$$\frac{d^2h}{d\Omega d\omega_S} = -\frac{\bar{A}\omega_I\omega_S^3\cos^2\theta}{2\pi^2c^4}\,[n(\omega)+1]\,|f^y|^2[\cos^2\theta|g^{xz}|^2 + \sin^2\theta|g^{zz}|^2$$

$$+ \sin\theta\cos\theta\{(g^{xz})^*g^{zz} + (g^{zz})^*g^{xz}\}]\;\mathrm{Im}\Big[\sum_{n,n'}\psi(B+\kappa_n)^*\,\psi(B+\kappa_{n'})$$

$$\times\{|K|^2\,\langle(m^x)^*;\,m^x\rangle - 2M_oG^*K\,\langle(m^y)^*;\,m^x\rangle - 2M_oG\,K^*\langle(m^x)^*;\,m^y\rangle$$

$$+ 4M_o^2|G|^2\,\langle(m^y)^*;\,m^y\rangle\}\Big] \qquad (86)$$

4.3. NON-HYBRIDIZED SPIN WAVES AND GREEN FUNCTIONS

To obtain the equations for the dipole-exchange SW frequencies and the Green functions, we consider a ferromagnetic film of finite thickness L magnetized to saturation along the z-axis by an external bias field of magnitude H_e. Specifically we take the case of the static magnetization (denoted by M_o) perpendicular to the film surfaces. Hence the xyz and XYZ axes coincide, and the film surfaces correspond to the planes z = 0 and z = -L (see Fig. 15).

Following Refs. 89 and 90, we represent the variable magnetization $\mathbf{m}(z,\mathbf{r},t)$ of the film in the form

$$\mathbf{m}(z,\mathbf{r},t) = M_o\sum_n \mathbf{m}_{nq}\,\Phi_n(z)\,\exp[i(\omega t - \mathbf{q}\cdot\mathbf{r})] \qquad (87)$$

where $\mathbf{q}$ and $\mathbf{r}$ are respectively the two-dimensional SW wave vector and position vector in the film plane, and $\Phi_n(z)$ (with n denoting a mode index) are the SW modes defined in Ref. 89. The variable driving field $\mathbf{h}(z,\mathbf{r},t)$ can be written in a similar form to Eq. (87). The SW

modes form a complete orthonormal set of functions that satisfy a differential operator of the second order (an operator of the inhomogeneous exchange interaction) and the exchange boundary conditions (Ref. 89). In the present case of perpendicular magnetization the boundary condition at z = 0 has the simple form

$$\frac{\partial m^x}{\partial z} + d_1 m^x = 0 , \qquad \frac{\partial m^y}{\partial z} + d_1 m^y = 0 \tag{88}$$

where d_1 is a pinning parameter (related to the surface anisotropy constant, as explained below), and there is an analogous boundary condition at z = -L involving another pinning parameter d_2. The SW modes are the modes of spin wave resonance (SWR), and they correspond to

$$\Phi_n(z) = A_n \{\cos[\kappa_n(z+L)] + (d_1/\kappa_n)\sin[\kappa_n(z+L)]\} \tag{89}$$

Here κ_n is a transverse SW wave number which takes discrete values determined by the condition (Ref. 89):

$$[(\kappa_n)^2 - d_1 d_2] \tan(\kappa_n L) = \kappa_n (d_1 + d_2) \tag{90}$$

Negative and positive pinning parameters correspond to "easy-plane" and "easy-axis" types of surface anisotropy, respectively.

The SW mode frequencies and the corresponding magnetic Green functions (linear response functions) can readily be obtained using the formalism of Ref. 89 and the expansion in Eq. (87) in the case of a perpendicularly-magnetized film. The results are found to be

different for the non-degenerate (see below) and degenerate (see Sec. 4.5) cases.

In the case of non-degenerate SW modes (corresponding to $\omega_{nq} \neq \omega_{mq}$ for $n \neq m$) the SW frequencies are given approximately by

$$\omega_{nq} = [\Omega_{nq} (\Omega_{nq} + \omega_M P_{nn})]^{1/2} \tag{91}$$

where we have defined

$$\Omega_{nq} = \omega_H + \alpha\omega_M(q^2 + \kappa_n^2) \tag{92}$$

Here $\omega_H = \gamma(H_e - 4\pi M_0)$, $\omega_M = \gamma(4\pi M_0)$, γ is the gyromagnetic ratio, α is an exchange constant, and $P_{nn}(qL)$ is the diagonal matrix element of the dipole-dipole interaction (Ref. 89), namely

$$P_{nn}(qL) = \frac{1}{L}\int_{-L/2}^{L/2} dz dz' \frac{q}{2} \exp\{-q|z-z'|\}\Phi_n(z)\Phi_n(z'). \tag{93}$$

We note that our exchange parameter α and pinning parameter d are related to the exchange term A and surface anisotropy constant K_s, which are sometimes used by other authors, by $\alpha = A/(2\pi M_0^2)$ and $d = K_s/A$. As q varies from zero to infinity P_{nn} satisfies $0 \leq P_{nn} \leq 1$. The spin-wave Green functions (response functions) $\hat{C}_{nn}$ in the wave-vector representation are defined by

$$\begin{bmatrix} m^x_{nq} \\ m^y_{nq} \end{bmatrix} = \hat{C}_{nn} \begin{bmatrix} h^x_{nq} \\ h^y_{nq} \end{bmatrix} \tag{94}$$

We find (Refs. 89, 95) that these take the simple form $\hat{C}_{nn} =$

$\hat{Y}_{nn}\omega_M/(\omega^2 - \omega_{nq}^2)$, where the elements of the 2 x 2 matrix $\hat{Y}_{nn}$ are $Y_{nn}^{xx} = \Omega_{nq} + \omega_M P_{nr}$, $Y_{nn}^{yy} = \Omega_{nq}$, and $Y_{nn}^{xy} = -Y_{nn}^{yx} = i\omega$.

We next examine the above results in the particular case of antisymmetric exchange boundary conditions when the pinning parameters have equal magnitudes, but opposite signs, at the film surfaces (Ref. 95):

$$d_1 = -d_2 \equiv d, \qquad (d > 0) \tag{95}$$

It is then clear from Eq. (90) that the SW spectrum of the film consists of an infinite number of bulk SW dispersion branches ($\kappa_n = n\pi/L$ with $n = 1,2,\ldots$) and one surface SW branch ($\kappa_n = id$). We note that, in this case of perpendicular magnetization, the surface branch for $q \rightarrow 0$ lies *below* the spectrum of bulk SW modes. For general pinning, the solutions for κ_n can be obtained numerically from Eq. (90).

4.4. BRILLOUIN LIGHT SCATTERING FROM NON-HYBRIDIZED SPIN WAVES

The response functions $C_{nn}^{\alpha\beta}$ defined in Eq. (94) can be identified with the magnetic Green functions $\langle (m^{\alpha})^*; m^{\beta} \rangle$ for mode n which enter into the BLS formalism ($\alpha,\beta = x,y$). When the imaginary parts of these Green functions are taken in the expressions for the differential cross section $d^2h/d\Omega d\omega_S$ [e.g., see Eqs. (85) and (86)], the predicted BLS spectrum consists of a series of δ-function peaks at the discrete SW frequencies found in Sec. 4.3. The integrated

intensity $(dh/d\Omega)_n$ for mode n is proportional to the strength of the corresponding δ-function and behaves for Stokes scattering at $\omega_S = \omega_I - \omega_{nq}$ as

$$\left(\frac{dh}{d\Omega}\right)_n \propto \frac{|\psi(B + \kappa_n)|^2}{\omega_{nq}^2} \left[K(\Omega_{nq} + \omega_M P_{nn})^{1/2} + 2M_0 G(\Omega_{nq})^{1/2}\right]^2 \qquad (96)$$

where ω_{nq} and Ω_{nq} are defined in Eqs. (91) and (92), and we have approximated the Bose-Einstein factor by assuming $\hbar\omega_{nq} \ll k_B T$ where T is the temperature, since this inequality usually applies in BLS experiments. We have taken polarizations $e_I = (\cos\theta, 0, \sin\theta)$ and $e_S = (0, 1, 0)$, the overall proportionality factor in Eq. (96) is a function of the angle θ, the in-plane wave vector q, and the optical parameters, as can be deduced from Eq. (85). However, this factor is independent of κ_n (equal to id for the surface SW mode and $n\pi/L$ for a bulk SW mode). The corresponding result in the case of anti-Stokes scattering is obtained by the replacement $K \longrightarrow -K$. Hence we predict a Stokes/anti-Stokes asymmetry when both K and G contribute to the light scattering; this is analogous to the effect observed (Refs. 4, 96) in bulk BLS measurements on YIG. In many materials the dominant magneto-optical coupling corresponds to the K term (Ref. 4), and Eq. (96) then simplifies.

The theory has been applied to the SW spectra and BLS from Fe films. The parameters for the Fe films are chosen as follows (Refs. 84, 93): the exchange constant $\alpha = 1.15 \times 10^{-13}$ cm^{-2}, $4\pi M_o = 21$ kG,

the external bias magnetic field H_e = 22.5 kOe, and the complex refractive index η = 2.72 + 2.86i at a wavelength λ = 488 nm for the incident light.

A numerical example of the predicted SW dispersion relations for perpendicularly-magnetized Fe films with antisymmetric pinning is given in Fig. 16. This corresponds to film thickness L = 20 nm and pinning parameter d = 2.5 $\times$ 10^5 cm^{-1}. There is no appreciable mode degeneracy and the surface branch lies below the first two (n = 1 and n = 2) bulk modes. Some numerical results are shown in Table 4.1 for the integrated BLS intensity I = $dh/d\Omega$ for the four lowest-frequency SW modes of a Fe film (surface mode S and n = 1, 2, 3 bulk modes) in this same case. We have taken angle θ = 45^0, implying q = 1.82 $\times$ 10^5 cm^{-1}. These results have obtained by employing Eq. (96) for the case of linear magneto-optical coupling only (G = 0), and the intensities are expressed relative to I_1 of the n = 1 bulk mode. The surface mode scattering is predicted to dominate in this example, and by analogy with experimental results in the parallel-magnetization geometry (Ref. 75) this would be expected for such a film thickness.

Table 4.1. Integrated intensities and frequencies for Brillouin scattering from an iron film

SW Mode	S	1	2	3
I/I_1	14.6	1	0.09	0.03
$\omega/2\pi$ (GHz)	7.20	21.5	71.2	154

For Fe films, in the case of different thickness or with different pinning parameters, we find that hybridization effects can become important. This is discussed in later sections.

The BLS results described so far are for cases where the light scattering processes do not involve *multiple* reflections of the incident or scattered light at the film surfaces. They are appropriate whenever the penetration depth of the light is less than the film thickness or if the (nonmagnetic) substrate has the same complex refractive index as the film itself. The formalism to include the multiple reflections in a very thin magnetic film has been given by Cottam (Ref. 93) and applied to transverse-magnetized films in a magnetostatic approximation. Now we summarize the method applied to perpendicular-magnetized films in our dipole-exchange theory and, in particular, we generalize Eq. (82) to include these effects, taking only the case of linear magneto-optical coupling ($G = 0$).

If the light incident from vacuum (in the region where $z > 0$)

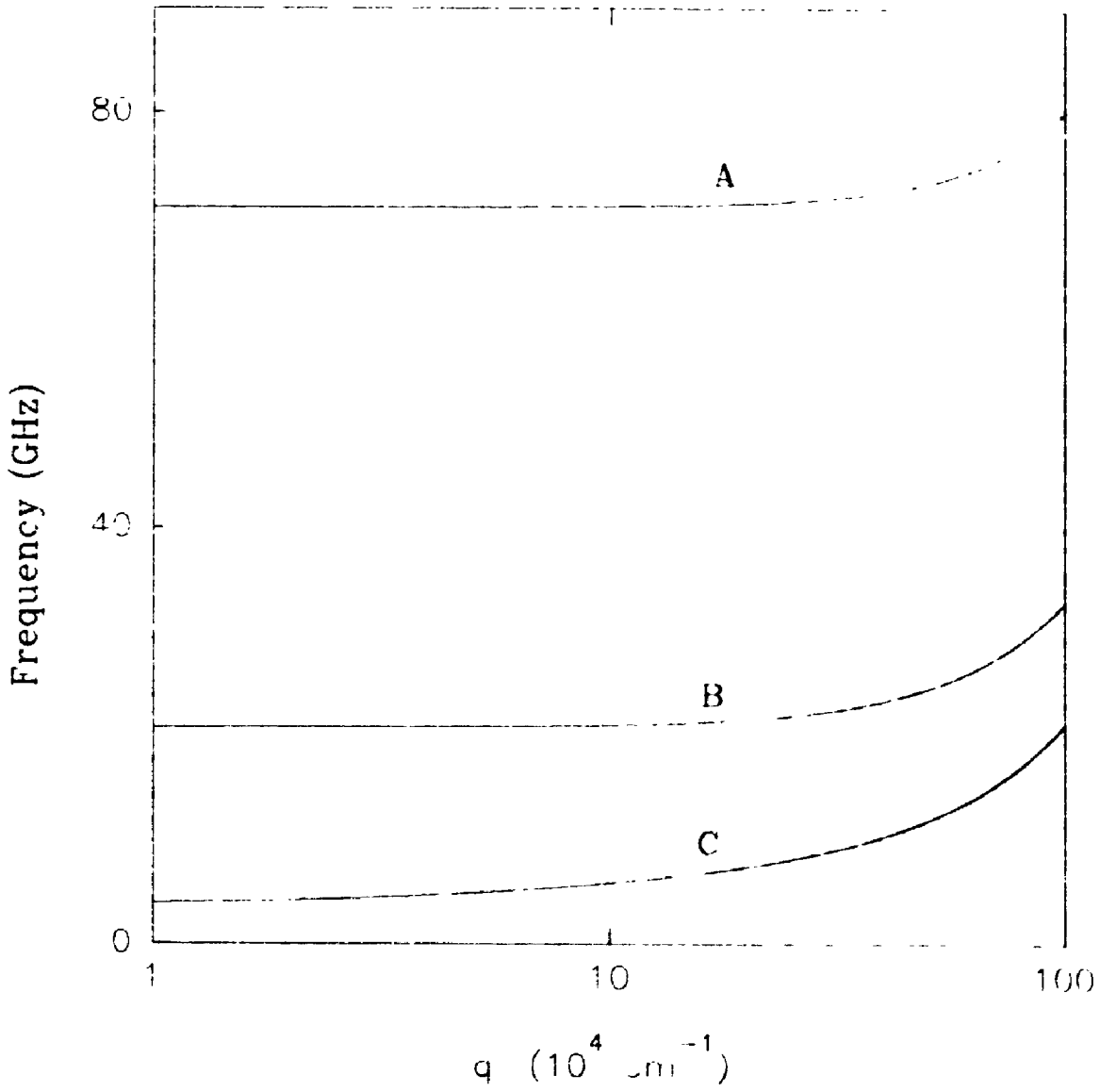

Fig. 16. The SW frequencies plotted against the in-plane wave vector q for a Fe film in the non-degenerate case, see text for the parameters. The n=1 and n=2 bulk modes (labeled B and A, respectively), and the surface mode (labeled C) are shown.

has electric field components $E_I^\nu \exp(-ik_I^z z)$, then the incident electric field components in the film are (Ref. 93):

$$E_I^\nu \left[f^\nu(k_I^z)\exp(-ik_I^z z) + F^\nu(k_I^z)\exp(ik_I^z z) \right] \qquad (97)$$

where, for convenience, we omit the common factor $\exp[i(\omega t - \mathbf{q}.\mathbf{r})]$. The coefficients f and F are, for example, given by

$$f^z(k_I^z) = -F^z(-k_I^z) = 2k_I^z(\varepsilon K_I^z + \varepsilon' k_I^z)/[(k_I^z + \varepsilon k_I^z)(\varepsilon K_I^z + \varepsilon' k_I^z) - (k_I^z - \varepsilon k_I^z)(\varepsilon K_I^z - \varepsilon' k_I^z)\exp(2ik_I^z L)] \qquad (98)$$

Here we follow the notation of Sec. 4.2 that k_I^z and k_I^z refer to wave-vector components in the vacuum and film respectively, and we denote the corresponding optical wave vector in the substrate by K_I^z. Also ε and ε' denote the complex dielectric functions of the film and substrate respectively. We note that, when $\mathrm{Im}(k_I^z L) \gg 1$, $f^z(k_I^z)$ becomes equal to the Fresnel coefficient in Eq. (77) and $F^z(k_I^z)$ vanishes.

For the choice of electric-field polarizations $e_I = (\cos\theta, 0, \sin\theta)$ and $e_S = (0, 1, 0)$, the required contribution to the electric field of the scattered light in the vacuum region that arises from magneto-optical coupling in the film with the $\exp(-ik_I^z z)$ term of Eq. (97) is (Ref. 93)

$$E_S^{(-)} = -(k_S^z)^2 P_{int} \exp(ik_S^z) \left[g_{yy}(k_S^z)\, \psi(k_I^z + k_S^z + \kappa_n) + g^{yy}(-k_S^z)\, \psi(k_I^z - k_S^z + \kappa_n) \right] \quad (99)$$

Here P_{int} is the polarization produced at the scattered light frequency due the coupling between the incident light and a SW with wave-vector component κ_n. The function ψ is defined in Eq. (79) and

$$g^{yy}(k_S^z) = (\omega_S/c)(K_S^z + k_S^z)/[(k_S^z + k_S^z)(K_S^z + k_S^z) - (k_S^z + k_S^z)(K_S^z + k_S^z)\exp(2ik_S^z L)] \quad (100)$$

The contribution $E_S^{(+)}$, which corresponds to the scattering produced from the coupling with the $\exp(ik_I^z z)$ term in Eq. (97), is given by a similar expression with k_I^z replaced by $-k_I^z$ in Eq. (99).

Finally, following the approach of Ref. 90 adapted to the present geometry, we conclude that Eq. (82) for the differential BLS cross section is generalized (in the case of linear magneto-optical coupling) by making the following replacement of factors:

$$|f^z g_{yy}|^2 [\psi(B + \kappa_n)]^* \psi(B + \kappa_n') \rightarrow \sum_{\sigma_I, \sigma_I', \sigma_S, \sigma_S'} \sigma_I \sigma_I' [f^z(\sigma_I k_I^z)]^* \times f^z(\sigma_I' k_I^z) [g_{yy}(\sigma_S k_S^z)]^* g^{yy}(\sigma_S' k_S^z) [\psi(\sigma_I k_I^z + \sigma_S k_S^z + \kappa_n)]^* \times \psi(\sigma_I' k_I^z + \sigma_S' k_S^z + \kappa_n) \quad (101)$$

where the σ indices are each summed over the values +1 and -1.

We have made further BLS calculations for EuO films, for which the exchange effects are weaker than for Fe. Also the optical penetration is larger (about 150 nm) in EuO, and so the multiple-reflection effects (including a dependence on the optical constants of the *substrate* as well as those of the magnetic film itself) become more important. For EuO films we take (Refs. 75, 84) $\alpha = 4.6 \times 10^{-15}$ cm^{-2}, $4\pi M_o = 23.8$ kG, $H_e = 25.3$ kOe, and $\eta = 1.6 + 0.25i$ at $\lambda = 514.5$ nm. However, it turns out that SW hybridization effects are significant for these parameter values in EuO, and so we discuss the BLS results later in Sec. 4.6.

4.5. HYBRIDIZED SPIN WAVES AND GREEN FUNCTIONS

In the previous section we pointed out certain cases where the hybridization of the SW modes should be taken into account. It is very difficult to treat analytically the hybridization of more than two modes at once. However, in most cases we encounter only the situation where the modes are degenerate in pairs. The occurrence of three or more dispersion branches of the spectrum almost crossing is very rare.

In the case of degeneracy of a pair of SW modes with numbers n and m ($\omega_{nq} = \omega_{mq}$) the hybridized SW dispersion branches ω_{nm} are found, following Ref. 89, to satisfy

$$2\,\omega_{nm}^2 = (\omega_{nq}^2 + \omega_{mq}^2) \pm \left[(\omega_{nq}^2 - \omega_{mq}^2)^2 + 4\,\Omega_{nq}\Omega_{mq}\omega_M^2\,P_{nm}^2\right]^{1/2} \qquad (102)$$

where P_{nm} is a non-diagonal matrix element of the dipole-dipole interaction (Ref. 89). We note that Eq. (27) is a secular equation which removes the degeneracy of "diagonal" dipole-exchange modes ω_{nq} and ω_{mq} by taking into account the *non-diagonal* dipole-dipole hybridization of these modes in the first order of standard perturbation theory. The small parameter of this perturbation theory is proportional to the ratio of the *non-diagonal* matrix element P_{nm} of the dipole-dipole interaction to the difference between the eigenfrequencies of the unperturbed modes, as discussed in detail in Ref. 89.

The spin-wave Green functions in the degenerate case are now expressible in terms of a 4 x 4 matrix, due to "mixing" between the modes. They can be derived following earlier work (Refs. 89, 90), except that it is more convenient here to use a representation in terms of the quantities $a_{nq} \equiv m^{+}_{nq} = m^{x}_{nq} + im^{y}_{nq}$ and $a^{*}_{nq} \equiv m^{-}_{nq} = m^{x}_{nq} - im^{y}_{nq}$ instead of m^{x}_{nq} and m^{y}_{nq}; these are the circular polarizations of the spin-wave mode with the label n and in-plane wave vector q. The corresponding result to Eq. (94) in the degenerate case is

$$\left(\hat{D}_{nm} + (\omega/\omega)\hat{L}_{nm} \right) a_{nmq} = h_{nmq} \qquad (103)$$

where $\hat{L}$ = diag(-1,1,-1,1) is a diagonal matrix and

$$\mathbf{a}_{nmq} = \begin{bmatrix} a_{nq} \\ a^{*}_{n,-q} \\ a_{m,q} \\ a^{*}_{m,-q} \end{bmatrix}, \qquad \mathbf{h}_{nmq} = \begin{bmatrix} h^{+}_{nq} \\ h^{-}_{n,-q} \\ h^{+}_{mq} \\ h^{-}_{m,-q} \end{bmatrix} \tag{104}$$

Here $h^{\pm}_{nq}$ are the polarizations of the external magnetic field (along the film normal) in the Fourier representation, and the 4x4 matrix $\hat{D}_{nm}$ (which contains the dipole-exchange and pinning effects) is given by

$$\hat{D}_{nm} = \frac{1}{2} \begin{bmatrix} 2N_n + P_{nn} & P_{nn} & P_{nm} & P_{nm} \\ P_{nn} & 2N_n + P_{nn} & P_{nm} & P_{nm} \\ P_{mn} & P_{mn} & 2N_m + P_{mm} & P_{mm} \\ P_{mn} & P_{mn} & P_{mm} & 2N_m + P_{mm} \end{bmatrix} \tag{105}$$

where $N_n = \Omega_{nq}/\omega_M$ and expressions for the dipole-dipole interaction matrix elements P_{nm} (which depend on the pinning conditions) are written explicitly in Ref. 89. From Eq. (103), the tensorial Green function for the linear-response relationship $\mathbf{a}_{nmq} = \hat{G}_{nm}\, \mathbf{h}_{nmq}$ can be written as

$$\hat{G}_{nm} = \left(\hat{D}_{nm} + (\omega/\omega_M)\hat{L}_{nm} \right)^{-1} \tag{106}$$

The hybridization (or mixing) of the SW dispersion branches is caused by the long-range dipolar interaction; it can be ignored only if the branches are well separated. To find the representation in which the matrix $\hat{G}_{nm}$ becomes diagonal we need to perform a general

Bogolyubov transformation which takes into account the interaction between the two modes (Ref. 97):

$$a_{nq} = U_{n1,q}\alpha_{1q} + U_{n2,q}\alpha_{2q} + V^{*}_{n1,-q}\alpha^{*}_{1,-q} + V^{*}_{n2,-q}\alpha^{*}_{2,-q}$$
$$a^{*}_{nq} = U^{*}_{n1,q}\alpha^{*}_{1q} + U^{*}_{n2,q}\alpha^{*}_{2q} + V_{n1,-q}\alpha_{1,-q} + V_{n2,-q}\alpha_{2,-q} \qquad (107)$$

and there are similar expressions for a_{mq} and a^{*}_{mq}. Here α_{gq} and α^{*}_{gq} (with g = 1,2) are the new canonical variables for the nm and mn hybridized modes (labeled arbitrarily above as 1 and 2). They are chosen for their Green functions to have the form:

$$\langle\langle \alpha_{gq}; \alpha^{*}_{g',q} \rangle\rangle = \delta_{gg'}/[\omega - \omega_g(q)] , \qquad (108)$$

$$\langle\langle \alpha^{*}_{gq}; \alpha_{g',q} \rangle\rangle = -\delta_{gg'}/[\omega + \omega_g(q)], \qquad (109)$$

with $\omega_g(q)$ being the hybridized frequencies as given by Eq. (102), or equivalently obtained from the roots of $\det[\hat{D}_{nm} + (\omega/\omega_M)\hat{L}_{nm}] = 0$. Note that, in the present geometry of a perpendicularly magnetized film, we have $\omega_g(q) = \omega_g(-q)$.

To calculate the light-scattering (BLS) spectra we need (see Sec. 4.2) the Green functions $\langle\langle m^{\mu}_{nq}; m^{\nu}_{mq} \rangle\rangle$ with $\mu,\nu = x,y$. We can rewrite them in the terms of a and a^{*}; for example

$$\langle\langle (m^{x}_{nq})^{*}; m^{x}_{mq} \rangle\rangle = \frac{1}{4}\left[G^{++}_{nm} + G^{+-}_{nm} + G^{-+}_{nm} + G^{--}_{nm}\right] \qquad (110)$$

where $G^{++}_{nm} = \langle\langle a^{*}_{nq}; a^{*}_{m,-q} \rangle\rangle$, $G^{+-}_{nm} = \langle\langle a^{*}_{nq}; a_{mq} \rangle\rangle$, $G^{-+}_{nm} = \langle\langle a_{n,-q}; a^{*}_{m,-q} \rangle\rangle$,

and $G^{--}_{nm} = \langle\langle a_{n,-q}; a_{mq} \rangle\rangle$.

Assuming a transformation as in Eq. (107), the coefficients U_{nm} and V_{nm} can be found from the requirement that the Hamiltonian has a diagonal form in α and $\alpha^{\dagger}$. This corresponds to the Green functions having the form of Eqs. (108) and (109). Then, using Eqs. (107)- (109) and the definitions following Eq. (110), we can write

$$G^{++}_{nm} = \frac{V_{n1,-q}U^{*}_{m1,-q}}{\omega - \omega_1(-q)} + \frac{V_{n2,-q}U^{*}_{m2,-q}}{\omega - \omega_2(-q)} - \frac{U^{*}_{n1,q}V_{m1,q}}{\omega + \omega_1(q)} - \frac{U^{*}_{n2,q}V_{m2,q}}{\omega + \omega_2(q)}$$

$$G^{--}_{nm} = \frac{U_{n1,-q}V^{*}_{m1,-q}}{\omega - \omega_1(-q)} + \frac{U_{n2,-q}V^{*}_{m2,-q}}{\omega - \omega_2(-q)} - \frac{V^{*}_{n1,q}U_{m1,q}}{\omega + \omega_1(q)} - \frac{V^{*}_{n2,q}U_{m2,q}}{\omega + \omega_2(q)}$$

$$G^{+-}_{nm} = \frac{V_{n1,-q}V^{*}_{m1,-q}}{\omega - \omega_1(-q)} + \frac{V_{n2,-q}V^{*}_{m2,-q}}{\omega - \omega_2(-q)} - \frac{U^{*}_{n1,q}U_{m1,q}}{\omega + \omega_1(q)} - \frac{U^{*}_{n2,q}U_{m2,q}}{\omega + \omega_2(q)}$$

$$G^{-+}_{nm} = \frac{U_{n1,-q}U^{*}_{m1,-q}}{\omega - \omega_1(-q)} + \frac{U_{n2,-q}U^{*}_{m2,-q}}{\omega - \omega_2(-q)} - \frac{V^{*}_{n1,q}V_{m1,q}}{\omega + \omega_1(q)} - \frac{V^{*}_{n2,q}V_{m2,q}}{\omega + \omega_2(q)} \qquad (111)$$

On the other hand, the above Green functions are also given by the elements of the matrix reciprocal to $[\hat{D}_{nm} + (\omega/\omega_M)\hat{L}_{nm}]$. Using Cramer's rule for the elements of the reciprocal matrix, we obtain:

$$G^{-+}_{nn} = \frac{\Delta_{11}(q,\omega)}{\Delta(q,\omega)}, \qquad G^{-+}_{mm} = \frac{\Delta_{33}(q,\omega)}{\Delta(q,\omega)} \qquad (112)$$

where $\Delta(q,\omega) = \det[\hat{D}_{nm} + (\omega/\omega_M)\hat{L}_{nm}]$ and $\Delta_{11}(q,\omega)$ and $\Delta_{33}(q,\omega)$ are the minors of the (1,1) and (3,3) elements, respectively. Next, taking into account that

$$\Delta(q,\omega) = \left(\omega - \omega_1(q)\right)\left(\omega - \omega_2(q)\right)\left(\omega + \omega_1(-q)\right)\left(\omega + \omega_2(-q)\right) \quad (113)$$

and making the expressions in Eqs. (111) and (112) equal for $\omega = \pm\omega_g(\pm q)$ for g = 1,2, we obtain the following expressions for the U and V coefficients:

$$U_{n1,q} = \left[\frac{\Delta_{11}(\omega_1^+)}{(\omega_1^+ - \omega_2^+)(\omega_1^+ + \omega_1^-)(\omega_1^+ + \omega_2^-)}\right]^{1/2} e^{i\psi_1(q)}$$

$$U_{n2,q} = \left[\frac{\Delta_{11}(\omega_2^+)}{(\omega_2^+ - \omega_1^+)(\omega_2^+ + \omega_2^-)(\omega_2^+ + \omega_1^-)}\right]^{1/2} e^{i\psi_2(q)}$$

$$V_{n1,q} = \left[\frac{\Delta_{11}(-\omega_1^+)}{(\omega_2^+ - \omega_1^+)\cdot(\omega_1^+ + \omega_2^-)(\omega_1^+ + \omega_1^-)}\right]^{1/2} e^{i\psi_1(q)}$$

$$V_{n2,q} = \left[\frac{\Delta_{11}(-\omega_2^+)}{(\omega_1^+ - \omega_2^+)(\omega_1^- + \omega_2^+)(\omega_2^+ + \omega_2^-)}\right]^{1/2} e^{i\psi_2(q)}$$

$$U_{m1,q} = \left[\frac{\Delta_{33}(\omega_1^+)}{(\omega_1^+ - \omega_2^+)(\omega_1^+ + \omega_1^-)(\omega_1^+ + \omega_2^-)}\right]^{1/2} e^{i\psi_1(q)}$$

$$U_{m2,q} = \left[\frac{\Delta_{33}(\omega_2^+)}{(\omega_2^+ - \omega_1^+)(\omega_2^+ + \omega_2^-)(\omega_2^+ + \omega_1^-)}\right]^{1/2} e^{i\psi_2(q)}$$

$$V_{m1,q} = \left[\frac{\Delta_{33}(-\omega_1^+)}{(\omega_2^+ - \omega_1^+)(\omega_1^+ + \omega_2^-)(\omega_1^+ + \omega_1^-)}\right]^{1/2} e^{i\psi_1(q)}$$

$$V_{m2,q} = \left[\frac{\Delta_{33}(-\omega_2^+)}{(\omega_1^+ - \omega_2^+)(\omega_1^- + \omega_2^+)(\omega_2^+ + \omega_2^-)}\right]^{1/2} e^{i\psi_2(q)} \qquad (114)$$

The phases $\psi_1(q)$ and $\psi_2(q)$ cannot be obtained using this approach. To determine them we can use the condition for the Bogolyubov transformation to be canonical, i.e., to keep unchanged the form of Hamilton's equations of motion:

$$\sum_j \left[U_{nj}U^*_{mj} - V_{nj}V^*_{mj}\right] = \delta_{nm} , \quad \sum_j \left[U_{nj}V_{mj} - V_{nj}U_{mj}\right] = 0 \qquad (115)$$

The analytical expressions for the phases $\psi_1(q)$ and $\psi_2(q)$ are rather cumbersome. However, when examining the conditions in Eq. (115) numerically, we found out that one can set the phases equal to either 0 or π, as appropriate, without any appreciable change of accuracy.

The expressions derived in Eq. (114) differ slightly from those in Ref. 97. This difference is due to the different choice of the Green functions in Eq. (112). However, our choice seems more appropriate, because it leads to expressions that are more symmetric with respect to the mode indices.

The Green functions in Eq. (110) can eventually be written, using the above Bogolyubov transformation and the solutions for the U and V coefficients, as

$$\ll (m^{x}_{nq})^{*};\ m^{x}_{mq} \gg \ = \ \frac{1}{2} \sum_{g=1,2} \left[\frac{A_{gnm}(q)}{\omega - \omega_g(q)} - \frac{(A_{gnm}(q))^{*}}{\omega + \omega_g(q)} \right] \qquad (116)$$

where

$$A_{gnm}(q) \ = \ \frac{S_{nm}(q,\omega)\ S^{*}_{mn}(q,\omega)}{2\omega_g(q)\ [\omega^2_g(q) - \omega^2_{3-g}(q)]}\ , \qquad (g = 1,2)\ ,$$

$$S_{nm}(q,\omega) \ = \ (\Delta_{11}(q,\omega))^{1/2} + (\Delta_{11}(q,-\omega))^{1/2} \qquad (117)$$

where $\Delta_{11}(q,\omega)$ has been defined earlier.

It is worthwhile mentioning that all the above-written expressions reduce to those for the non-degenerate case for those values of wave vector q that are far from the region of repulsion of the SW branches. This is due to the fact that, far from the region of repulsion, the small parameter of the perturbation theory, which is proportional to $P_{nm}/(\omega^2_n - \omega^2_m)$, approaches zero.

4.6. BRILLOUIN LIGHT SCATTERING FROM HYBRIDIZED SPIN WAVES

We now assume, as in Sec. 4.5, that for any given in-plane wave number q we have only two SW modes (labeled n and m) that are appreciably hybridized. For simplicity, we restrict attention to the usual case of linear magneto-optical coupling, so that only the Green function $\ll (m^{x})^{*};\ m^{x} \gg$ is required [see Eqs. (85) and (86)]. Using results from Sec. 4.4, we eventually find that the contribution to $d^2h/d\Omega d\omega_S$ from the hybridized modes is proportional to

$$\sum_{g=1,2} \frac{1}{\omega_g(q)} \left[|\psi(B + \kappa_n)|^2 A_{gnn}(q) + |\psi(B + \kappa_m)|^2 A_{gmm}(q) \right.$$

$$\left. + 2\,\mathrm{Re}[\psi^*(B + \kappa_n)\psi(B + \kappa_m)\, A_{gnm}(q)] \right] \left[\delta(\omega - \omega_g) + \delta(\omega + \omega_g) \right] \tag{118}$$

The integrated intensities for BLS are given by strengths of the δ-functions in Eq. (118) multiplied by the appropriate Fresnel coefficients and magneto-optical constants.

In Fig. 17, which corresponds to L = 50 nm and d = 2.5×10^5 cm^{-1} for a Fe film, we have an example of a degeneracy near q ~ 1.1×10^5 cm^{-1} between the surface and n = 1 bulk modes, and the resulting hybridized modes (full lines) are calculated using Eq. (102). In Fig. 18 we display the dependences of the SW eigenfrequencies on the pinning parameter d, taking fixed in-plane wave vector q = 1.82×10^5 cm^{-1}. The surface-mode frequency decreases with increasing d, going to zero at a characteristic value d_o, which lies far from the hybridization region of the dispersion curves and can be approximately deduced from the non-degenerate dispersion relationship $\omega_S = \omega_H + \alpha\omega_M(k^2 - d_o^2) = 0$; it is of interest for the light scattering behavior. The softening of this mode (labeled C in the non-hybridized case and E in the hydridized case) occurs because the pinning at one of the surfaces behaves like an effective anisotropy field that opposes the applied magnetic field. Also some SW dispersion curves showing hybridization effects for EuO films of

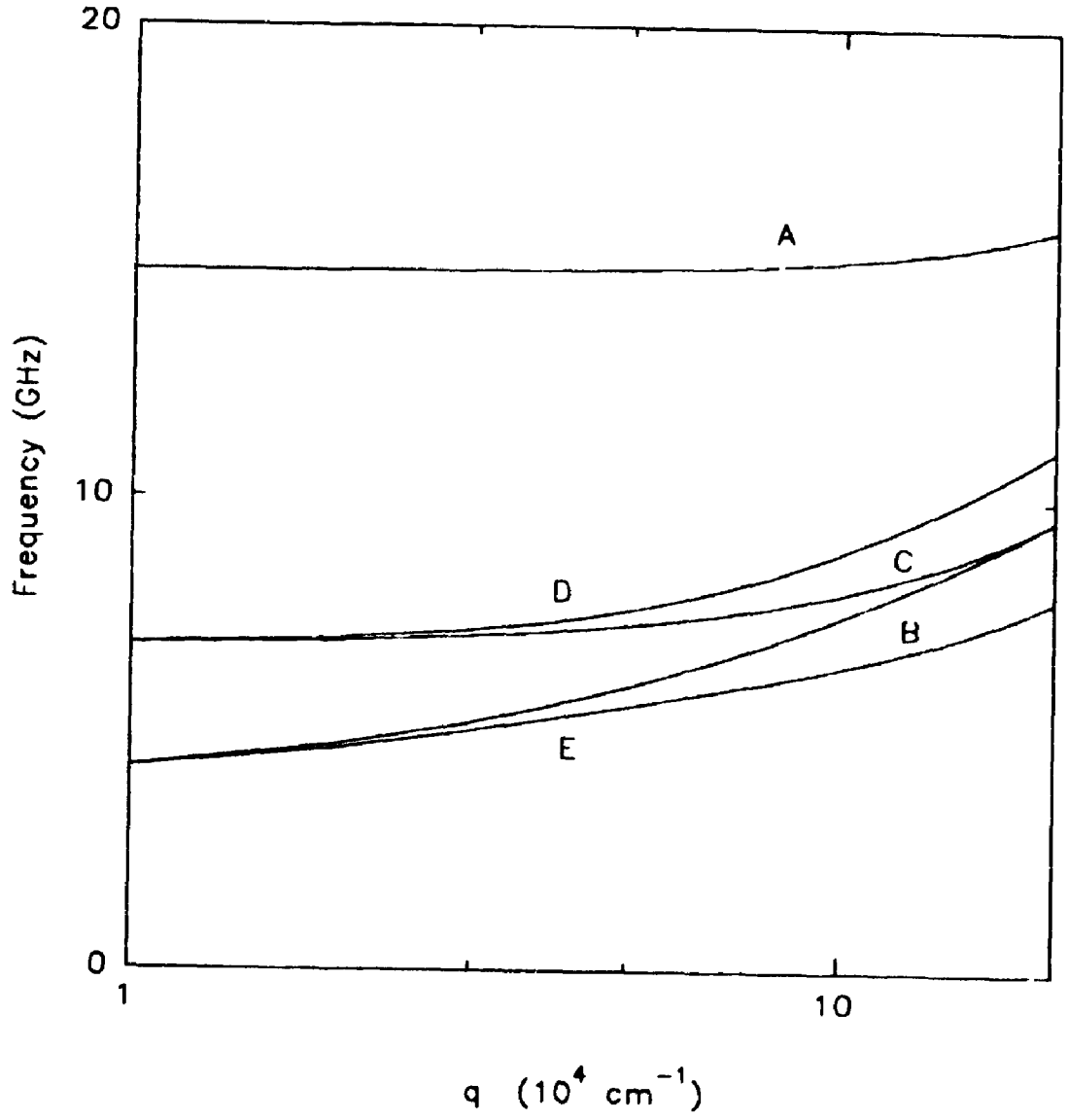

Fig.17. The SW dispersion relations for a Fe film; see text for the parameters. The notations are: A – the n=2 bulk mode; D,E – the hybridized n=1 bulk and surface modes; B,C – the non-hybridized n=1 bulk and surface modes.

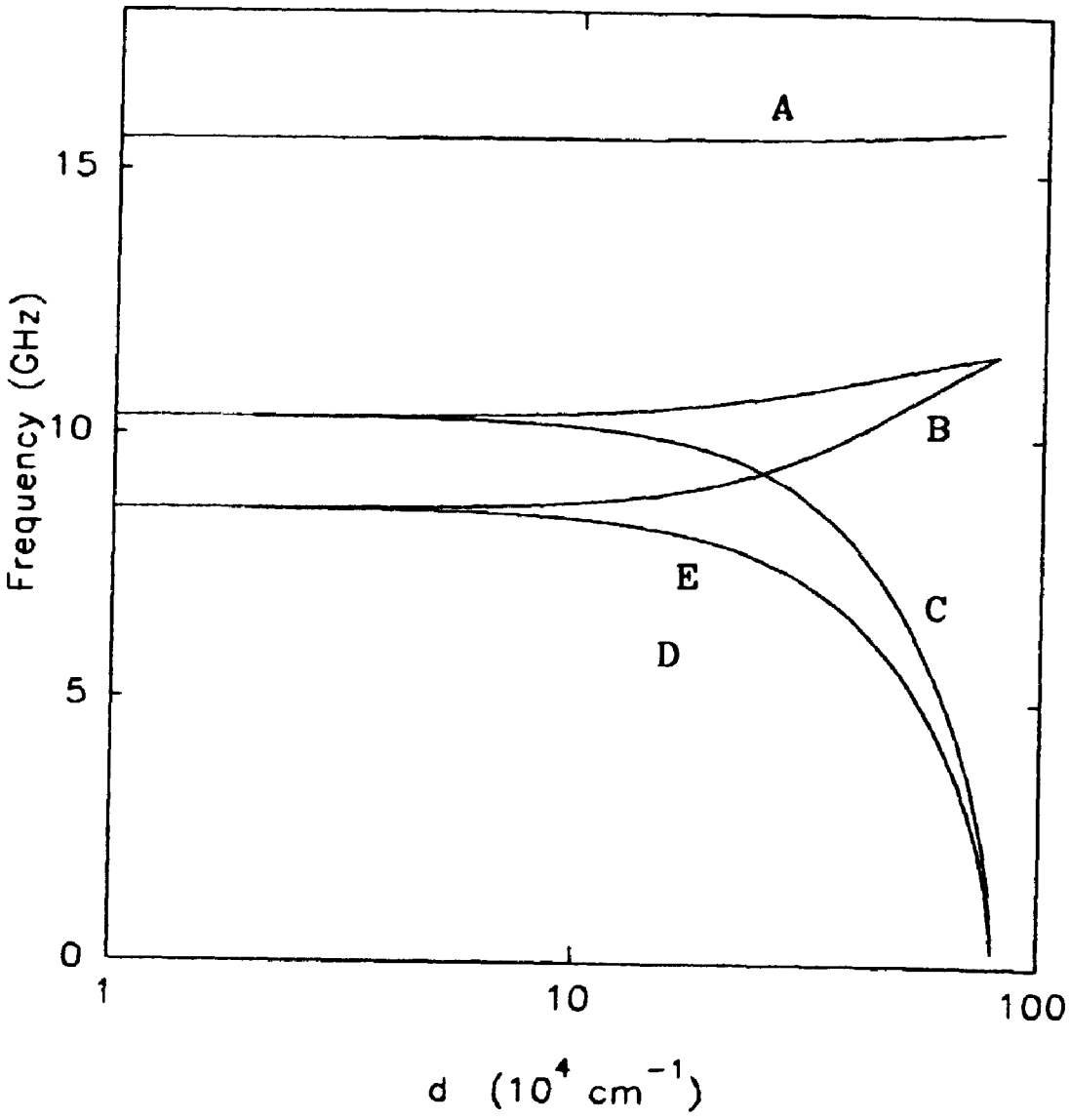

Fig.18. The SW eigenfrequencies versus pinning d for a Fe film, see text for the parameters. The mode hybridization occurs at around $d = 2*10^5$ cm^{-1}. The notations are the same as for Fig. 17.

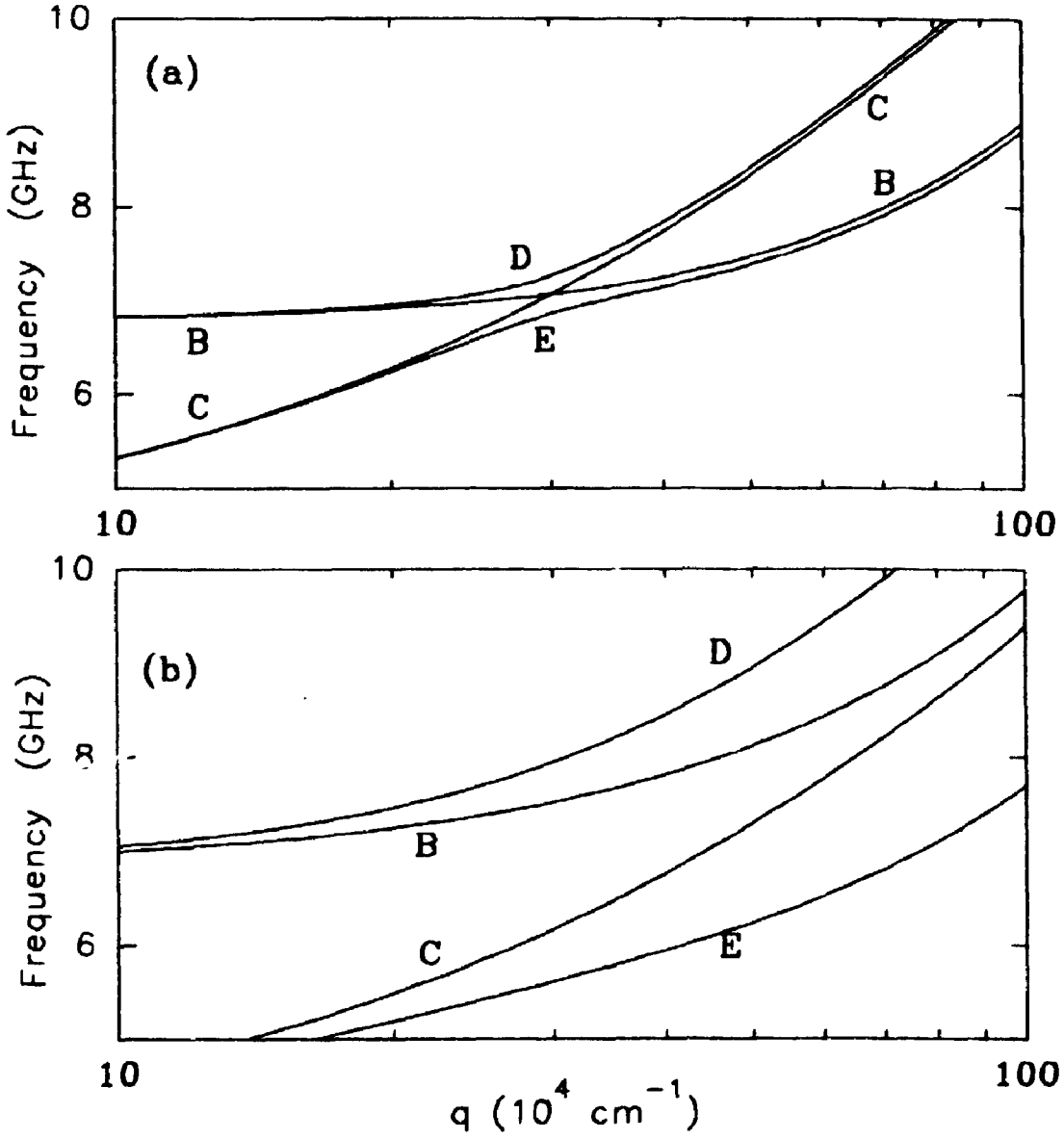

Fig.19. The SW dispersion relations for a EuO film for two different values of the pinning parameter: (a) $d=2*10^5$ cm^{-1}; (b) $d=1.4*10^5$ cm^{-1}; see text for the other parameters. The notations are: D, E – the hybridized n=1 bulk and surface modes; B,C – the non–hybridized n=1 bulk and surface modes.

thickness 10 nm are shown in Fig. 19, taking two different values of d.

For other values of the parameters, the hybridization effects may strongly influence the BLS intensities. A plot of the integrated intensities of the scattered light from the hybridized n = 1 bulk and surface modes versus d is given in Fig. 20 for the same Fe film as in Fig. 17 with angle $\theta = 45^0$. The specific features in the behavior of both curves around $d \cong 2 \times 10^5$ cm^{-1} become clear when account is taken that this is the region of the hybridization of the dispersion relationships. The increase of the integrated BLS intensity from the mode labeled D corresponds to d approaching the value d_o (implying that the unhybridized surface SW frequency becomes very small). Because the optical penetration depth of Fe is relatively small (about 15 nm), we can neglect the multiple reflection of the scattered light from the lower surface of the film for the given film thicknesses.

We have made further BLS calculations for EuO films, for which multiple-reflection effects and a dependence on the (nonmagnetic) substrate material become important, as discussed at the end of Sec. 4.4. Using the parameter values quoted earlier, we show some numerical calculations in Fig. 21. In the main figure the BLS integrated intensity is plotted against film thickness L for two different choices of substrate material, namely silicon (with complex

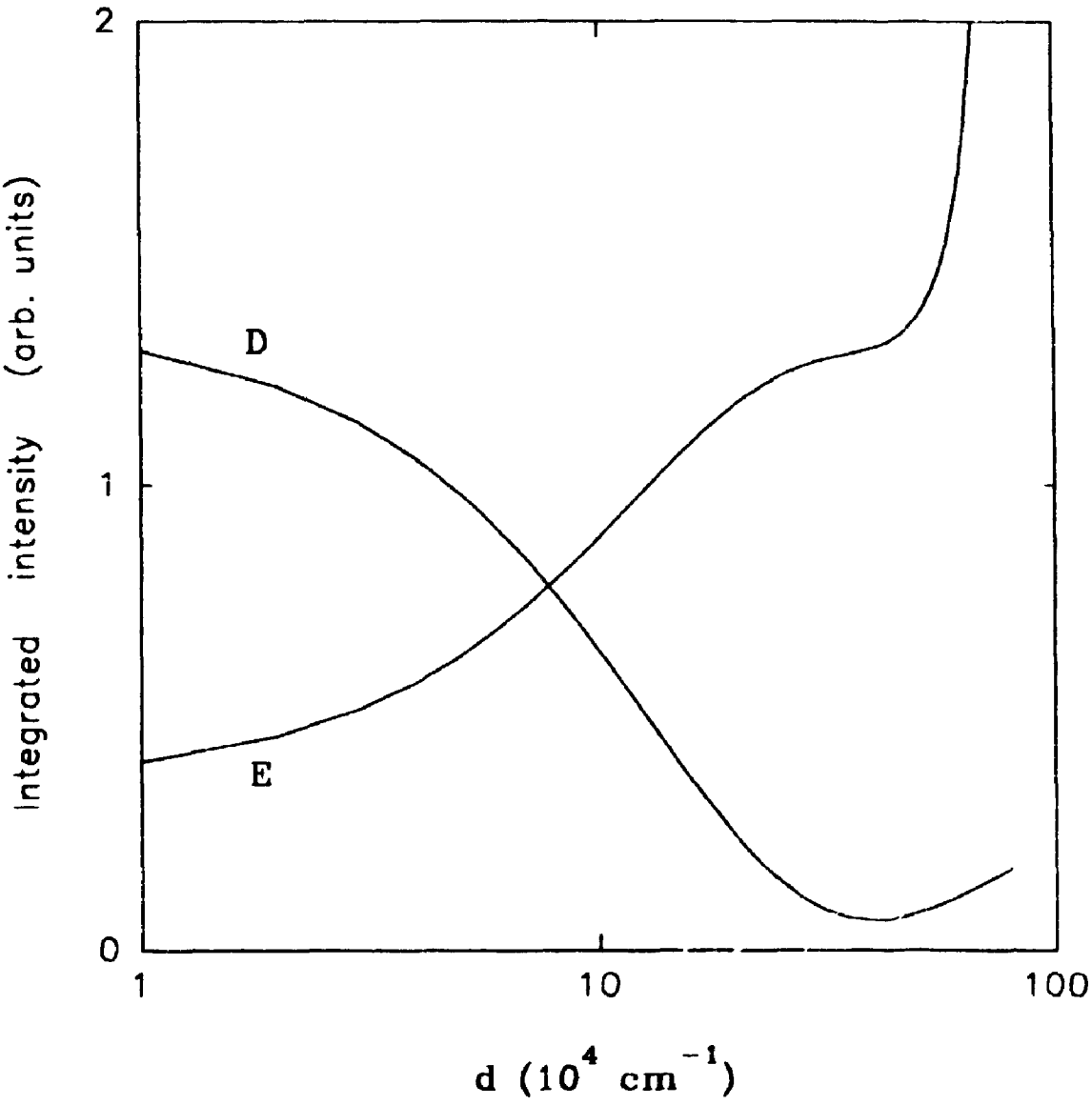

Fig. 20. The integrated intensities of the BLS for a Fe film with backscattering angle equal to 45^0 versus pinning parameter d, using the same parameters, as in Fig. 17. The curves D and E correspond to the hybridized n=1 bulk and surface modes.

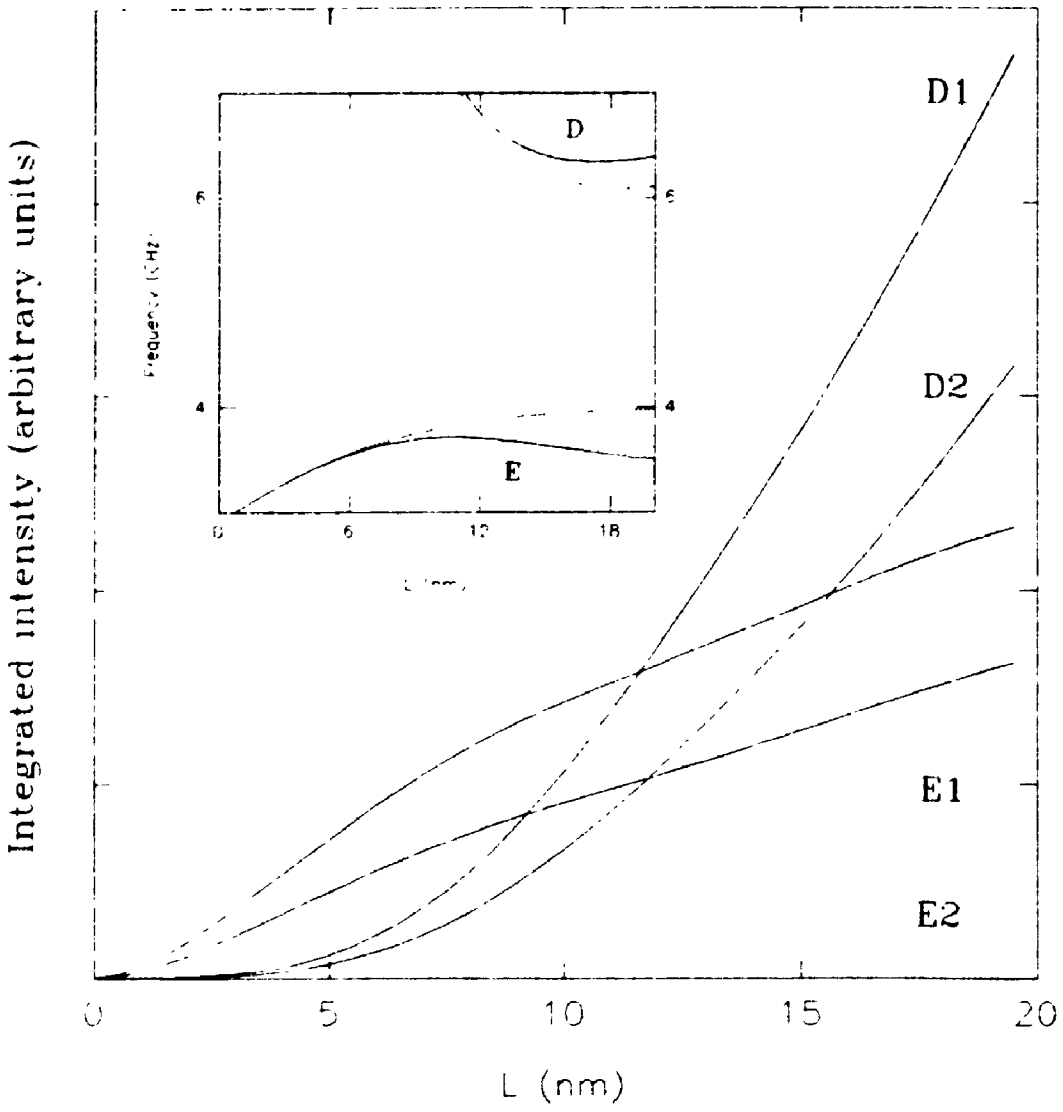

Fig.21. The integrated BLS intensities and SW frequencies (see inset) for a EuO film for the hybridized surface and n=1 bulk SW modes. The BLS results are shown as a function of film thickness L for two choices of substrate corresponding to silicon (curves D1 and E1, respectively) and to sapphire (curves D2 and E2). See the text for parameter values.

refractive index (4.3 + 0.1i) and sapphire (1.77 + 0.01i). We have used the BLS formalism described in Sec. 4.4, and it should be noted that the surface SW mode and the n = 1 bulk SW mode are strongly hybridized for part of the range of L being considered (see the inset to Fig. 21). For larger values of L, the surface mode becomes hybridized, in turn, with the bulk SW modes of larger n.

4.7. MODIFICATION OF PINNING CONDITIONS

The case of antisymmetric pinning is of physical interest, because there are effective ways to control the magnitude and sign of the pinning at each film surface (Ref. 95). Nevertheless, experimentally it is hard to achieve *purely* antisymmetric pinning, and so we discuss the situation when the pinning conditions are not exactly antisymmetric.

The general equation for the SW perpendicular wavenumber κ_n in the case of pinning d_1 and d_2 at the two surfaces is given in Eq. (90). In the purely antisymmetric case, the solutions are just the bulk waves with $\kappa_n = n\pi/L$ and the surface wave with $\kappa_n = \pm id$, as discussed earlier. If κ^* denotes any one of these solutions , then for the case of not purely antisymmetric pinning we may define $\kappa_n = \kappa^*(1 + \delta)$, with $d_1 \equiv d$ and $d_2 \equiv -d(1 + \varepsilon)$, assuming $|\varepsilon| << 1$ and $|\delta| << 1$. We then find, by linearizing Eq. (90), that the approximate solutions correspond to (in terms of δ):

$$\delta \simeq \begin{cases} \varepsilon[1 - \exp(-2dL)]^{-1} , & \text{for a surface wave} \\ -\varepsilon(d/L)[(n\pi/L)^2 + d^2]^{-1} , & \text{for bulk wave n} \end{cases} \quad (119)$$

For any value of ε in the linear regime, we see that *real* solutions for δ occur in both above cases. Hence the wavenumber κ_n corresponding to the surface wave remains imaginary, and the bulk wave wavenumber remains real.

A numerical analysis shows that, within the given range of the parameters, the ratio δ/ε for the bulk wave is rather small. This leads us to conclude that the bulk wave is relatively stable with respect to deviations from the antisymmetric case. For a surface wave, we conclude from Eq. (119) that δ/ε becomes larger as the pinning parameter d becomes smaller. However, the dispersion relationships in the regime of small d are rather flat, and so even a significant shift in κ_n does not change the frequency appreciably (e.g., the change is only a few percent or less). Some numerical results for the dependence of δ/ε on d are shown in Fig. 22, taking as an example $\varepsilon = 0.3$.

4.8. CONCLUSIONS

We have demonstrated in this chapter a simple analytic approach to the calculation of cross sections and intensities for Brillouin light scattering from dipole-exchange spin waves in magnetic thin

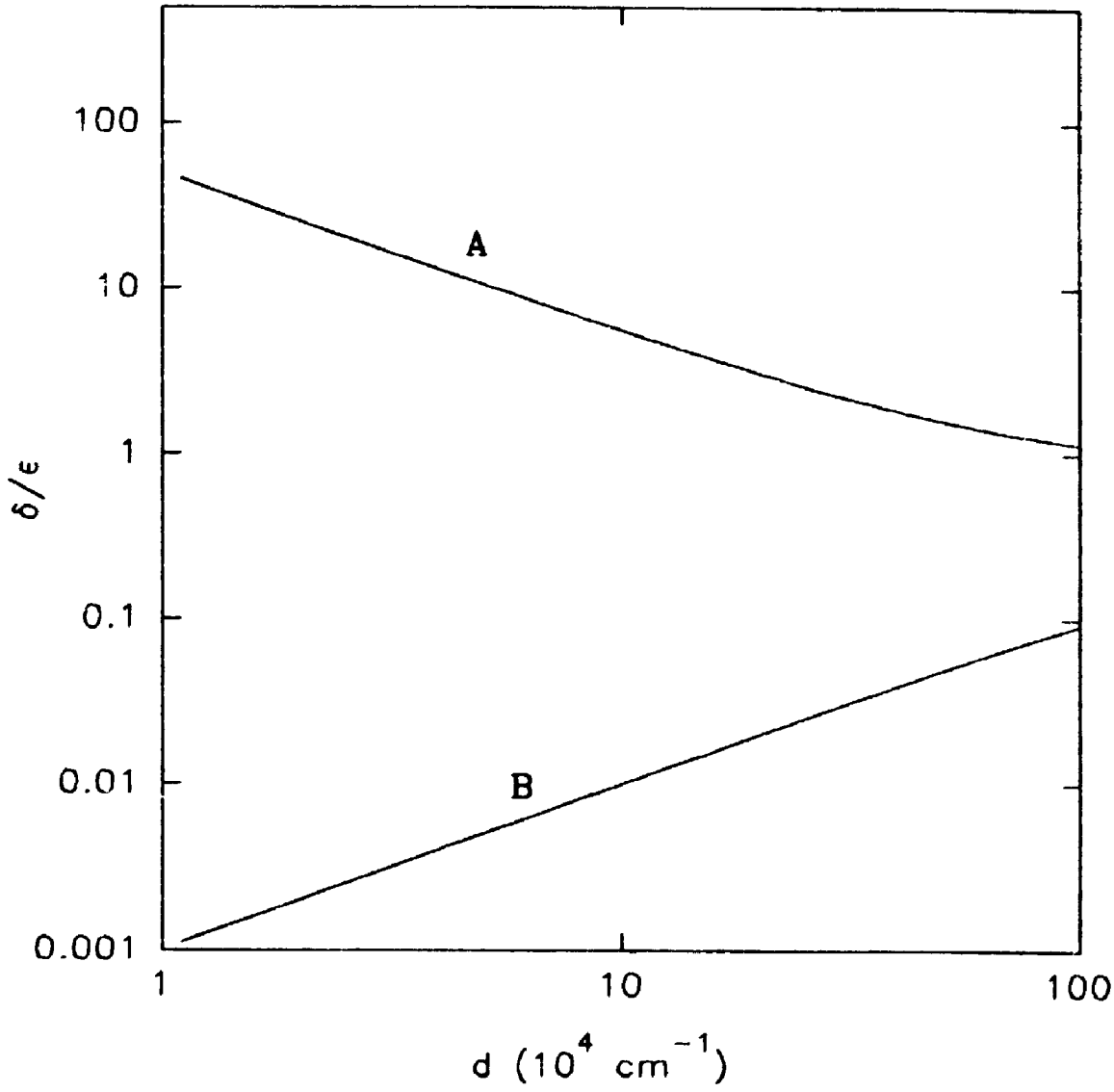

Fig. 22. The shift in the perpendicular SW wave vector (expressed in terms of the dimensionless parameter δ/ϵ for a fixed ϵ) as a function of d for the n=1 bulk mode (curve A) and the surface mode (curve B). We have taken ϵ =0.3 and L=10 nm.

films. We concentrated on the case of perpendicularly magnetized films with surface anisotropy (pinning) effects included. An advantage of this approach over previous methods, which were largely numerical, lies in the possibility to carry out the calculations analytically, e.g., in estimating analytically pinning effects or the relative contributions to the spectrum of BLS of such effects as dipole-dipole and exchange interactions.

The tensorial Green-function formalism for the spin-wave spectrum in magnetic films, which forms the basis of our approach, has recently been generalized for the case of anisotropic magnetic films magnetized in an arbitrary direction to the film normal (Ref. 105). Thus, using these results, it is straightforward to extend the above BLS formalism to the cases of anisotropic films and different static magnetization directions.

The results of our theoretical study of the BLS from the thin magnetic films have been published in several papers (see refs. 85, 86, 87).

CHAPTER 5.

SPIN WAVE SPECTRA IN THE MAGNETIC MULTILAYER STRUCTURES

5.1. INTRODUCTION

Recently considerable attention has been attracted to spin wave phenomena in sandwich, or multilayer, structures consisting of alternating magnetic and non-magnetic layers (see a detailed review of the most recent results in Ref. 106 and references therein).

A typical multilayer structure is depicted in Fig. 23. The magnetic layer usually represents a metallic (Fe, Co, Ni, etc) thin film, the spacer consisting of a nonmagnetic metal (Pd, Pt, Cu, Au, Ag, etc). The thicknesses of the magnetic layer and spacer may vary, in general being of the order of 10 to 100 Å. As well, a number of investigations has been devoted to the special case of a bilayer structure, e.g. $Ni_{0.8}Fe_{0.2}/Pd/Ni_{0.8}Fe_{0.2}$ (Ref. 99) or Co/Au/Co (Ref. 112).

The magnetic layers in the system can be treated as non-interacting only in the zero-order approximation. First of all, there is a substantial long-range dipole-dipole (magnetostatic) interaction between the magnetic layers across the thickness of the nonmagnetic spacer layers. Second, recently in a number of publications and conference presentations the effect of an exchange

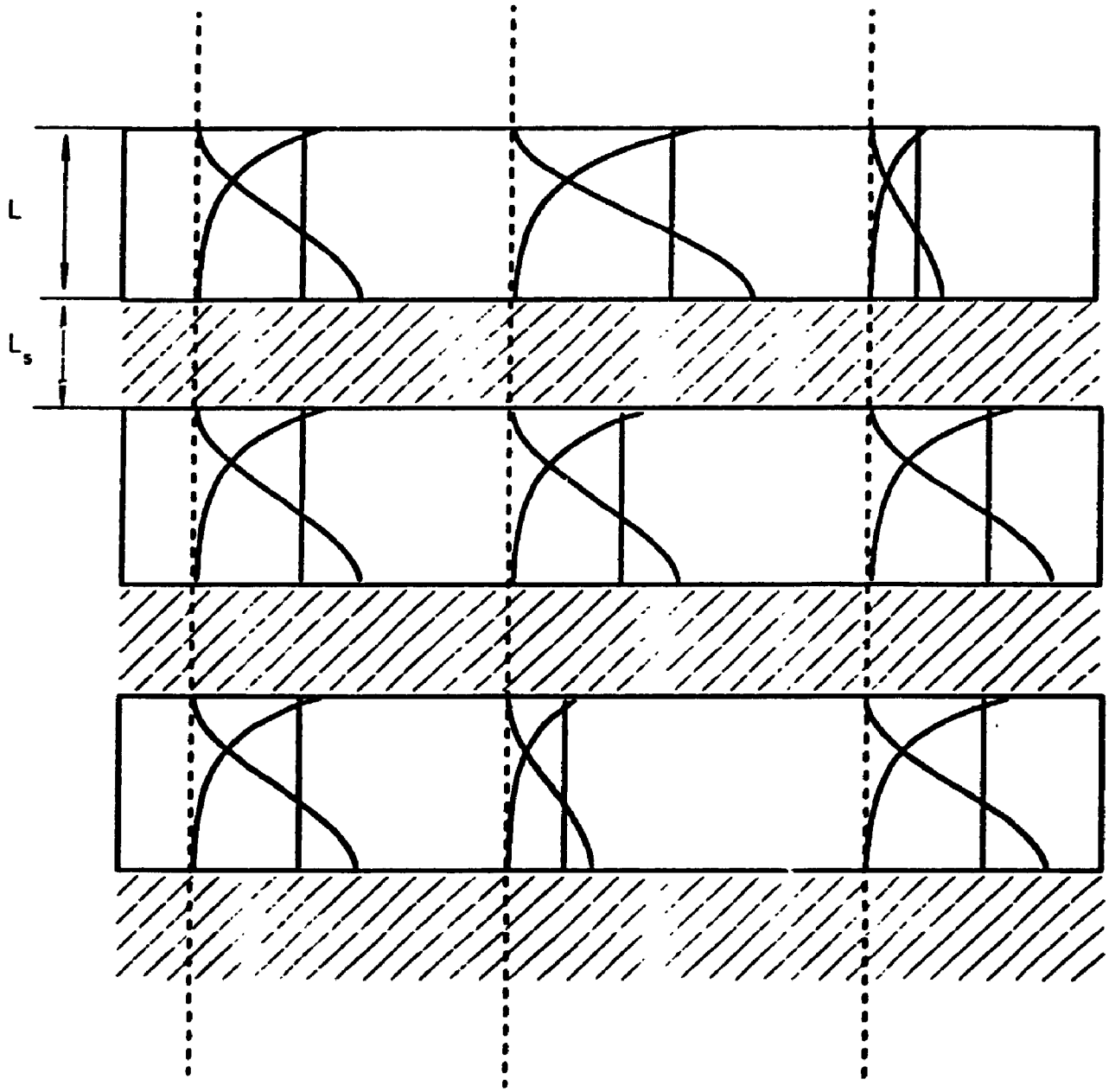

Fig. 23. A typical multilayer structure. The curves show schematic mode amplitudes to illustrate the concept of composite modes.

interaction across the spacer has been discussed (see, e.g. the review Ref. 106, as well as Refs. 111, 110, 107, 108, 109). This exchange can have ferromagnetic, antiferromagnetic or oscillatory character and, in general, it depends on the spacer thickness and the magnetic properties of the magnetic layers. A major goal of the experimental and theoretical study of magnetic multilayers is to provide an opportunity to control the magnetic parameters, such as surface exchange anisotropy and intra- and interlayer exchange.

There are two basic techniques commonly used to investigate spin waves in such structures, namely, Magnetic Resonance (MR) (see Refs. 103, 107, 108) and Brillouin Light Scattering (BLS) (Refs. 99, 109). We note that the MR technique is designed to investigate the properties of the spin wave excitations with the in-plane wave vector $q=0$, whereas the BLS method operates within the range of $q \sim 10^5$-10^6 cm^{-1} as discussed in Chapter 4. Hence the influence of dipole-dipole interactions is different in the two cases.

A frequently used approach for a theoretical interpretation of BLS or MR in magnetic multilayers is that by Hillebrands et al (Refs. 109, 112, 100, 113). It is based on writing a set of coupled equations of motion for a multilayer structure to account for the different types of interactions of spins within the magnetic layers

as well as the interlayer interactions and different types of surface anisotropy. These equations are then solved numerically with the appropriate boundary conditions and the dispersion relationships of the SW excitations and the mode profiles are obtained. An advantage of this method is that it is relatively straightforward to apply to real systems and it is capable of giving a good quantitative interpretation for a number of experiments (see, e.g. Refs. 113, 99). However, the method, being completely numerical, does not provide analytical expressions for the the SW spectra. Although theoretical curves obtained adequately describe the existing experimental SW data, the theory involves lengthy numerical calculations of a rather cumbersome system of initial equations.

An alternative, analytical approach for magnetic multilayers is developed here (see as well Ref. 102). This approach is exactly analogous to the one discussed in Chapter 4 for the thin films and constitutes a Hamiltonian formalism combined with perturbation theory. Theoretically, there are two main ways to account for the interactions in the system within the framework of a Hamiltonian formalism. First, one can include all the interactions in the Hamiltonian, which then is appropriately diagonalized. Second, one can realize some of the interactions as the constraints, or boundary

conditions (like the pinning conditions described in Chapter 4). The connection between the two approaches, which are analytically equivalent, is made possible through the variational analysis technique (see e.g. Ref. 10). However, if one uses perturbation theory to diagonalize the Hamiltonian and obtain the dispersion relationships and SW mode profiles, the two approaches are not equivalent any more, because the perturbation technique results are known to be dependent on the choice of zero order eigenfunctions.

In this chapter we shall study the SW and BLS spectra of magnetic multilayers with the exchange-dipole interlayer and intralayer interactions included. The basic technique will be the same as used for the film geometry in the Chapter 3, but generalized by incorporating interlayer effects. Starting with the simplest case, in Section 5.2 we investigate the SW spectrum of a double magnetic layer system. We account for the interlayer exchange interaction by applying linearized Hoffmann boundary conditions. This corresponds to the second of the two approaches discussed above. The numerical results and application to the light scattering from the surface waves are presented in Section 5.3.

In Section 5.4. we study a multilayer structure with an arbitrary number of layers, including the interlayer exchange as an

energy term in the Hamiltonian. We propose a model for the envelope SW profiles in a multilayer constructed from the single film SW modes and discuss its applicability and limitati ns. As a special case of the general theory, we compare the obtained analytical expressions when there are just two magnetic layers with those derived in Section 5.2. As well, we discuss the interpretation of MR and BLS results for multilayers. Some concluding remarks are made in Section 5.5.

5.2. SPIN WAVE SPECTRUM FOR THE EXCHANGE-COUPLED DOUBLE-LAYER SYSTEM

Here we develop a simple, analytic approach, which is based on the same Green function formalism discussed in the previous Chapter 4 and accounts for dipole-dipole and exchange interactions within each ferromagnetic layer as well as dipole-dipole and exchange couplings between different layers.

Let us consider a perpendicularly magnetized layered structure consisting of two ferromagnetic films (labeled 1 and 2) of thicknesses L_1 and L_2, separated by a nonmagnetic layer of thickness b. The pinning constants $d_1^{s,i}$ and $d_2^{s,i}$ characterize pinning on the outer surface (s) and interface (i), respectively, of each film. The z axis is taken to be perpendicular to the planar surfaces and interfaces (with z=0 corresponding to the middle of the non-magnetic

spacer layer).

We assume that the interlayer exchange interaction is characterized by a phenomenological parameter $\beta_j = A_{12}/A_j$. Here A_j is a coefficient of overall exchange within layer j, and A_{12} is an interlayer exchange coefficient (see Refs. 98, 100 for the definitions). We should note here that, as the intralayer exchange represents interaction within the *bulk* of a layer, while interlayer exchange is effectively an interaction between the *surfaces* of different layers, the constants A_{12} and A_j have different units. Consequently, the parameter β is usually expressed in cm^{-1}. The typical experimental behavior of β as a function of spacer thickness b is discussed elsewhere (Refs. 99, 101). Depending on the materials and the structure, it can be positive, negative or oscillatory, being generally of the order of magnitude 10^6 cm^{-1}, when b is within the range of 10 - 100 Å. In our theory we use β as an empirical parameter already known either from microscopic calculations or from experiment.

The procedure of obtaining the SW spectrum for a multilayer system has already been developed (Refs. 102, 103) for the case of purely dipolar coupling between the layers. By analogy to Eq. (87) from Chapter 4, it is based on the expansion of the variable part of

variable part of magnetization $\mathbf{m}_j(\mathbf{R},t)$ and the dipolar field $\mathbf{h}^{dip}(\mathbf{R},t)$ of the layer j as a Fourier series of the following kind:

$$\mathbf{m}_j(\mathbf{R},t) = M_o \sum_{\mathbf{k}} \sum_{n} \mathbf{m}_{\mathbf{q}jn}\, \phi_{jn}(z)\, \exp[-i(\mathbf{q}\cdot\mathbf{r}-\omega t)] \qquad (120)$$

$$\mathbf{h}_j^{dip}(\mathbf{R},t) = \sum_{\mathbf{k}} \sum_{n} \mathbf{h}_{\mathbf{q}jn}^{dip}\, \phi_{jn}(z)\, \exp[-i(\mathbf{q}\cdot\mathbf{r}-\omega t)] \qquad (121)$$

where the functions $\phi_{jn}(z)$ for the case of two layers should be taken in the form:

$$\phi_{1n}(z) = A_{1n}\cos\left[\kappa_{1n}\left(z + \frac{b}{2} + L_1\right)\right] + B_{1n}\sin\left[\kappa_{1n}\left(z + \frac{b}{2} + L_1\right)\right]$$

$$\phi_{2n}(z) = A_{2n}\cos\left[\kappa_{2n}\left(z - \frac{b}{2} - L_2\right)\right] + B_{2n}\sin\left[\kappa_{2n}\left(z - \frac{b}{2} - L_2\right)\right] \qquad (122)$$

where κ_{jn} are the transverse discrete wave numbers, $\mathbf{R}=(\mathbf{r},z)$ is a three-dimensional position vector, $\mathbf{r}$ being its in-plane component. Below we sometimes drop one or both subscripts of κ_{jn}, where this does not cause ambiguity. To incorporate the effects of interlayer exchange coupling into the theory (Ref. 102), we require that the eigenfunctions (122) satisfy the linearized Hoffmann boundary conditions (Ref. 99):

$$-\frac{\partial\phi_{1n}}{\partial z} + d_1^s\phi_{1n}\Big|_{z=-\left(L_1+\frac{b}{2}\right)} = 0$$

$$\frac{\partial \phi_{2n}}{\partial z} + d_2^s \phi_{2n}\Big|_{z=\left(L_2+\frac{b}{2}\right)} = 0$$

$$\frac{\partial \phi_{1n}}{\partial z} + \left(d_1^i + \beta_1\right)\phi_{1n}\Big|_{z=-\frac{b}{2}} - \frac{M_{o1}}{M_{o2}}\beta_1 \phi_{2n}\Big|_{z=\frac{b}{2}} = 0$$

$$-\frac{\partial \phi_{2n}}{\partial z} + \left(d_2^i + \beta_2\right)\phi_{2n}\Big|_{z=\frac{b}{2}} - \frac{M_{o2}}{M_{o1}}\beta_2 \phi_{1n}\Big|_{z=-\frac{b}{2}} = 0 \qquad (123)$$

where M_{oj} is the static magnetization in the film j, and $d_j^{s,i}$ are the pinning parameters at the outer surface and interface, respectively. In particular, in the case of a symmetric structure consisting of two identically magnetized layers (i.e., $L_1 = L_2 \equiv L$, $d_1^{i,s} = d_2^{i,s} \equiv d^{i,s}$, $\beta_1 = \beta_2 \equiv \beta$, $M_{o1} = M_{o2} \equiv M_o$), there are two types of SW modes - one symmetric and one antisymmetric with respect to the mid-plane of the structure. We can show that for this case Eqs. (123) lead to

$$\left(\kappa^2 - d^s d^i\right)\tan(\kappa L) = \kappa\left(d^s + d^i\right) \qquad (124)$$

for the *symmetric* modes, i.e., the modes with the variable magnetization in the both layers distributed symmetrically, and

$$\left(\kappa^2 - d^s(d^i+2\beta)\right)\tan(\kappa L) = \kappa\left(d^s + (d^i+2\beta)\right) \qquad (125)$$

for the *antisymmetric* modes.

Equation (124) is formally the same as Eq. (90) for a single

(uncoupled) layer of thickness L. Equation (125) has a similiar form but with a modification of the interface pinning due to the interlayer exchange β, i.e., $d^i \rightarrow d^i + 2\beta$. Thus we conclude that the interlayer coupling affects only antisymmetric modes. In particular, in the case of unpinned surface spins ($d^i = d^s = 0$) we recover from Eq. (125) all the results for transverse wave numbers of antisymmetric modes obtained in Ref. 98. It also follows from earlier results (Refs. 89, 104) that when $d^i = d^s = 0$ for $\beta > 0$ we get only *real* solutions for κ (bulk modes). On the other hand, for $\beta < 0$, along with the infinite number of bulk solutions, we obtain one (lowest energy) surface solution with imaginary κ. By making the replacement $d^i \rightarrow d^i + 2\beta$, we can apply all the conclusions of the previous Chapter to describe quantitatively the SW dispersion in exchange coupled magnetic double layers.

Using Eqs. (124) and (125) to calculate the transverse SW wave numbers κ_n and the formalism (Ref. 102) developed for dipolar coupling of magnetic layers we can derive an approximate dispersion relation for SW propagating in a magnetic double layer consisting of two identical magnetic films coupled by both dipole-dipole and exchange interactions. In the particular case of the coupling of two identical modes (with label n) in both films we get the following

dispersion relation for a double layer:

$$(\omega_n^{\pm})^2 = \Omega_n(\Omega_n + \omega_M P_{nn}) \pm (\omega_M \Omega_n P_{nn}^{12}) \qquad (126)$$

where the "+" sign corresponds to antisymmetric modes, the "-" sign corresponds to symmetric modes, and $\Omega_n = \Omega(\kappa_n)$ is the eigenfrequency of the SW mode n of a single film in the purely exchange limit defined by Eq. (92). We do not reproduce here the lengthy expressions for the diagonal $P_{nn} = P_{nn}^{11} = P_{nn}^{22}$ and off-diagonal P_{nn}^{12} dipole matrix elements in coupled magnetic films, as the procedure of their analytical evaluation is well developed by analogy with Chapter 4 (see also Refs. 89, 102). We note that, as the expressions for P_{nn} and P_{nn}^{12} depend on transverse wave number κ_n (and therefore on the exchange coupling coefficient β), so does the splitting of the spectral branches. Thus the dipole-dipole and exchange splitting of the dispersion branches should not be considered separately. Both types of splitting influence the spectrum and, although interlayer exchange mainly affects the frequencies of antisymmetric SW modes near $q = 0$ [see Eq. (125)], it will also significantly change the dipole-dipole branch repulsion in the short-wavelength ($qL \gg 1$) region probed by BLS.

5.3. NUMERICAL RESULTS AND APPLICATIONS FOR SURFACE WAVES

We are interested here in surface SW modes of a double layer that correspond to the solutions of Eqs. (124)- (126) for imaginary κ_n. The numerical analysis shows, that, depending on the values of d^i, d^s, and β, there may exist two, one, or zero such solutions. When both of the effective pinning parameters d^i, d^s are negative and sufficiently large in magnitude, there are two imaginary solutions for κ_n, while for non-negative values of one of these parameters a single solution exists only if the second parameter is negative. The same kind of analysis can be applied to the dependence of the κ_n values on the exchange coupling coefficient β. As the symmetric modes are not affected by the interlayer exchange, the κ_n values for the symmetric modes remain the same for all values of β. Contrary to that, for the antisymmetric modes the effective interface pinning changes with β and so do the κ_n values.

We have calculated the dependence of the imaginary transverse wave numbers (corresponding to surface SW modes) on the interlayer exchange parameter β for the system Fe/spacer/Fe. We used the following set of parameters: the exchange parameter α, the field H_e and the static magnetization $4\pi M_o$ are taken as in Chapter 4, the film thickness L = 200 Å, and the pinning parameters are $d^s = d^i$

$= d = -1 \times 10^6$ cm^{-1}. The values of β were taken to vary from -5×10^5 to 1×10^5 cm^{-1}. The results are presented in Fig. 24. For the given set of parameters there exist one surface branch for the symmetric mode (horizontal line A) and two surface branches for the antisymmetric mode (curves B and C). Curve C ends at the point $\beta = 0$, where the corresponding branch of the SW spectrum meets the bulk continuum.

The existence of an imaginary solution for κ_n, however, does not guarantee the existence of a corresponding branch in the SW spectrum. This becomes clear from the analysis of the dispersion equation (126). The dipole matrix elements P_{nn}^{ik} are always positive. However, the sign of Ω_n depends on the values of $|q|$ and κ_n, and sometimes becomes negative. In this case if P_{nn}^{ik} are sufficiently large, the right hand side of Eq. (126) becomes negative.

The above conclusions are confirmed by the results of our calculations of the SW spectrum and the BLS integrated intensities for the system Fe/spacer/Fe for the given values of the parameters. The Green function formalism for BLS from multilayered magnetic structures is well established (see Ref. 4 and references therein) and can be considered as a direct generalization of the results obtained in Chapter 4 for thin films. Since the appropriate Green

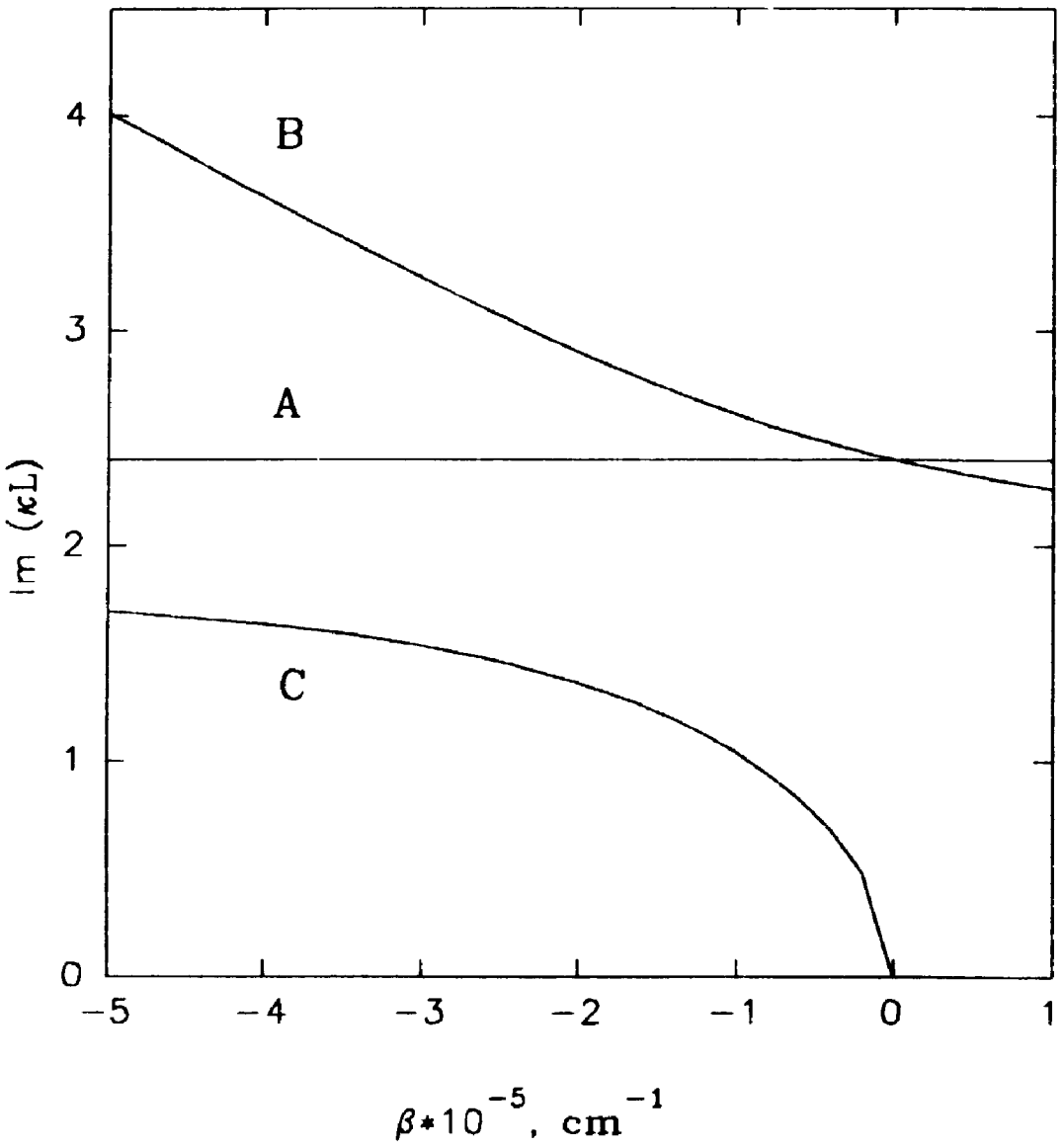

Fig. 24. The dependence of imaginary perpendicular SW wavenumbers on the interlayer exchange coefficient β for a Fe/spacer/Fe structure (see text for the parameters and details).

functions have been calculated from the formalism described earlier, it is straightforward in principle to determine the light scattering intensities associated with the various SW modes. In the general case it is necessary to take account of the internal multiple reflections of the incident and scattered light at the surfaces and interfaces of the sample. In the present work we avoid this difficulty by restricting attention to the case when the optical penetration depth of the light in the sample is smaller than L (e.g., as would be typically in the case of Fe films), thereby making the multiple reflection effects negligible. Within the framework of our approach we can conclude that all the scattering processes take place in the upper layer, which makes all the formal expressions for the BLS integrated intensities derived in Chapter 4 for a single film geometry applicable here, the interactions with the second layer affecting only the SW spectrum of the system.

We used the same 180^0 backscattering geometry and the parameters of the experiment as previously (see Chapter 4), taking the scattering angle $\theta = 45^o$. This provides for the in-plane wavenumber of the SW to be $|q| \cong 1.8 \times 10^5$ cm^{-1}. In Fig. 25. we display the dependences of the surface modes frequencies on β. It can be seen that, although the imaginary κ for symmetric mode exists, there is no

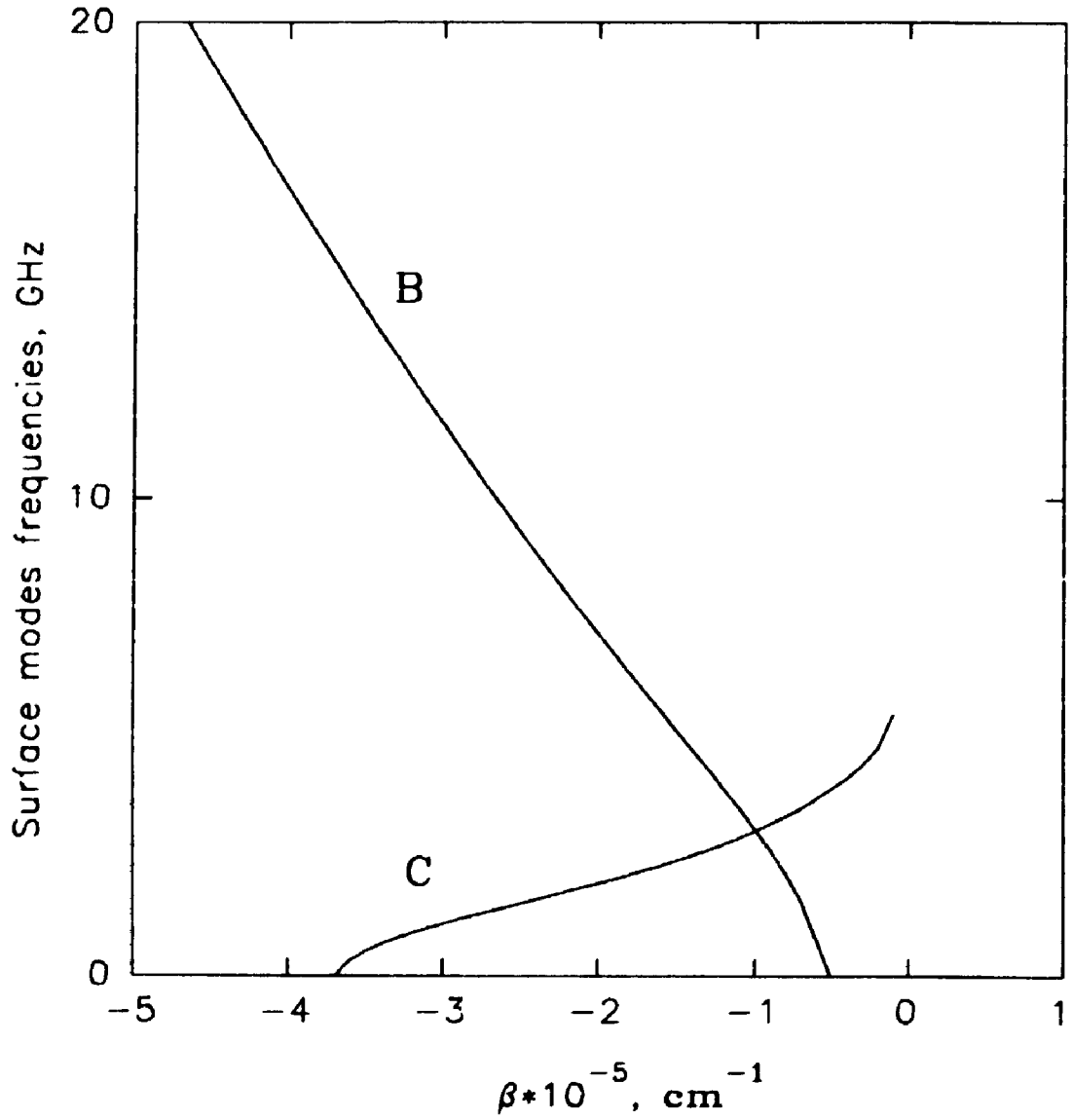

Fig. 25. The dependences of surface SW frequencies on the interlayer exchange coefficient β for a Fe/spacer/Fe structure (see text for the parameters and details).

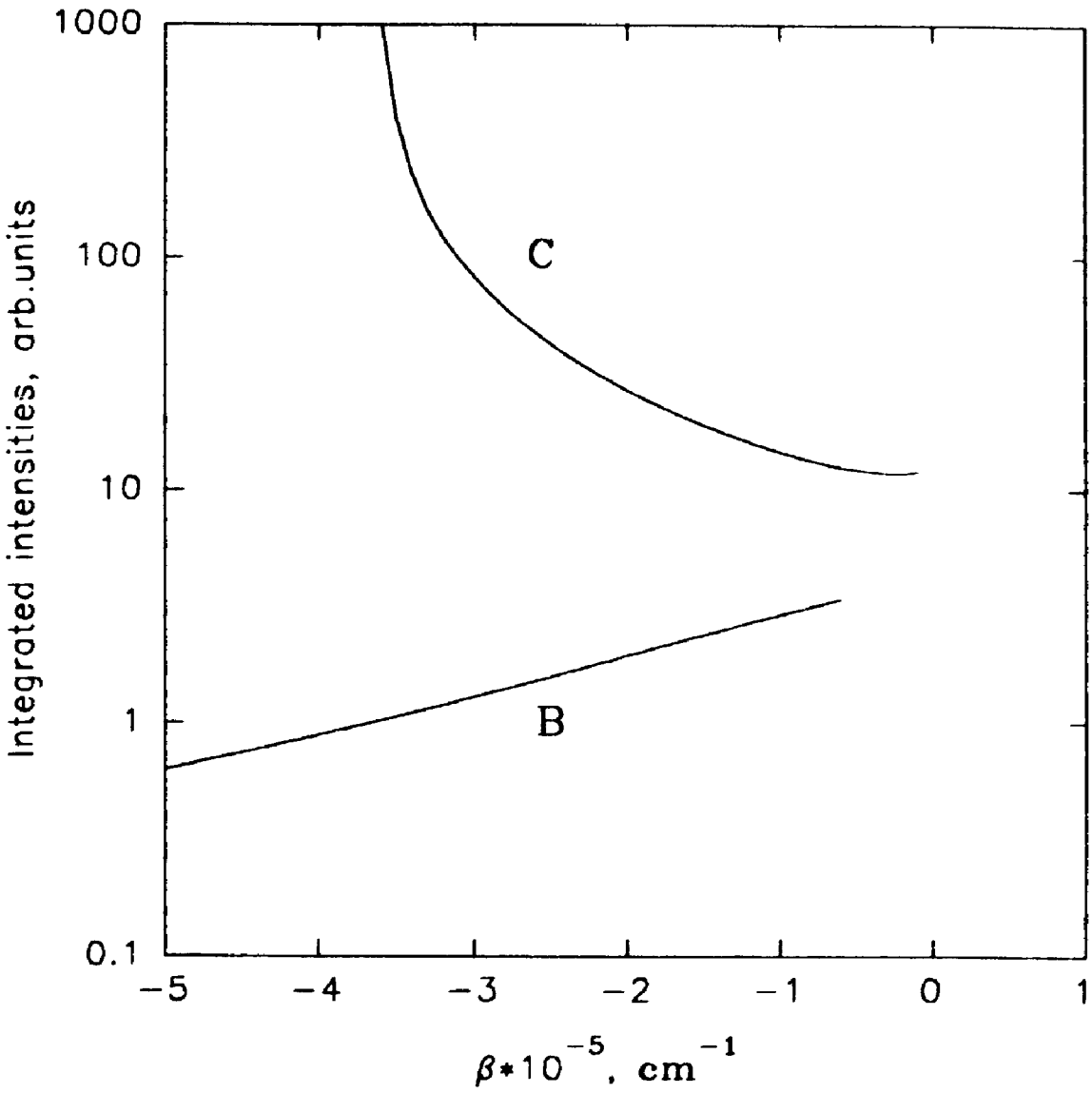

Fig. 26. The dependences of the integrated intensities of Brillouin light scattering from the surface SW on the interlayer exchange coefficient β for a Fe/spacer/Fe structure (see text for the parameters and details).

corresponding branch in the SW spectrum. As well, the branch C in Fig. 25, corresponding to the curve C in Fig. 24, appears only when the β values are in the interval from about -3.6×10^5 to 0 cm^{-1}. In the same way, the branch B ceases to exist when $\beta \geq -0.5 \times 10^5 cm^{-1}$ while the corresponding κ dependence (curve B in Fig. 24) still shows the existence of the solution. Basically the same characteristic features can be seen in Fig. 26, where the BLS integrated intensities are depicted. The labeling of the branches is the same as for the previous two plots.

5.4. SPIN WAVE SPECTRUM IN MULTILAYERS WITH INTERLAYER EXCHANGE AND DIPOLE COUPLING. A SEMI-EMPIRICAL APPROACH.

5.4.1. The Hamiltonian and the spin wave representation

We extend our previously developed analytic theories of BLS from dipole-exchange spin waves in magnetic films (Chapter 4) and magnetic double layers (Sections 5.2 and 5.3) to the cases of perpendicularly-magnetized magnetic superlattices consisting of alternating layers of a ferromagnet and a nonmagnetic spacer. The effects of dipole-dipole and exchange interactions (both intralayer and interlayer) are included. We obtain explicit approximate

expressions for the spectrum of the collective SW modes of a superlattice.

We assume a perpendicularly magnetized multilayer structure consisting of an arbitrary number N of identical magnetic layers, each separated by identical nonmagnetic spacers. The energy density W of the system can be written as

$$W = \frac{1}{4VN}\sum_{i,j}\int dR dR' M^{*}_{Ri}\left[2\hat{G}^{ii}_{RR'}\delta_{ij}+\hat{G}^{ij}_{RR'}\right]M_{R'j} - \frac{1}{VN}\sum_{j}\int dR\ H^{j}_{R}M^{z}_{Rj} \qquad (127)$$

where V is the volume of each magnetic layer (labeled by i and j) and M_{Ri} is the total magnetization at position R in layer i. The second term describes the Zeeman interaction with the static magnetic field, assumed to have the same value H in all layers. The tensor $\hat{G}^{ij}_{RR'}$ represents dipole and exchange interactions, with the diagonal term $\hat{G}^{ii}_{RR'}$ corresponding to a single film case. We take the dipole and intralayer exchange interaction tensors in the same form as for a single film (see Chapter 4 and references therein) and assume for the interlayer exchange energy density to be of the form:

$$-\frac{\pi\alpha}{\tilde{L}NV}\sum_{i,j}\beta\int dR dR' M^{*}_{Ri}M_{R'j}\delta(r-r') \qquad (128)$$

where $\tilde{L}$ is the superlattice periodic length (i.e., the sum of a spacer thickness and a magnetic layer thickness), M_o (the saturation

magnetization) is assumed to be the same in all layers, and β is defined as in previous sections. The sum is over the *adjacent* layers, and r and r' are the in-plane components of R and R'. The simplified form of (128) should be satisfactory within the framework of this semi empirical approach given the short-range character of the exchange interaction.

Next we rewrite W using the linearized Holstein-Primakoff representation and we transform the spin-wave (SW) polarizations a_{R_i} and $a^{\bullet}_{R_i}$ with respect to any complete orthonormal basis $\phi_k(R)$, indexed by label k:

$$a_{R_i} = \sum_k a_k \, \phi_k(R, i), \quad a^{\bullet}_{R_i} = \sum_k a^{\bullet}_k \, \phi^{\bullet}_k(R, i) \tag{129}$$

The quadratic part W_2 of the energy density is then written in the canonic form of

$$W_2 = \sum_{12} A_{12} a^{\bullet}_1 a_2 \; + \frac{1}{2}\Big(\sum_{12} B^{\bullet}_{12} a_1 a_2 + \text{c.c.} \Big) \tag{130}$$

where

$$A_{12} = \frac{gM_o}{2V\bar{N}} \sum_{i,j} \int dR dR' \Big[\phi^{\bullet}_1(R, i) \phi_2(R', j) \Big(\big(\hat{G}^{++}_{RR'ij} + \hat{G}^{--}_{R'Rji} \big)(1+\delta_{ij}) - 2\delta(R-R')\delta_{ij} \Big(\sum_j \int dR' \hat{G}^{zz}_{RR'ij} + \frac{H}{M_o} \Big) \Big] \tag{131}$$

$$B_{12} = \frac{gM_o}{VN} \sum_{i,j} \int dR dR' \phi_1(R,i) \phi_2(R',j) \hat{G}^{+-}_{RR',ij} (1+\delta_{ij}) \qquad (132)$$

Here indices 1 and 2 stand for k_1 and k_2, and the superscripts +, -, and z denote the correspondi , components of the interaction tensor in terms of $M^{\pm} = M^x \pm iM^y$ and M^z, as in Chapter 4.

As far as the linear operator $\hat{G}_{RR'}$ is additive,

$$\hat{G}_{RR',ij} \equiv \hat{G}^{ex}_{RR',ij} + \hat{G}^{d}_{RR',ij}, \qquad (133)$$

we can deal with the exchange (ex) and dipolar (d) contributions separately. To choose the orthonormal basis $\phi_k(R,i)$ we assume that:

(i) the interlayer interaction is weak. This assumption enables the SW modes of a multilayer to be constructed from the single layer SW modes S_n (SWSL), which are identical to the single film modes discussed in Chapter 4, with only the envelope being dependent on the interlayer interaction.

(ii) the individual layers are thin enough for the different SWSLs to be well separated in frequency. Indeed, the separation of the neighboring bulk modes frequencies in the thin film can be roughly estimated as

$$\Delta\omega \sim \alpha\omega_M \left(\frac{\pi}{L}\right)^2 \qquad (134)$$

For the parameters of an iron film with L=50 Å, the value of $\Delta\omega$ appears to be of the order of 10^{11}Hz, the frequencies being at least

one order of magnitude less. This means that we can use the SWSL's with the same number n for all the layers of a multilayer. We note that there might be situations when the second assumption is not true. For example, if the pinning parameters at the surfaces of the film (layer) are close in magnitude but have opposite signs, there might be two surface modes with close frequencies.

With the two quoted assumptions the SW modes of a multilayer can be represented as composite SW modes (CSWM) of the following form:

$$\phi_k(R,i) \equiv \phi_{qnQ}(R,i) = L_{niQ}S_n(z_i)\exp(-iq\cdot r) \qquad (135)$$

where q is the in-plane wave vector, and z_i is the spatial coordinate perpendicular to the layers measured from the center of layer i. The orthonormality condition is

$$\sum_{nj} L^*_{njQ}L_{njQ'} = N\delta_{QQ'} \qquad (136)$$

5.4.2. Multilayer energy density in the CSWM approximation

We now substitute (135) and (136) into (131) and (132), and after some algebraic manipulations obtain:

$$A_{12}\equiv A_{qnQQ'} = \frac{1}{N}\sum_{i,j} L^*_{niQ}L_{njQ'}A_{qnij'}$$

$$B_{i2} \equiv B_{qnQQ'} = \frac{1}{NL} \sum_{i,j} L^{*}_{niQ} L_{niQ'} B_{qnij'} \tag{137}$$

with

$$A_{qnij} = \frac{gM_o}{2V} \int dr dr' \exp\{iq\cdot(r-r')\} \int_{-L/2}^{L/2} dz dz' S^{*}_{n}(z) S_{n}(z') A\left(r, z; r', z' + (i-j)\tilde{L}\right)$$

$$B_{qnij} = \frac{gM_o}{V} \int dr dr' \exp\{iq\cdot(r-r')\} \int_{-L/2}^{L/2} dz dz' S^{*}_{n}(z) S_{n}(z) B\left(r, z; r', z' + (i-j)\tilde{L}\right) \tag{138}$$

Here A(R,R') and B(R,R') are defined by

$$A(R;R') = \left[\left(\hat{G}^{++}_{RR'ij} + \hat{G}^{--}_{R'Rji}\right)(1+\delta_{ij}) - 2\delta(R-R')\delta_{ij}\left(\sum_{j} \int dR' \hat{G}^{zz}_{RR'ij} + \frac{H}{M_o}\right)\right], \tag{139}$$

$$B(R;R') = \left[\hat{G}^{+-}_{RR'ij}(1+\delta_{ij})\right]. \tag{140}$$

To have the orthonormality conditions (136) satisfied we expect the coefficients L_{njQ} to have the form:

$$L_{njQ} = R_n \exp\left(-iQ_n j\right) + T_n \exp\left(iQ_n j\right) \tag{141}$$

Here Q_n plays the role of a dimensionless wave number of a CSWM constructed from the SWSL's with the number n. The coefficients R_n

and T_n generally depend on the anisotropy of the interlayer exchange between the boundary layers of a multilayer and the neighbouring ones. Empirically we may describe these anisotropies by analogy with the single film case (Chapter 4, Eq. (88)), i.e. via boundary conditions utilizing a concept of *effective macroscopic pinning*:

$$a_1 + D_{Un}(a_2 - a_1)=0, \qquad a_N + D_{Ln}(a_N - a_{N-1}) = 0, \tag{142}$$

where a_m denotes the SW polarizations in the mth layer, and D_{Un} and D_{Ln} being the effective pinning constants for the n-th mode at the top and at the bottom of the multilayer, respectively. Using (142), we can easily write down the consistency conditions for (141), assuming that a_m also has a dependence like in (141) on the layer number:

$$(R_n + T_n)(1-D_{Un}) + D_{Un}(R_n/X + T_nX)=0,$$

$$(R_n/X^{N-1} + T_nX^{N-1})(1+D_{Ln}) - D_{Ln}(R_n/X^{N-2} + T_nX^{N-2})=0, \tag{143}$$

where $X=\exp(iQ_n)$. In the simple case of $D_{Un}=D_{Ln}=0$ we get

$$L_{njQ} = (2-\delta_{Qm})^{1/2}\cos\left(\frac{\pi m}{N}(j-\frac{1}{2})\right), \quad m=0,1,2,3,\ldots N-1. \tag{144}$$

which is analogous to the situation of the free surface spins in the case of a single film.

5.4.3. Calculation of the matrix elements.

We now specify the form of the dipole and exchange interaction tensors. The dipole interaction tensor is taken as previously (see Ref. 89, 102, Chapter 4 and earlier this chapter) to be in the magnetostatic form. In the case of a *perpendicularly magnetized structure* this reads in the mixed q-z representation as:

$$\hat{G}^{d}_{q}(z,z') = \pi \begin{bmatrix} G_p & G_p & 2iG_p \cdot \mathrm{sign}(z-z') \\ G_p & G_p & 2iG_p \cdot \mathrm{sign}(z-z') \\ 2iG_p \cdot \mathrm{sign}(z-z') & 2iG_p \cdot \mathrm{sign}(z-z') & 4\left(G_p - \delta(z-z')\right) \end{bmatrix}. \tag{145}$$

where $G_p(z,z') = \frac{q}{2} e^{-q|z-z'|}$.

The exchange intralayer contribution has to be treated separately from the interlayer exchange contribution. Using Eq. (6) we get the operator $\hat{G}^{ex}_{RR'}$ of the intralayer exchange given by the following matrix in the (+,-,z) representation:

$$\hat{G}^{ex}_{RR'} = -\pi\delta(R-R') \begin{bmatrix} \alpha\Delta & 0 & 0 \\ 0 & \alpha\Delta & 0 \\ 0 & 0 & 2\alpha\Delta \end{bmatrix}. \tag{146}$$

Here Δ denotes the three-dimensional Laplace operator, and α is the exchange constant as defined in Chapter 4.

The interlayer exchange energy, taken in the form (128), produces the following contribution to the interaction tensor $\hat{G}_{RR'}$:

$$-\frac{\pi\alpha\delta(r-r')}{\tilde{L}}\begin{bmatrix}\beta_{ij} & 0 & 0\\ 0 & \beta_{ij} & 0\\ 0 & 0 & 2\beta_{ij}\end{bmatrix} \qquad (147)$$

with

$$\beta_{ij} = \beta((1-\delta_{iN})\beta_{j,i+1} + (1-\delta_{i1})\beta_{j,i-1}) \qquad (148)$$

which corresponds to our assumption of only adjacent layers interacting via interlayer exchange.

Let us now calculate the matrix elements involved in (137) and (138). We have for the interaction tensor in the mixed qn-ij representation (138):

i) Dipole contribution:

$$A^{d}_{qnij} = \pi g M_o\left((1+\delta_{ij})P_{nnij}(q) - 4\delta_{ij}\right),$$
$$B^{d}_{qnij} = \pi g M_o P_{nnij}(q)(1+\delta_{ij}); \qquad (149)$$

ii) Intralayer exchange contribution:

$$A^{e1}_{qnij} = 4\pi\alpha g M_o \delta_{ij}\left(q^2 + (\kappa_n)^2\right)$$
$$B^{e1}_{qnij} = 0; \qquad (150)$$

iii) The Zeeman interaction contribution:

$$A^{z}_{qnij} = gH\delta_{ij}$$

$$B^{z}_{qnij} = 0; \qquad (151)$$

iv) Interlayer exchange contribution:

$$A^{e2}_{qnij} = \frac{2\pi\alpha g M_o}{\tilde{L}}\left(\delta_{ij}\left(\sum_m \beta_{im}\right) - \beta_{ij}\right)$$

$$B^{e2}_{qnij} = 0; \qquad (152)$$

Finally, we get:

$$A_{qnij} = \frac{\omega_M}{4}\left[P_{nnij}(q) - \frac{2\alpha\beta_{ij}}{\tilde{L}}\right] +$$

$$+ \delta_{ij}\left[\omega_H + \alpha\omega_M\left(q^2 + (\kappa_n)^2\right) + \frac{\omega_M}{4}P_{nnii}(q) + \frac{\alpha\omega_M}{2\tilde{L}}\sum_m \beta_{im}\right];$$

$$B_{qnij} = \frac{\omega_M}{4}(1+\delta_{ij})P_{nnij}(q); \qquad (153)$$

Next we calculate the dipole matrix elements $P_{nnij}(q)$ in the same way as in Ref. 89 and Eq. (93). We can write the integral expressions for these elements in the form:

$$P_{nnij}(q)= \frac{1}{L}\int dzdz' \frac{q}{2}\exp\left(-q|z-z'+ (i-j)\tilde{L}|\right)S_n^*(z)S_n(z') \qquad (154)$$

where $q=|q|$. We note here that if i=j then $P_{nnij}(q)\equiv P_{nn}(q)$, which is the diagonal dipole matrix element for the single film case (see Ref. 89). If i>j, then the integration in (154) can be written as:

$$P_{nnij}(q)= \frac{q}{2}\exp(-q|i-j|\tilde{L})\frac{1}{L}\left[\int dz\exp(-qz)S_n^*(z)\right]\left[\int dz'\exp(qz')S_n(z')\right]. \qquad (155)$$

We now take the trial SWSL modes $S_n(z)$ in the form appropriate for the free surface spins , i.e.

$$S_n(z)= \left(\frac{2}{1+\delta_{0n}}\right)\cos\left(\frac{\pi n}{L}(z+\frac{L}{2})\right) \qquad (156)$$

In this case we get from (155):

$$P_{ooij}(q) = \frac{\exp(-q|i-j|\tilde{L})}{2qL}\left(\exp(qL)+\exp(-qL)-2\right),$$

$$P_{nnij}(q) = \frac{\exp(-q|i-j|\tilde{L})}{\left((\pi n)^2+(qL)^2\right)^2}(qL)^3\left[(-1)^n\left(\exp(qL)+\exp(-qL)\right)-2\right] \qquad (n\neq 0) \qquad (157)$$

We note that the following factorization is possible:

$$P_{nnij}(q) = \mathfrak{G}_{pq}(i,j)P_n(q), \tag{158}$$

where

$$\mathfrak{G}_{pq}(i,j) = \frac{q}{2}\exp(-\,q|i\tilde{L}-j\tilde{L}|) \tag{159}$$

is the macroscopic analogue of the function G_p from (145) for an individual film.

Now we substitute the above expressions into (138):

$$A_{qnQQ'} = \delta_{QQ'}\left(\omega_H + \alpha\omega_H\left(q^2 + (\kappa_n)^2\right) + \frac{\omega_M}{4}P_{nn}(q)\right) + \frac{\omega_M}{4}U_{qnQQ'} + \frac{\omega_M}{2}V_{qnQQ'};$$

$$B_{qnQQ'} = \frac{\omega_M}{4}P_{nn}(q) + \frac{\omega_M}{4}U_{qnQQ'} \tag{160}$$

where

$$U_{qnQQ'} = \frac{1}{N}\sum_{i,j} L^{*}_{niQ}L_{njQ'}P_{nnij}(q),$$

$$V_{qnQQ'} = \frac{\alpha}{\tilde{L}N}\sum_{i,j} L^{*}_{niQ}L_{njQ'}\left[\delta_{ij}\left(\sum_{m}\beta_{im}\right) - \beta_{ij}\right] = 2\alpha\frac{\beta}{\tilde{L}}\delta_{Q_nQ'}\left(1 - \cos Q_n\right) \tag{161}$$

The final expression for $V_{qnQQ'}$ above is obtained by taking the form (144) for the functions L_{njQ}. We should note that, technically speaking, it is possible to distinguish experimentally only a few

composite modes with the lowest Q_n. In this case we can rewrite (161) as follows:

$$V_{qnQQ'} = \frac{\alpha\beta}{\tilde{L}} \delta_{QQ'} Q_n^2. \tag{162}$$

and also we have

$$A_{qnQQ'} = \delta_{QQ'} \left(\omega_H + \alpha\omega_M \left(q^2 + (\kappa_n)^2 + \frac{\beta}{2\tilde{L}}(Q_n)^2\right) + \frac{\omega_M}{4} P_{nn}(q)\right) + \frac{\omega_M}{4} U_{qnQQ'}; \tag{163}$$

The interlayer dipole matrix element between two composite modes

$$U_{qnQQ'} = \frac{1}{N}\sum_{i,j} L^*_{niQ} L_{njQ'} P_{nnij}(q) = P_n(q) \frac{1}{N}\sum_{i,j} L^*_{niQ} L_{njQ'} \mathfrak{G}_{pq}(i,j), \tag{164}$$

can be calculated within an assumption that the number of layers is sufficiently large to replace the summation in (164) by integration. If we neglect the hybridization of the composite modes, the required matrix element U_{qnQQ} can be written as:

$$U_{qnQQ} \sim \mathfrak{P}_{QQ} P_n \tag{165}$$

where the expression for $\mathfrak{P}_{QQ}$ formally corresponds to the matrix element P_{nn} for the case of a single film with free surface spins:

$$\mathfrak{P}_{QQ} = P_{nn}(q\tilde{L}N) \tag{166}$$

Finally, using the expressions (160)- (166), we are able to calculate the frequencies of the non-hybridized composite modes, using the same approach as in the single film case:

$$\omega^2_{qnQ} = A^2_{qnQQ} - |B_{qnQQ}|^2 = \left[\Omega_{qnQ} + \frac{\omega_M}{4}\left(U_{qnQQ} + P_{nn}(q)\right)\right]^2 -$$

$$- \left[\frac{\omega_M}{4}\left(U_{qnQQ} + P_{nn}(q)\right)\right]^2 = \Omega_{qnQ}\left[\Omega_{qnQ} + \frac{\omega_M}{2}\left(U_{qnQQ} + P_{nn}(q)\right)\right] \tag{167}$$

where

$$\Omega_{qnQ} = \omega_H + \alpha\omega_M\left(q^2 + (\kappa_n)^2 + \frac{\beta}{2\tilde{L}}(Q_n)^2\right) . \tag{168}$$

5.4.4. Analysis of the obtained expressions.

We have to stress that (167) is valid only within the assumption of small Q_n. In this case the form of the dispersion relationship (167) is formally analogous to the one for a single film. Moreover if we assume no interlayer exchange and dipole coupling, (167) reduces exactly to the single film dispersion relationship. If, however, we cannot consider Q_n small (for example, for multilayers with a small number of layers), we have to use (167) with Q_n^2 replaced by $2(1-\cos(Q_n))$.

First, it is instructive to make a simple comparison to the case of a bilayer (N=2), which was studied previously in Section 5.2. If we put N=2 in our recent theory, there are only two allowed values of Q_n for any n, corresponding to $1-\cos(Q_n)$ taking the values of 1 and

0. The former can be associated with the antisymmetric mode of a bilayer, while the latter is a symmetric mode. By analyzing (164) we can conclude that the interlayer exchange does not affect the frequencies of the symmetric mode, in accordance with our previous results. On the other hand, we should not expect to obtain *exact* correspondence with our previous results for the bilayer analytically, as previously the interlayer exchange was introduced via Hoffmann boundary conditions. These conditions were then linearized, which makes the set of approximations different from the ones employed here. However, in the limit of free surface spins, small $\kappa_n L$ and thin spacer ($L \cong \tilde{L}$), we obtain exact analytical correspondence, as the dispersion relationship (168) leads to:

$$\Omega_{qnQ} = \omega_H + \alpha\omega_H\left(q^2 + \frac{2\beta}{\tilde{L}}\right) . \qquad (169)$$

which corresponds to our results of Section 5.2 applied to the situation of free surface spins. We note here that the assumption of a thin spacer is reasonable, because otherwise either there is no interlayer exchange or the continuous medium approximation is not valid.

Second, let us consider the more interesting situation where the number of layers is taken to be large. In this case Eqs. (166)- (167) describe a multilayer in an "effective medium" approximation. Indeed,

we can rewrite (166)- (167) as follows:

$$\omega^2_{qnQ} = \Omega_{qnQ}\left[\Omega_{qnQ} + \omega_M \tilde{P}_{nn}(q)\right],$$

$$\Omega_{qnQ} = \tilde{\omega}_H + \alpha\omega_M\left(q^2 + \tilde{Q}^2_n\right); \qquad (170)$$

where

$$\tilde{P}_{nn}(q) = \frac{1}{2}\left(U_{qnQQ} + P_{nn}(q)\right);$$

$$\tilde{\omega}_H = \omega_H + \alpha\omega_M\kappa^2_n;$$

$$\tilde{Q}_n = \left[\frac{\beta}{2\tilde{L}}\right]^{1/2} Q_n \qquad (171)$$

Equation (170) has exactly the same form as for the single film case, with the film parameters renormalized according to (171).

In view of the above, we can make predictions concerning the types of composite excitations occurring in different experimental situations. First, if the interlayer exchange has no "macrosurface" anisotropy, i.e. the interaction between the first (or the last) layer and its adjacent one is spherically symmetric, we predict no pseudosurface (Im Q_n>0) composite modes. In this case the lowest frequency excitation will be the uniform precession mode (L_{njQ}=const), which is the one typically excited in FMR experiments. This conclusion follows from the direct analogy of the Eqs. (170 - 171) for a multilayer with the corresponding expressions for a single

film, for which if the pinning parameters at both surfaces of the film are equal zero, the surface solutions do not exist and the uniform precession is the lowest SW mode.

Second, if the interlayer exchange acting on on the end layers of a multilayer is not completely isotropic and we can talk about the effective macropinning, we predict the existence of pseudosurface composite modes as well as bulk modes. The consistency equation, analogous to Eq. (90) from Chapter 4 would read as follows:

$$\left(\frac{\beta}{2\tilde{L}}Q_n^2 - D_{Un}D_{Ln}\right)\tan\left(\left[\frac{\beta}{2\tilde{L}}\right]^{1/2} Q_n N\tilde{L}\right) = \left[\frac{\beta}{2\tilde{L}}\right]^{1/2} Q_n\left(D_{Un} + D_{Ln}\right) \qquad (172)$$

with the parameters D_{Un} and D_{Ln} characterizing the anisotropy of the interlayer exchange at the top and at the bottom of the multilayer structure (see above). By fitting the solutions of (172) to the experimental curves we can deduce the dependence of β on the spacer thickness.

We may use our theory for a qualitative analysis of the results of the experiment from Refs. 107 and 108. In our opinion, the two branches of FMR obtained in 108 can be associated with the hybridized pseudosurface and first pseudobulk composite modes, which exist due to the effective surface anisotropy of the interlayer exchange. The hybridization occurs as the spacer thickness becomes

greater than 5Å and is due to mixing of the branches with different κ_n but close frequencies in the composite modes. We predict small macropinning constants as the first pseudobulk composite mode has a relatively small resonance amplitude. We note, however, that although our approach is capable of predicting the behavior of the FMR dispersion relationships, it provides no simple way to explain hybridization. The reason is that for q=0, as in the case of FMR experiments, the branch dipolar hybridization is ruled out as the dipole Green function (145) goes to zero. The possible mechanism for hybridization is mixing of single film modes with different transverse wave vectors but close frequencies, occurring due to the micropinning dependence on the spacer thickness. This mechanism is beyond the assumptions of our present theory, as it implies that different composite modes are constructed of the SWSL's which in general are not orthogonal to each other. It would be worthwhile, however, to develop a numerical perturbation theory of the kind used in Ref. 112 that would take our analytical expressions as a zero-order approximation.

For the case of the BLS experiments, where $q \sim 10^5$ cm^{-1}, the above mentioned effects will be much less important as the main role in the hybridization will be played by the dipole interlayer interaction,

which is relatively easy to account for within the framework of our approach.

5.4.5. Numerical results

We apply the CSWM formalism to Fe/Spacer multilayers with the parameters: $\alpha = 1.15 \times 10^{-13}$ cm^2, $4\pi M_o = 21$ kOe, $H_e = 22.5$ kG, L = 100 Å, spacer thickness 10 Å, and zero macro- and micro-pinning. It is straightforward to confirm numerically that for these parameters there is no noticeable hybridization of the modes with different n. In Fig. 27 we display the boundaries of the bulk bands for multilayers with $\beta = 10^5$ cm^{-1} and different values of N. One of the boundaries (at $Q = \pi$), is independent of N within the given q interval. This can be explained by the vanishing of the dipolar contribution for the modes with high Q. The other boundary (at Q = 0) does not depend on the interlayer exchange, but the dipolar contribution to this branch is significant and depends on N. From our analysis we expect a scaling behavior with the dimensionless universal variable being $q\tilde{L}N$. Indeed, in Fig. 27 we see that the crossings, denoted by arrows are equidistant in the logarithmic q-scale. In Fig. 28 we show the dispersion branches for Fe/spacer multilayers with N = 5 and different values of β corresponding to ferromagnetic and antiferromagnetic interlayer exchange. The branch

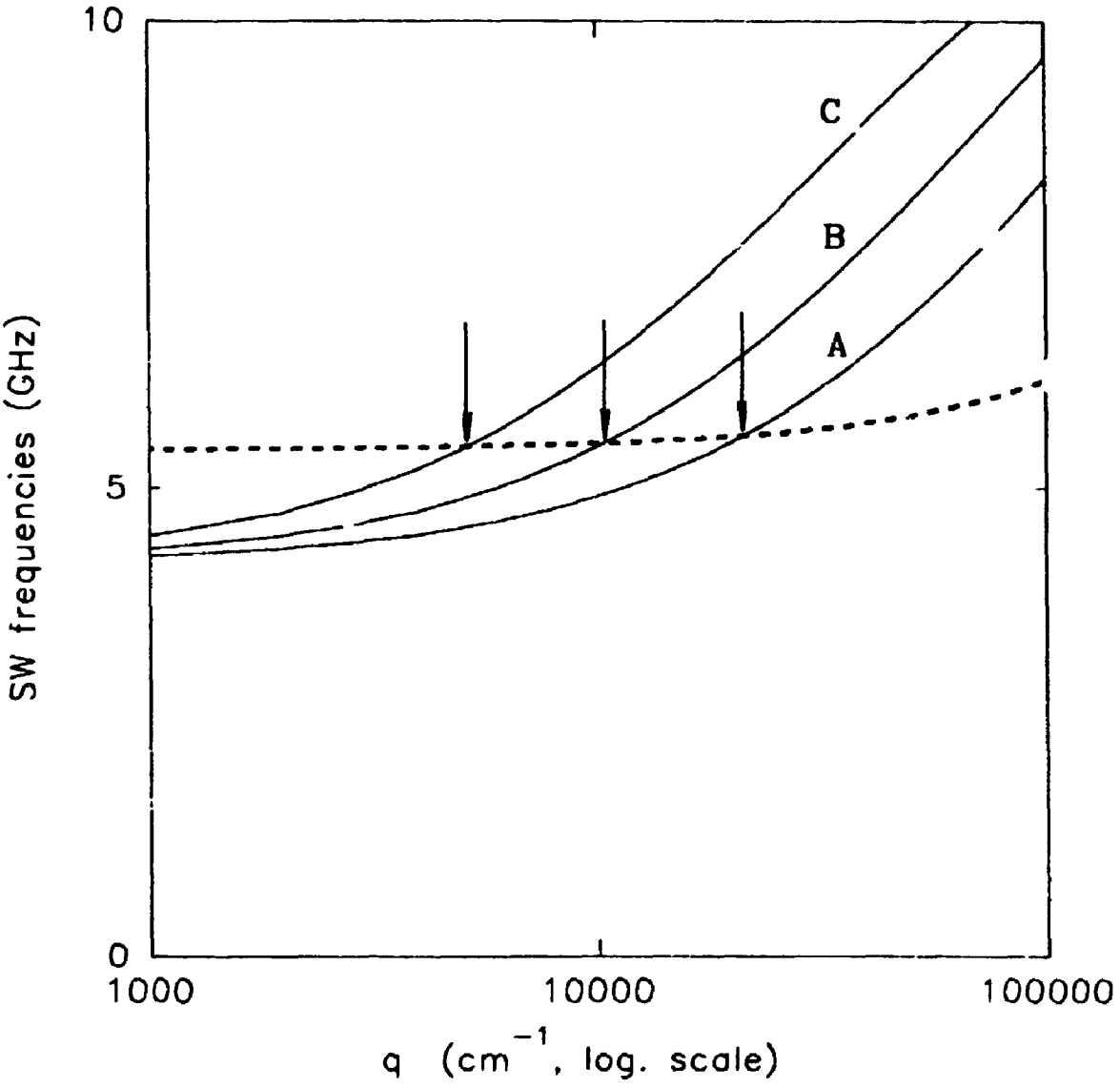

Fig. 27. The boundaries of the bulk SW frequency bands for multilayers with interlayer exchange coefficient $\beta=10^5 cm^{-1}$. Broken line represents N- independent boundary, corresponding to $Q=\pi$. Solid lines correspond to $Q=0$. Numbers of layers are: N=10 (curve A), N=20 (curve B) and N=40 curve (C). See text for the details.

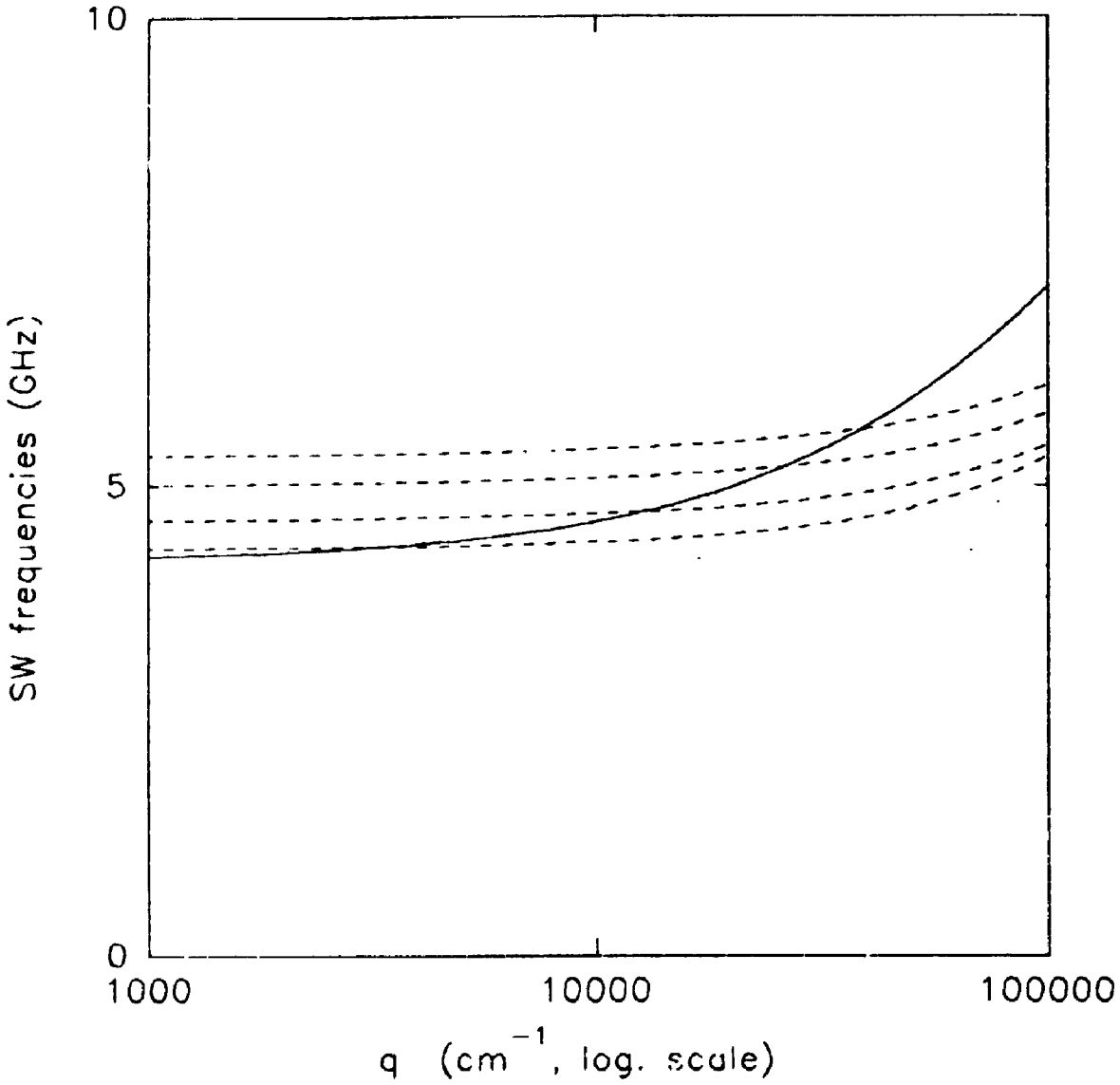

Fig. 28.Dispersion branches for a multilayer with N=5. The solid line corresponds to the purely dipole branch; dashed and dotted lines correspond to $\beta=10^5$ and $\beta=-10^5$ cm^{-1}, respectively.

separation for the low q region, which is directly measurable from the BLS spectrum, is directly proportional to $|\beta|$. This provides a convenient way of measuring β.

The extention of the above to obtain the BLS intensities follows a well-established procedure, generalizing our results (Ref. 85, 86) for thin films and double layers. Basically, the scattering cross section can be expressed in terms of a weighted summation over magnetization-dependent Green functions $\langle\langle m^{\mu}_{nq}; m^{\nu}_{n',q} \rangle\rangle$ with $\mu,\nu = x,y$. The weighting factors depend on temperature, magneto-optical coupling, electric-field polarizations, scattering geometry, and optical transmission coefficients at the various surfaces and interfaces. Once the appropriate Green functions have been calculated from the formalism described earlier (by linear-response methods), it is straightforward to determine the BLS intensities associated with the various SWCM modes. In general, it is necessary to take account of the various internal multiple reflections of the incident and scattered light at the surfaces and interfaces of the sample (Refs. 86, 87), but we can avoid this difficulty by restricting attention to the case where the optical penetration depth of the light in the sample is smaller than L (e.g., as would be typically in the case of Fe/spacer multilayers).

5.5 Conclusions

In the present chapter we suggested some analytical approaches to the multilayer magnetic systems, which have traditionally been treated by means of numerical methods. In our opinion, the discussed analytical approaches yield sufficient accuracy for quantitative and qualitative description of the recent BLS and FMR experiments, yet being simple to use in applied calculations.

The main results of this chapter have been published in recent papers (Refs. 85, 86 and 87).

CHAPTER 6.

CONCLUSIONS

The aim of this brief chapter is to summarize the main results of the thesis and sketch some further developments that could be made along the lines of the present research.

The critical properties of the Heisenberg S=1/2 quantum thin films: A Monte-Carlo study. In Chapters 2 and 3 we presented the results of our research in the field of Monte-Carlo simulation of the quantum spin lattices. We devised a formal procedure of creating the variants of the Monte-Carlo method within the Handscomb approach and we demonstrated that most of the previous modifications of the method fit into our proposed scheme.

We accomplished a Monte-Carlo study of the critical properties of the films with one, two and three layers. To our knowledge, this is the first investigation of this kind. We have confirmed the validity of the renormalization-group theory results (Ref. 62) for a one layer film for a wider range of temperatures than before. We showed that a ferromagnetic film with the number of monolayers $M \leq 3$ is unlikely to undergo a paramagnetic-ferromagnetic phase transition at finite temperatures. Our finite-scaling analysis is important in view of discussing how the finite size of the system affects its behaviour in the vicinity of T_c for the thermodynamic limit. We presented

numerical data for the behaviour of the effective exchange renormalization constant and its dependence on the interlayer exchange and the surface dilution. On the basis of our numerical data we analyzed the experimental data for critical behaviour of the ^{3}He film on a graphite substrate. The results of our research has led to several journal papers (see, e.g., Refs 64, 65, 73).

Among a number of possible developments of the presented research we can mention the extensions of our calculations to the case of layered systems with a greater number of layers, and to the case of anisotropic Heisenberg ferro- and antiferromagnetic thin films. The latter calculations are important when studying the critical behaviour of certain magnetic superconductors, such as doped La_2CuO_4, which is now commonly assumed to be an effectively bilayer Heisenberg antiferromagnet.

Spin waves and Brillouin Light Scattering in thin films and multilayers. In Chapters 4 and 5 we presented the results of our research in the field of the Brillouin Light Scattering from spin waves in layered magnetic structures. We presented a relatively simple *analytic* theory, based on a perturbation method, to describe the dipole-exchange SW spectra in the magnetic thin films and multilayers. We devised the approach to calculate the SW mode frequencies and the BLS intensities in a case of an arbitrarily

magnetized system, giving explicit expressions for a particular case of a perpendicularly magnetized film. On the basis of our theory we analyzed the influence of the surface anisotropy (or "pinning") on the SW spectra and BLS intensities. The same approach was applied to a bilayer magnetic system, for which the surface SW spectra and the BLS intensities were calculated. For the multilayer structures we devised a semi-empirical theory which explains the properties of the composite modes of the whole structure in terms of effective "macropinning". The results of our research have led to several publications (see, e.g., Refs. 85, 86, 87).

Some further developments of the presented approach, to mention a few, are: the explicit calculations of the SW spectra in tangentially magnetized systems, the detailed comparison of our results with purely numerical calculations of the spectra and with the experiments, and the systematic development of the semi-empirical theory for the multilayer structures on the basis of a transfer matrix approach (that would establish correspondence between the macropinning parameters and the properties of the surface layers). Also a great potential for development lies in extending our, presently linear, theory to the situations where the nonlinear SW interactions play a significant role in the SW spectrum, as may be the case in certain experiments.

REFERENCES:

1. Heisenberg, W., Z.Phys., **49**, 619 (1928)

2. K.W.H. Stevens, *Spin Hamiltonians*, in Magnetism, G.T.Rado and H.Suhl, eds., NY, Academic, 1963.

3. Lifschitz, E.M., and Pitaevski, L.P., *Theoretical Physics*, vol.IX, *Statistical Physics*, Moscow, NAUKA, 1978, pp. 337-369 (in Russian).

4. M.G. Cottam and D.J. Lockwood, *Light Scattering in Magnetic Solids*, Wiley, New York, 1986.

5. Kuni, F.M., *Statistical Physics*, LGU Publishing House, Leningrad 1982 (in Russian).

6. R.Balescu, *Equilibrium and Nonequilibrium Statistical Mechanics*, vol.2., J.Wiley & Sons, NY, 1975.

7. Lvov, V., *Nonlinear Spin Waves*, Moscow, Nauka, 1982, Chapters 1-3.

8. Phase Transitions and Critical Phenomena, C.Domb and M.S.Green, eds., N.Y.,Academic, 1972, vol.1, Chapters 5-7.

9. Cottam, M.G. and D.R.Tilley, *Introduction to Surface and Superlattice Excitations*, Cambridge Univ. Press, Cambridge, 1989.

10. Akhiezer, A.I., Baryakhtar, V.G., Peletminskii, S.V., *Spin Waves*, Amsterdam, North-Holland Pub. Co., 1968.

11. N.Metropolis, A.W.Rosenbluth, M.N.Rosenbluth, A.H.Teller, J.Chem.Phys., **21**, 1087 (1953)

12. *Monte Carlo Methods in Statistical Physics*, ed. by K.Binder, Springer-Verlag, 1979.

13. Bloch, F., Z.Phys., **61**, 206 (1930)

14. Holstein, T., and Primakoff, H., Phys.Rev., **58**, 1098 (1940)

15. Elliott, R.J. and Loudon, R., Phys.Lett., **4**, 189 (1963).

16. P.A. Fleury, S.P.S. Porto, L.E. Cheesman, and H.J. Guggenheim, Phys. Rev. Lett. **17**, 84 (1966).

17. J.R. Sandercock and W. Wettling, Solid State Comm. **13**, 1729 (1973).

18. J.R. Sandercock, Solid State Comm. **15**, 1715 (1974).

19. P. Grunberg and F. Metawe, Phys. Rev. Lett. **39**, 1561 (1977).

20. J.R. Sandercock and W. Wettling, IEEE Trans. Magnet. **14**, 442 (1978).

21. M. Grimsditch, A.P. Malozemoff, and A. Brunsch, Phys. Rev. Lett. **43**, 711 (1979).

22. P. Grunberg, M.G. Cottam, W. Vach, C.M. Mayr, and R.E. Camley, J. Appl. Phys. **53**, 2078 (1982).

23. M. Grimsditch, M.R. Khan, A. Kueny, and I.K. Schuller, Phys. Rev. Lett. **51**, 498 (1983).

24. de Raedt H. and Lagendjik A., *Monte Carlo simulation of quantum statistical lattice systems*, Phys.Rep., **127**, 233 (1985).

25. Cullen J.J. and Landau D.P., *Monte Carlo studies of one-dimensional quantum Heisenberg and XY models*, Phys.Rev.B, **27**(1), 297, (1983).

26. Handscomb D.C. , *The Monte-Carlo Method in Quantum Statistical Mechanics*, Proc.Camb.Phil.Soc., **52**, 594 (1962).

27. Handscomb D.C., *Monte-Carlo Method and the Heisenberg*

Ferromagnet, Proc.Camb.Phil.Soc., **60**, 115 (1964).

28. Lyklema J.W., Phys.Rev.Lett., **49**(1), 82-5 (1982).

29. Lyklema J.W., *Critical properties of Heisenberg chains at T=0*, Phys.Rev.B, **27**(5) (1983).

30. D.Betts, *Spin 1/2 XY-Model*, in Phase Transitions and Critical Phenomena, C.Domb and M.S.Green, eds., N.Y.,Academic, 1974, vol.3

31. Favorski I.A., A.G. Gutman, A.P. Lubartsev, I.V. Rozhdestvenskii, *Monte Carlo Study of Quantum and Classical Spin Lattice Systems with Long-Range Potentials*, Preprint Institute for Theoretical Physics, Ukrain. Acad. of Science, ITP-85-94R, Kiev 1985 (in Russian).

32. ırtazayev,A.K., Favorski I.A., *Investigation of the cooperative phenomena in the quantum spin lattice systems by means of Monte-Carlo methods*, VINITI manuscript, UDK 539.2, P.6250-B87, Leningrad 1987 (in Russian).

33. Chakravarty S. and Stein D.B., *Monte Carlo Simulation of Quantum Spin Systems* ,Phys.Rev.Lett.,**49**(8), 582-5, (1982).

34. Rozhdestvensky I.V., Favorsky I.A. and Murtazayev A.K. , *"The Study of Quantum Spin Models of Magnetics and Ferroelectrics by Means of Numerical Experiment"*, preprint Ukrain.Acad.Sc., Institute for Theor. Phys.,ITP-87-158P, Kiev, 1988 (in Russian).

35. Branco, N.S., S.L.A. de Queiroz and R.R. dos Santos, *Heisenberg and Ising spins in three dimensions with site-bond-correlated dilution*, Phys.Rev.B, **42**, 458 (1990).

36. Jochims, M., T.Holey and M.Fahnle, *Monte-Carlo simulations for pure and site-diluted simple cubic classical Heisenberg system*,

Phys.Stat.Sol. (b), **166**, 277 (1991).

37. Favorsky, I.A., A.G. Gutman, E.M.Ushakova, *Magnetic and thermal properties of the Heisenberg ferromagnet* $CuK_2Cl_4 \cdot 2H_2O$. *A Monte Carlo calculation*, Sov.Phys-Fizika Tverdogo Tela, **29**(5), 1582-5 (1987)

38. Foster, F.G., *On the stochastic matrices associated with certain queuing processes*, Ann.Math.Statist., **24**, 355-60 (1953)

39. Lee D.H., Joannopulos J.D., and Negele J.W., *Monte-Carlo Solution of Antiferromagnetic Quantum Heisenberg Spin Systems*, Phys.Rev.B, **30**(3), 1599 (1984).

40. Chakravarty S. and Stein D.B., *Monte Carlo Simulation of Quantum Spin Systems*, Phys.Rev.Lett., **49**(8), 582-5 (1982).

41. Manousakis E. and Salvador R., *Monte Carlo study of the two-dimensional spin-1/2 quantum Heisenberg model: Spin correlations in* $La_2Cu\ O_4$, Phys.Rev.B, **39**(1), 575-85 (1989).

42. Gomez-Santos G., Joannopulos D. and Negele J.W., *Monte Carlo Study of the Quantum Spin-*$\frac{1}{2}$ *Heisenberg Antiferromagnet on the Square Lattice*, Phys.Rev.B, **39**(7), 4435-43 (1989).

43. R.Blinc, B.Zeks, and J.Nelmes, *Proton Tunnelling in* KH_2PO_4, Ph.Transitions, **3**, 2.3 (1983).

44. Y.-L.Wang, and B.R.Cooper, *Collective Excitations and Magnetic Ordering in Matherials with Singlet Crystal Field Ground State*, Phys.Rev., **185**(5), 539 (1968).

45. I.V.Rozhdestvensky, I.A.Favorsky, *Handscomb Monte-Carlo Method for S=1/2 Transverse Ising Model*, Mol.Simulations, **9**, 213-22 (1992).

46. S.Kadowaki and A.Ueda, *A New Monte Carlo Approach to Quantum Spin Systems.II*, Progr.Theor.Phys., 82(3), 493-506 (1989).

47. A.W.Sandwik and J.Kurkijarvi, *Quantum Monte Carlo simulation method for spin systems*, Phys.Rev.B, 43(7), 5950-61 (1990).

48. T.V.Kuznetsova and P.N.Vorontsov-Velyaminov, *Monte Carlo computation of the free energy in quantum two-dimensional Heisenberg ferromagnets using the expanded-ensemble method*, J.Phys: Condens.Matt., 5, 717-24 (1993).

49. M.Takahashi, *Quantum Heisenberg Ferromagnets in One and Two Dimensions at Low Temperature*, Progr.Theor.Phys., Supplement No.87, 233-46 (1986).

50. H. Godfrin, R.R. Ruel, and D.D. Osheroff, Phys. Rev. Lett. 60, 305 (1988).

51. N.Franco, R.E.Rapp, and H Godfrin, Phys. Rev. Lett., 57, 1161 (1986).

52. P.Schiffer, M.T.O'Keefe, H.Fukuyama and D.D.Osheroff, Phys. Rev. Lett., 71, 1403 (1993).

53. P.Shiffer, M.T. O'Keefe, D.D.Osheroff and H.Fukuyama, J. Low Temp. Phys., 94, 489 (1994).

54. H.Fukuyama, P.Schiffer, M.T.O'Keefe, D.D.Osheroff, *Proceedings of the 20th International Conference on Low Temperature physics*, Physica B (1988).

55. P. Zhou, J.E. Drumheller, B. Patyal, and R.D. Willett, Phys. Rev. B 45, 12365 (1992).

56. N.D. Mermin and H. Wagner, Phys. Rev. Lett. 17, 1133 (1966).

57. M. Takahashi, Phys. Rev. *B* **40**, 2494 (1989).

58. N.E. Stanley, Phys. Rev. **158**, 546 (1967).

59. J.Kosterlitz and D.Thouless, J.Phys.C., **6**, 1181 (1973).

60. L.Biferale and R.Petronzio, *Renormalization group study of XY and Heisenberg models in two dimensions*, Nucl.Phys.B, **328**, 677-700 (1989).

61. K. Yamaji and J. Kondo, Phys. Lett. **45A** 317 (1973).

62. Kopietz P. and Chakravarty S., *Low-temperature behavior of the correlation length and the susceptibility of a quantum Heisenberg ferromagnet in two dimensions*, Phys.Rev.B, **40**(7), 4858 (1989).

63. I.A. Favorsky, T.V. Kuznetsova, P.N. Vorontsov-Velyaminov, J. Phys. Condens. Matt. **4**, 2629 (1992).

64. I.V. Rojdestvensky and I.A. Favorski, J. Phys. Condens. Matt. **5**, L279 (1993).

65. I.V. Rojdestvenski, M.G. Cottam, and I.A. Favorski, J. Appl. Phys., **75**(10), 5823 (1994).

66. Y.C. Chen, H.H. Chen, and F. Lee, Phys. Rev. *B* **43**, 11082 (1991).

67. S.-W. Cheong, A.S. Cooper, L.W. Rupp, Jr., B. Batlogg, J.D. Thompson, and Z. Fisk, Phys. Rev. B **44**, 9739 (1991).

68. M. Takahashi and H. Ikeda, Phys. Rev. B **47**, 9132 (1992).

69. M. Takahashi, S. Ikeda, and H. Ikeda, J. Phys. Soc. Jpn. **60**, 387 (1991).

70. F. Suzuki, K. Takayama, K. Watanabe, and C. Ishii, J. Phys.

Soc. Jpn. **60**, 3242 (1991).

71. J. Behre and S. Mivashita, J. Phys. A **25**, 4745 (1992).

72. E.F. Talbot, Phys. Rev. B **33**, 4906 (1986).

73. I.V. Rojdestvensky, M.G.Cottam, I.A. Favorski, T.Kuznetsova and P.N. Vorontsov-Velyaminov, Surf.Rev. and Lett., 1(2&3) (1994)

74. P. Grunberg, Progress in Surf. Science, **18**, 1 (1985).

75. P. Grunberg, in Light Scattering in Solids V, eds. M. Cardona and G. Guntherodt (Springer-Verlag, Heidelberg, 1989), p.303.

76. J.R. Dutcher, in Linear and Nonlinear Spin Waves in Magnetic Films and Superlattices, ed. M.G. Cottam (World Scientific, Singapore, 1994), p. 287.

77. R.W. Damon and J. Eshbach, J. Phys. Chem. Solids **19**, 308 (1961).

78. R.E. Camley, T.S. Rahman, and D.L. Mills, Phys. Rev. B **23**, 1226 (1981).

79. J.F. Cochran and J.R. Dutcher, J. Magn. Magn. Mat. **73**, 299 (1988).

80. R.E. De Wames and T. Wolfram, J. Appl. Phys. **41**, 987 (1970).

81. R.L. Stamps and B. Hillebrands, Phys. Rev. B **43**, 3532 (1991).

82. V.V. Gann, Sov. Phys. - Solid State **8**, 2537 (1967) [Fiz. Tverd. Tela, **9**, 3167 (1966)].

83. B.N. Filippov, Phys. Met. Metall. **32**, 911 (1971) [Fiz. Met. Metalloved. **29**, 1131 (1970)].

84. M.G. Cottam and A.N. Slavin, IEEE Trans. Magnetics **27**, 5489

(1991).

85. I.V. Rojdestvensky, M.G. Cottam, and A.N. Slavin, J. Appl. Phys. 73, 7001 (1993).

86. I.V. Rojdestvensky, M.G. Cottam, and A.N. Slavin, Phys. Rev. B, 48, 12768-82 (1993).

87. A.N. Slavin, I.V. Rojdestvensky, and M.G. Cottam, J. Appl. Phys., 69(8), 6549-51 (1994).

88. O.G. Vendik and D.N. Chartorizhskii, Sov. Phys. - Solid State 12, 2537(1970) [Fiz. Tverd. Tela 12, 1538 (1970)].

89. B.A. Kalinikos and A.N. Slavin, J. Phys. C 19, 7013 (1986).

90. B.A. Kalinikos and A.N. Slavin, Acta Phys. Pol. A75, 541 (1989).

91. M.G. Cottam and A.N. Slavin, in Linear and Nonlinear Spin Waves in Magnetic Films and Superlattices, ed. M.G. Cottam (World Scientific, Singapore, 1994), p. 1.

92. B.A. Kalinikos, in Linear and Nonlinear Spin Waves in Magnetic Films and Superlattices, ed. M.G. Cottam (World Scientific, Singapore, 1994), p. 89.

93. M.G. Cottam, J. Phys. C 16, 1573 (1983).

94. N. Zubarev, Sov.Phys.-Uspekhi, 3, 320 (1960)

95. N.M. Salanskii and M.S. Erukhimov, *Physical Properties and Application of Magnetic Films* (Nauka, Novosibirsk, 1975), p. 38 [in Russian].

96. W. Wettling, M.G. Cottam, and J.R. Sandercock, J.Phys. C 8, 211 (1975).

3 of/de 3

PM-1 3½"x4" PHOTOGRAPHIC MICROCOPY TARGET
NBS 1010a ANSI/ISO #2 EQUIVALENT

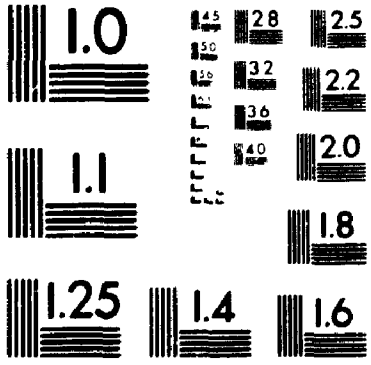

PRECISION[SM] RESOLUTION TARGETS

97. V.N. Krivoruchko and D.A. Yablonskii, Phys. Stat. Sol. (b) **103**, K41 (1981).

98. K. Vayhinger and H. Kronmuller, J. Mag. Magn. Mat. **72**, 307 (1988).

99. M. Vohl, J. Barnas, and P. Grunberg, Phys. Rev. B **39**, 12003 (1989).

100. B. Hillebrands, Phys. Rev. B **41**, 530 (1990).

101. B. Heinrich, Z. Celinski, J.F. Cochran, A.S. Arrott, K. Myrtle, and S.T. Purcell, Phys Rev. B **47**, 5077 (1993).

102. B.A. Kalinikos and P.A. Kolodin, Izv. Vuzov-Radiofizika **32**, 1290 (1989).

103. K. Vayhinger and H. Kronmuller, J. Mag. Magn. Mat. **62**, 159 (1986).

104. R.C. Moul and M.G. Cottam, J. Phys. C **16**, 1307 (1983).

105. B.A. Kalinikos, M.P. Kostylev, N.V. Kozhus, and A.N. Slavin, J. Phys. Cond. Mat. **1**, 9861 (1990).

106. B.Heinrich and J.F.Cochran, *Ultrathin metallic magnetic films: magnetic anisotropies and exchange interactions*, Advances in Physics, **42**(5), 523-639 (1993).

107. Z. Zhang, P.E. Wigen, S.S.P. Parkin, J. Appl. Phys. **69**, 5649 (1991).

108. Z. Zhang, P.E. Wigen, T. Suzuki, J. Magn. Soc. Jpn. **17S1**, 119 (1993).

109. B.Hillebrands, A. Boufelfel, C.M.Falco, P.Baumgart, G.Guntherodt, E.Zirngiebl and J.D.Thompson, *Brillouin scattering*

from collective spin waves in magnetic superlattices, J.Appl.Phys., **63**(8), 3880-4 (1988).

110. F.Hoffmann, A.Stankoff and H.Pascard, *Evidence for an Exchange Coupling at the Interface between Two Ferromagnetic Films*, Journ.Appl.Phys., **41**(3), 1022-3 (1979)

111. J.J. de Vries, P.J.H.Bloemen, M.T.Johnson, J. aan de Stegge, A.Reinders and W.J.M de Longe, *Oscillation of the interlayer coupling in Co/Au(111)/Co*, J. Appl. Phys. **73** (1993)

112. B. Hillebrands, *Calculating of spin waves in multilayered structures including interface anisotropies and exchange contributions*, Phys. Rev. B **37**, 9885-8 (1988).

113. B. Hillebrands, J.V.Harzer, G.Guntherodt, C.D.England and C.M.Falco, *Experimental evidence for the existence of the exchange-dominated collective spin-wave excitations in multilayers*, Phys. Rev. B **42**(10), 6839-41 (1988).